

A COCKTAIL OF THERMALLY STABLE, CHEMICALLY SYNTHESIZED CAPTURE AGENTS FOR
THE EFFICIENT DETECTION OF ANTI-GP41 ANTIBODIES FROM HUMAN SERA AND
TECHNIQUES

Thesis by

Jessica A. Pfeilsticker

In Partial Fulfillment of the Requirements
for the Degree of
Doctor of Philosophy



California Institute of Technology

Pasadena, California

2014

(Defended December 2, 2013)

© 2014

Jessica A. Pfeilsticker

All Rights Reserved

ACKNOWLEDGEMENTS

I begin by thanking my advisor Professor James Heath for his incredible guidance and talent. His enthusiasm for science is unrivaled, and his uncanny ability to absorb ideas and tie them together in creative and interesting ways has been a wonderful model for how to conduct research. I have enjoyed my time in his lab immensely, and am grateful to have learned from him for the last three and a half years.

I also want to thank Professor Daniel Weitekamp, from whom I learned many fundamental scientific principles. He helped me transition as a young graduate student from someone who takes classes and obtains grades to someone who thinks about and conducts research. For that, and for sharing with me some of his incredible ideas and vast intellect during my first three years at Caltech, I am thankful.

I want thank my committee members Professor Robert Grubbs, Professor Mitchio Okumura, and Professor William Clemons for their guidance and insight. More than once I sought their advice on how to navigate graduate school, and always received encouragement and enthusiasm in return.

Next, I thank my family. They originally inspired an interest in the natural world and the wish to explore it when I was a child, and then supported me as I pursued my education in science. To Dad and Penny, Mom and Ed, thank you for being my parents and offering love and advice. John and Jason, thanks for being the coolest brothers anyone could ask for. You both have incredible futures in front of you, and I know that

your deep thoughtfulness and curiosity will ensure a never ending supply of fun and interest as you pursue your own paths.

I want to thank my lab mates for their instrumental role in my graduate experience. Valerie Norton, Jason Ollerenshaw, Eduard Chekmenev, Jan Höevener, and Daniel Rowlands in the Weitekamp group; Aiko Umeda, Kaycie Deyle, Blake Farrow, Ryan Henning, Alex Sutherland, Joey Varghese, JingXin Liang, Arundhati Nag, Samir Das, Marilena Dimotsantou, Ann Chung, Steve Millward, Errika Romero, and Connie Hsueh in the Heath group; and Heather Agnew, Bert Lai, Rosemary Rohde, and Suresh Pitram at InDi Molecular. You all kept me sane, and offered much needed scientific and personal feedback and assistance during our time as friends and colleagues. Thank you for being my biggest allies; this experience was made so much richer because you all were in it.

I also need to thank the many members of Caltech staff who make research possible. Agnes Tong, thank you for all that you do to keep chemistry running smoothly. David VanderVelde, thank you for your enthusiasm and interest in sharing your knowledge of NMR. Mona Shahgholi, Jie Zhou, Felicia Rusnak, Darryl Willick, Joe Drew, Cora Carriedo, Steve Gould, Paul Carroad, Art Seiden, Mike Roy, Richard Gerhart, Jose Mendez, Engracia Alvarez, and countless others, thank you all for making the department exist and function. All of you have personally touched my time here in some way, and I wouldn't have been able to do this without you.

Finally, it is imperative that I thank the many friends who make up my support network. Lisa Sherer, thank you for being my pseudo-sister for the last 13 years. Caitlin

Murphy, Lisa Mauger, Tucker Jones, Nick Stadie, Luke Boosey, and Patrick Sanan, thank you for being an awesome group of people who bonded so quickly and tightly when we all first arrived at Caltech as wide-eyed first years. Keenan Crane, thank you for being so thoughtful and kind, and for helping me through all manners of crisis, both personal and professional. Cole DeForest, Robin DeForest, Anya Demianenko, and Michael McCoy, thank you for kindness, compassion, wine and foie gras. Young In Oh and Jean Li, thank you for mutual support in the face of adversities. Sang Tae Park, thank you for unconditionally having my back and being someone I could always rely on for personal and technical advice. Maggie Buckles, Tony Roy, and Kellie Roy, thank you for being smart, kind, wonderful people who gave me balance and kept me sane. Jon-Michael Sanchez, thank you for keeping life exciting, and for becoming someone with whom I could explore new ways to express myself. I love all of you, and thank you so much for being in my life.

ABSTRACT

This thesis reports on a method to improve *in vitro* diagnostic assays that detect immune response, with specific application to HIV-1. The inherent polyclonal diversity of the humoral immune response was addressed by using sequential *in situ* click chemistry to develop a cocktail of peptide-based capture agents, the components of which were raised against different, representative anti-HIV antibodies that bind to a conserved epitope of the HIV-1 envelope protein gp41. The cocktail was used to detect anti-HIV-1 antibodies from a panel of sera collected from HIV-positive patients, with improved signal-to-noise ratio relative to the gold standard commercial recombinant protein antigen. The capture agents were stable when stored as a powder for two months at temperatures close to 60°C.

TABLE OF CONTENTS

LIST OF FIGURES, SCHEMES, AND TABLES.....	xiii
--	-------------

CHAPTER 1: Introduction.....	1
-------------------------------------	----------

1.1 PCC Agent Cocktail for HIV-1 Diagnostics.....	2
---	---

1.2 References.....	5
---------------------	---

CHAPTER2: Developing a PCC Agent Cocktail for the Detection of Anti-HIV

Antibodies.....	7
------------------------	----------

2.1 Introduction.....	8
-----------------------	---

2.2 <i>In Situ</i> Click.....	9
-------------------------------	---

2.3 Anchor Selection.....	10
---------------------------	----

2.4 Screening.....	11
--------------------	----

2.5 Biligand Characterization.....	16
------------------------------------	----

2.6 Materials and Methods.....	21
--------------------------------	----

2.6.1 Anchor Synthesis.....	21
-----------------------------	----

2.6.2 OBOC Screens.....	22
-------------------------	----

2.6.3 Biligand Synthesis.....	24
2.6.4 Assays.....	27
2.7 Conclusion.....	29
2.8 Acknowledgements.....	29
2.9 References.....	31
CHAPTER 3: PCC Agent Based Assay for the Detection of Anti-HIV Antibodies from Human Sera.....	33
3.1 Introduction.....	34
3.2 Patient Sample Assay.....	34
3.3 PATH Sample Assay.....	37
3.4 Stability Assay.....	39
3.5 Materials and Methods.....	41
3.5.1 Patient Serum ELISA.....	41
3.5.2 PATH Samples ELISA.....	41
3.5.3 Stability Assay.....	42
3.6 Conclusion.....	43

3.7 Acknowledgements.....	44
3.8 References.....	45
CHAPTER 4: A Selective ^{15}N-to-^1H Polarization Transfer Sequence for More Sensitive	
Detection of ^{15}N-Choline.....	46
4.1 Abstract.....	47
4.2 Introduction.....	48
4.3 Theory.....	49
4.4 Experimental.....	56
4.5 Results and Discussion.....	61
4.6 Conclusion.....	68
4.7 Acknowledgements.....	68
4.8 References.....	69
APPENDIX A: Understanding PCC Agent Binding to Single Point Mutation E17K of Akt1	
Pleckstrin Homology Domain through Molecular Dynamics.....	71
A.1 Introduction.....	72

A.2 Peptide Capture Agent Against E17K Mutation of Akt1 PHD.....	73
A.3 Construction of E17K and WT Systems.....	73
A.3.1 yleaf-tosyl-biotin.....	73
A.3.2 Ligand/Protein Complexes.....	74
A.4 Molecular Dynamics.....	78
A.5 Binding Energy.....	80
A.6 Conclusion.....	85
A.7 Acknowledgements.....	85
A.8 References.....	86
APPENDIX B: Peptide-Based General Antibody Detection Agent.....	87
B.1 Introduction.....	88
B.2 Wells Peptide.....	88
B.3 Biligand Screen.....	89
B.4 1,4 Triazole Linked Biligand Characterization.....	92
B.5 1,5 Triazole Linked Biligand Characterization.....	92
B.6 Click Cyclized Wells.....	97

B.7 Materials and Methods.....	100
B.7.1 Anchor Synthesis.....	100
B.7.2 OBOC screen.....	100
B.7.3 Biligand Synthesis.....	102
B.7.4 Click Cyclized Wells Synthesis.....	103
B.7.5 Assays.....	104
B.8 Conclusion.....	106
B.9 Acknowledgements.....	106
B.10 References.....	107
APPENDIX C: Algorithm for Peptide Clustering.....	108
C.1 Introduction.....	109
C.2 Persistence Clustering.....	109
C.3 Algorithm Description.....	111
C.4 Output.....	111
C.5 Function Code.....	117
C.6 Conclusion.....	123

C.7 Acknowledgements.....	123
C.8 References.....	124
APPENDIX D: A cocktail of thermally stable, chemically synthesized capture agents for the efficient detection of anti-gp41 antibodies from human sera (<i>PloS one</i> 2013, 8, e76224).....	125
APPENDIX E: A Selective ^{15}N-to-^1H Polarization Transfer Sequence for More Sensitive Detection of ^{15}N-Choline (<i>Journal of Magnetic Resonance</i> 2010, 205, 125-129).....	131

LIST OF FIGURES, SCHEMES, AND TABLES**FIGURES, Chapter 2:**

Figure 2.1. Differential detection of 3D6 and 4B3 by anchor ligands.....	12
Figure 2.2. Structures of peptide ligands in PCC Agent cocktail.....	17
Figure 2.3. Apparent affinity of A21 and biligands directed against 3D6 as determined by SPR.....	18
Figure 2.4. Apparent affinity of A22 and biligand directed against 4B3 as determined by SPR.....	19
Figure 2.5. Performance of PCC agent cocktail to detect 3D6 and 4B3 from human serum.....	20

FIGURES, Chapter 3:

Figure 3.1. Patient sample ELISA.....	36
Figure 3.2. PATH sample ELISA.....	38
Figure 3.3. Stability assay.....	40

FIGURES, Chapter 4:

Figure 4.1. A refocused INEPT pulse sequence for polarization transfer from ^{15}N to ^1H for detection.....	51
Figure 4.2. The structure of ^{15}N -choline.....	52
Figure 4.3. Selective refocused INEPT pulse sequence for coherent polarization transfer from ^{15}N to methyl ^1H in ^{15}N -choline.....	57
Figure 4.4. Numerical simulation of the selective ^{15}N -to- ^1H INEPT pulse sequence acting on a simplified spin system.....	60
Figure 4.5. Comparison of ^1H spectrum using selective ^{15}N -to- ^1H INEPT sequence to ^{15}N spectrum.....	62
Figure 4.6. Measurement of the ^{15}N longitudinal relaxation time of ^{15}N -choline in D_2O solution using a modified version of selective ^{15}N -to- ^1H INEPT sequence.....	63
Figure 4.7. Amplitude of the methyl ^1H signal observed in ^{15}N -to- ^1H INEPT spectra of ^{15}N -choline using selective and non selective pulses.....	65

FIGURES, Appendix A:

Figure A.1. Structure of yleaf-tosyl-biotin.....	75
--	----

Figure A.2. Top three ZDOCK predicted conformations.....	76
Figure A.3. Selected ligand conformation complexed with the mutant and wild type PH domains.....	77
Figure A.4. Rmsd plots for the MD trajectories and restarted trajectories of the E17K and WT complexes.....	79
Figure A.5. Energy landscapes obtained from Rosetta <i>ab initio</i> structure prediction simulations on Rosetta@home.....	81
Figure A.6. Energy landscape for E17K complex.....	82
Figure A.7. Energy landscape for WT complex.....	83
Figure A.8. Structures of the E17K and WT reference states.....	84

FIGURES, Appendix B:

Figure B.1. Structures of peptide biligands identified in screen against IgG Fc.....	93
Figure B.2. Apparent affinity of Wells and biligands directed against Fc as determined by sandwich ELISA.....	94
Figure B.3. Structure of 1,5 triazole linked biligand.....	95

Figure B.4. Apparent affinity of Wells and 1,5 triazole linked WA directed against Fc as determined by sandwich ELISA.....	96
Figure B.5. Structure of Cu(I) click cyclized Wells peptide.....	98
Figure B.6. Performance of click cyclized Wells peptide variants compared to Wells peptide tested by sandwich ELISA.....	99

FIGURES, Appendix C:

Figure C.1. Discs formed around points with growing radius ϵ	110
Figure C.2. Illustrative example of how lifetimes of clusters are computed.....	112
Figure C.3. Projection of the peptides onto the top two eigenvectors taken from the diagonalization of the covariance matrix.	114
Figure C.4. Plot of eigenvectors vs. their associated eigenvalues.....	115
Figure C.5. Visual representation of the components of the top four eigenvectors.....	116

SCHEMES, Chapter 2:

Scheme 2.1. Screening strategy for selecting capture agents against
anti-HIV antibodies 3D6 and 4B3.....14

SCHEMES, Appendix B:

Scheme B.1. Screening strategy for selecting capture agents against
human IgG Fc.....90

TABLES, Chapter 2:

Table 2.1. Biligand screen results.....15

TABLES, Appendix B:

Table B.1. Biligand screen results.....91

TABLES, Appendix C:

Table C.1. List of clusters and their associated lifetimes calculated for the hits
resulting from the A22/4B3 screen.....113

Chapter 1

Introduction

1.1 PCC AGENT COCKTAIL FOR HIV-1 DIAGNOSTICS

Accurate diagnoses are critical for effective healthcare. Misdiagnoses carry large personal and societal costs, especially in cases where the disease is transmissible or carries a large social stigma. HIV is one such disease, and HIV misdiagnoses can lead to psychosocial difficulties and have dangerous public health implications [1]. According to the World Health Organization (WHO), roughly 40 million people were living with HIV as of the end of 2004, and some regions have adult prevalence as high as 15-39%. Many countries with high incidence of HIV are resource limited and rely on easy-to-use rapid detection tests for diagnosis; however, the performance of these tests is variable. A study of the WHO HIV two-test diagnostic algorithm, where two positive rapid detection tests are used alone for diagnosis, showed an unacceptably high rate of false-positive results (10.5%), likely due to non-selective cross reactivity [2].

HIV diagnoses are often made indirectly through the detection of anti-HIV antibodies [3]. The current gold standard detection reagents are biologically-produced, and are expensive, susceptible to thermal and biological degradation, and have batch to batch performance variability; all of which can adversely affect the accuracy of diagnostic assays [4,5,6]. Typically in HIV diagnostic assays, multiple immunogenic and conserved antigens from HIV are expressed as regions of a single chimeric protein. That chimeric protein is then used to capture specific antibodies from the body fluid (e.g. blood, saliva or urine) of potentially infected patients; a positive assay result implies infection. However, the antigen has been shown to have poor signal to noise [7],

possibly related to the off-target reactivity responsible for false negative results seen in rapid detection tests.

Robust detection reagents are needed that recognize relevant biomarkers with high sensitivity and selectivity, and that perform well in resource limited areas where controlled laboratory environments are not readily available. Protein Catalyzed Capture agents (PCC agents) are peptide-based detection agents that rival the affinity and selectivity of biological reagents, and that are chemically, physically, and biologically robust. As synthetic reagents, they are also highly modular and can be easily altered for incorporation into different assay platforms. Previous work has identified a number of PCC agents that detect multiple disease relevant biomarker proteins through the process of iterative *in situ* click screening [8,9,10], many of which were engineered to be specifically epitope targeted, and some of which have inhibiting or activating functionalities.

The application of PCC agent technology to anti-HIV antibody detection is not as straightforward as targeting a single biomarker; the polyclonal diversity of antibodies across patient populations can translate into large variations in assay performance from patient to patient. To selectively capture the diversity of anti-HIV antibodies while minimizing serological cross-reactivity, a cocktail of PCC agents was developed against multiple representative anti-HIV antibodies.

Chapter 2 reports on the use of iterative *in situ* click chemistry [8,11] to prepare a cocktail of chemically synthesized PCC agents that is designed to sample the polyclonal diversity of an antibody-based immune response. Three PCC agents, derived from the

same epitope on HIV-1 envelope protein gp41, were raised against two representative anti-HIV antibodies to create a cocktail of capture agents that sample the variations between the representative antibodies, thus increasing the reagent's potential to detect an anti-HIV immune response across multiple patients.

Chapter 3 then describes a PCC agent-based assay developed to detect human antibodies that bind a conserved region of the HIV-1 envelope glycoprotein gp41, using the PCC Agent cocktail described in Chapter 2. The performance is compared against the gold standard chimeric protein antigen using sera collected from a cohort of HIV-1-positive human subjects are tested, plus controls. The assay was also used to detect anti-HIV antibodies from a validation panel of HIV-1 specific IgG containing plasma samples that were rated HIGH, MED, LOW, or NEG in accordance with the titer of anti-HIV antibodies. Additionally, the thermal stability of the capture agent cocktail is reported, with an eye towards point-of-care HIV diagnostics assays that are needed in environments where refrigeration chains may not exist. Chapters 2 and 3 were taken in part from *PloS one* **2013**, *8*, e76224 (see Appendix D).

1.2 REFERENCES

1. Bhattacharya R, Barton S, Catalan J (2008) When good news is bad news: psychological impact of false positive diagnosis of HIV. *AIDS care* 20: 560-564.
2. Klarkowski DB, Wazome JM, Lokuge KM, Shanks L, Mills CF, et al. (2009) The evaluation of a rapid in situ HIV confirmation test in a programme with a high failure rate of the WHO HIV two-test diagnostic algorithm. *PLoS one* 4: e4351.
3. Fanales-Belasio E, Raimondo M, Suligoi B, Butto S (2010) HIV virology and pathogenetic mechanisms of infection: a brief overview. *Ann Ist Super Sanita* 46: 5-14.
4. Daskalakis D (2011) HIV diagnostic testing: evolving technology and testing strategies. *Top Antivir Med* 19: 18-22.
5. Ginocchio CC, Carman WF, Arens MQ (2011) Update on HIV diagnostic testing algorithms. Editors' introduction. *J Clin Virol* 52 Suppl 1: S1.
6. Alvarez M, Chueca N, Guillot V, Bernal Mdel C, Garcia F (2012) Improving Clinical Laboratory Efficiency: Introduction of Systems for the Diagnosis and Monitoring of HIV Infection. *Open Virol J* 6: 135-143.
7. Tiwari RP, Jain A, Khan Z, Kumar P, Bhargava V, et al. (2012) Designing of novel antigenic peptides cocktail for the detection of antibodies to HIV-1/2 by ELISA. *Journal of immunological methods*.
8. Agnew HD, Rohde RD, Millward SW, Nag A, Yeo WS, et al. (2009) Iterative in situ click chemistry creates antibody-like protein-capture agents. *Angew Chem Int Ed Engl* 48: 4944-4948.
9. Millward SW, Henning RK, Kwong GA, Pitram S, Agnew HD, et al. (2011) Iterative in Situ Click Chemistry Assembles a Branched Capture Agent and Allosteric Inhibitor for Akt1. *Journal of the American Chemical Society* 133: 18280-18288.

10. Arundhati Nag SD, Mary Beth Yu, Kaycie M. Deyle, Steven W. Millward, James R. Heath
(2013) A Chemical Epitope-Targeting Strategy for Protein Capture Agents: The Serine
474 Epitope of the Kinase Akt2. *Angewandte Chemie International Edition* In press.
11. Millward SW, Henning RK, Kwong GA, Pitram S, Agnew HD, et al. (2011) Iterative in situ click
chemistry assembles a branched capture agent and allosteric inhibitor for Akt1. *J Am
Chem Soc* 133: 18280-18288.

Chapter 2

Developing a PCC Agent Cocktail for the Detection of Anti-HIV Antibodies

2.1 INTRODUCTION

Detecting the immune response to an infectious agent can provide a useful *in vitro* diagnostic surrogate relative to direct pathogen detection [1]. Such assays are commonly used for detecting HIV infection because of its characteristic immunopathology [2]. Direct detection of HIV viral RNA and p24 antigen is only effective at an early stage of infection, approximately 2-6 weeks of initial exposure [3,4]. Antibodies against HIV envelope proteins emerge in patients' blood around 3-4 weeks of infection [2,5] as the viral RNA and p24 levels decline as a result of immunocomplex formation [6]. The high serum level of anti-HIV IgG is maintained throughout the course of clinical latency (2-20+ years), during which time viral antigens are under detection limits until the onset of acquired immunodeficiency syndrome (AIDS) [2,5]. Typically in these assays, immunogenic and conserved antigens from the HIV are expressed as regions of a single chimeric protein. That chimeric protein is then used to capture specific antibodies from the body fluid (e.g. blood, saliva or urine) of potentially infected patients; a positive assay result implies infection. However, the polyclonal diversity of antibodies across a patient population can translate into large variations in assay performance from patient to patient. In addition, the chimeric recombinant proteins are biological reagents, and so may have limitations related to shelf life and batch-to-batch variability. These limitations can adversely influence the performance of a diagnostic test [3,5,7], especially one that is deployed in harsh physical environments.

Previous work in the Heath group has demonstrated the ability to selectively target biologically relevant proteins with PCC Agents [8,9]. Targeting anti-HIV antibodies requires selective detection of anti-HIV antibodies over other IgG and serum proteins while maintaining sensitivity to variations in immune response across patients. This chapter reports on the discovery, synthesis, and characterization of a cocktail of capture agents that selectively target different anti-HIV antibodies to increase the target capture probability while minimizing cross reactivity with other proteins in sera.

2.2 *IN SITU* CLICK

The development of a PCC Agent against a protein target utilizes the target itself to promote the 1,3-dipolar cycloaddition between an acetylene and an azide group to form a triazole linkage (the *in situ* 'click' reaction) [10]. The protein effectively plays the role of an extremely selective, but much less efficient, variant of the Cu(I) catalyst that is commonly used for such couplings [11,12]. For the present work, the two reacting species are peptides – one peptide (the anchor) is a chemically modified variant of a conserved, immunogenic epitope on the HIV-1 gp41 protein, and the second peptide is selected via an *in situ* click screen from a large (10^6 element) one-bead-one-compound (OBOC) [13] peptide library. The protein targets are human monoclonal antibodies raised against variants of the gp41 epitope represented by the anchor peptide.

2.3 ANCHOR SELECTION

The PCC Agents developed here were designed to capture antibodies that are selective for residues 600-612 (IWCGSGKLICTTA) of gp41. Previous studies have shown that a large fraction of HIV-1-positive patients develop antibodies against this epitope [14,15]. Our strategy for sampling the polyclonal diversity of such antibodies was to develop PCC Agents that exhibited both differential, as well as similar avidities for human monoclonal antibodies (mAbs) raised against different parts of this epitope. To select the anchor peptides, we modified the polypeptide fragment corresponding to residues 600-612 of gp41 with artificial amino acids at multiple locations, and tested the ability of these modified cyclic peptides to detect two different monoclonal anti-gp41 antibodies 3D6 and 4B3 (Polymun, Klosterneuburg, Austria). The 3D6 mAb was raised against the epitope SGKLIC, whereas the 4B3 mAb was raised against SGKLICTTA. One anchor peptide, A21, was synthesized by adding a propargyl glycine (Pra) residue at the C-terminus of the residues 600-612 of gp41. This anchor peptide was also N-terminally tagged with a polyethylene glycol (PEG) oligomer bridge and a biotin label. For a second anchor peptide (A22), Leu-607 was substituted with Pra. A22 also included an N-terminal PEG-biotin label. A21 equally detected 3D6 and 4B3 with an estimated dissociation constant (K_d) of 1-50 nM, while A22 differentially detected 3D6 ($K_d >10 \mu\text{M}$) and 4B3 ($K_d = 1-50 \text{ nM}$) (Figure 2.1). A21 and A22 were then separately developed into PCC agents against 3D6 and 4B3, respectively.

2.4 SCREENING

The *in situ* click screens are illustrated in Scheme 2.1. The target IgG is incubated with an excess of the selected anchor peptide and a large OBOC library at 4°C overnight (see Materials and Methods). The OBOC library is synthesized on TentaGel resin (Rapp Polymere, Tuebingen, Germany), and is a comprehensive library of 5-mers with a 6th amino acid at the N-terminus presenting an azide functionality. To help ensure chemical and biochemical stability, the OBOC library is comprised of non-natural (D) stereoisomers of the 20 natural amino acids, excluding cysteine and methionine. The *in situ* screen is designed to identify a secondary (2^o) peptide that, when coupled to the anchor, forms a biligand with increased selectivity and/or affinity for the target IgG.

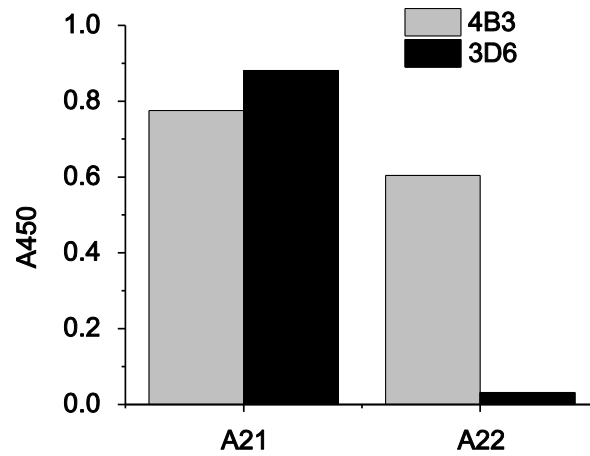
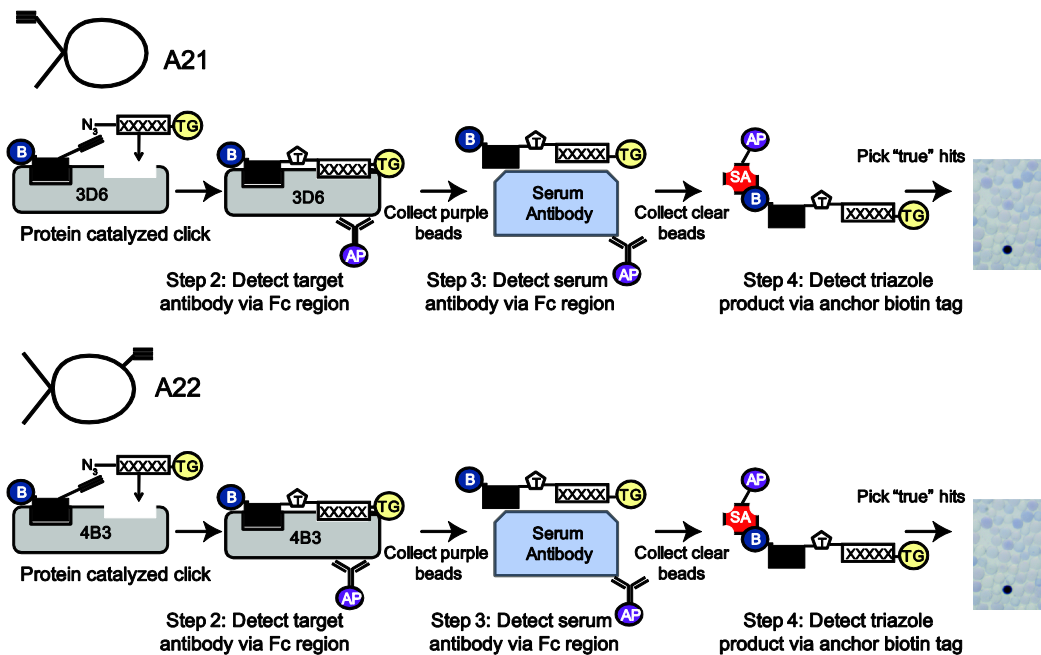


Figure 2.1. Differential detection of 3D6 and 4B3 by anchor ligands. Relative affinities of A21 and A22 for 3D6 and 4B3 were determined by sandwich ELISA. Biotinylated anchor ligands A21 and A22 were immobilized on streptavidin-coated 96-well plated at a concentration of 100 nM, and incubated with the solutions of target anti-HIV antibodies 3D6 and 4B3 at 100 nM in TBS. Captured antibody was detected by peroxidase-conjugated anti-human IgG antibody.

The screen proceeds stepwise. In the first step (not shown in Scheme 2.1) the OBOC library is cleared of beads that exhibit non-specific binding to alkaline phosphatase-conjugated streptavidin (SA-AP), which is used as a detection reagent in a later step. Step 2 is a target screen, and so is designed to detect the presence of the bound IgG target to specific beads, and defines possible hits. The step 3 screen is designed to remove those beads from the pool of potential hits that also exhibit binding to off-target serum proteins. Step 4 is called a product screen, and is unique to sequential *in situ* click screens [16]. This screen is designed to detect for the presence of *in situ* clicked reaction products, which are those hit beads containing the triazole-linked anchor peptide. Typically, Step 2 yields a few hundred hits (~0.05% of the OBOC library). Step 3 reduces that pool by a factor of 2 or 3 to about 100 hits, and Step 4 further reduces the number of hits to around 10. This is a manageable number, meaning that each hit can be separately synthesized as a biligand using Cu(I) catalyzed click chemistry to couple the anchor and 2° peptides. A complete list of the hits for the A21/3D6 and A22/4B3 screens is given in Table 2.1.



Scheme 2.1. Screening strategy for selecting capture agents against anti-HIV antibodies 3D6 and 4B3. The flow chart represents the use of the A21 and A22 cyclic peptides as anchor ligands for separate in situ click screens against a large OBOC azide-presenting peptide library.

	X ₁	X ₂	X ₃	X ₄	X ₅
Az4	d	k	G	l	p
Az4	v	a	d	p	a
Az4	n	i	d	n	G
Az4	p	G	v	t	f
Az4	s	r	r	r	s
Az4	d	q/e	G	a	f
Az4	y	w	d	y	n

Az4	h	l	l	y	q
Az4	s	G	a	q	s
Az4	d	d	w	a	i
Az4	q	i	d	l	r
Az4	t	f	L	q	s
Az4	h	n	p	f	k
Az4	w	G	e	h	p

Az4	q	n	d	w	K
Az4	l	t	s	r	Y
Az4	d	i	k	s	p
Az4	e	i	h	n	y
Az4	q	p	i	d	q
Az4	k	i	d	r	v
Az4	q	s	p/d	w	l
Az4	e	q	t	f	d

Table 2.1. Biligand screen results. List of pentapeptide “hits” from OBOC biligand screens performed with A21/3D6 and A22/4B3. The selected secondary ligands corresponding to (i), (ii), and (iii) are shown in red, blue, and green respectively (shown in Figure 2.2).

2.5 BILIGAND CHARACTERIZATION

The performance of these biligands is then characterized using immunoprecipitation (pulldown) assays detected by Western blotting from spiked serum samples for specificity (data not shown), and sandwich ELISAs and surface plasmon resonance (SPR) assays for affinity estimations (Figure 2.3-2.4). This approach yielded two equivalently performing biligands against 3D6, and one biligand against 4B3. These three PCC agents (Figure 2.2) were combined, in equal parts, to form a capture agent cocktail. The cocktail slightly outperformed both the standard commercial chimeric antigen and A21, when tested against healthy human serum spiked with both 3D6 and 4B3 (Figure 2.5). A21 is the equivalent of the original antigenic epitope of gp41.

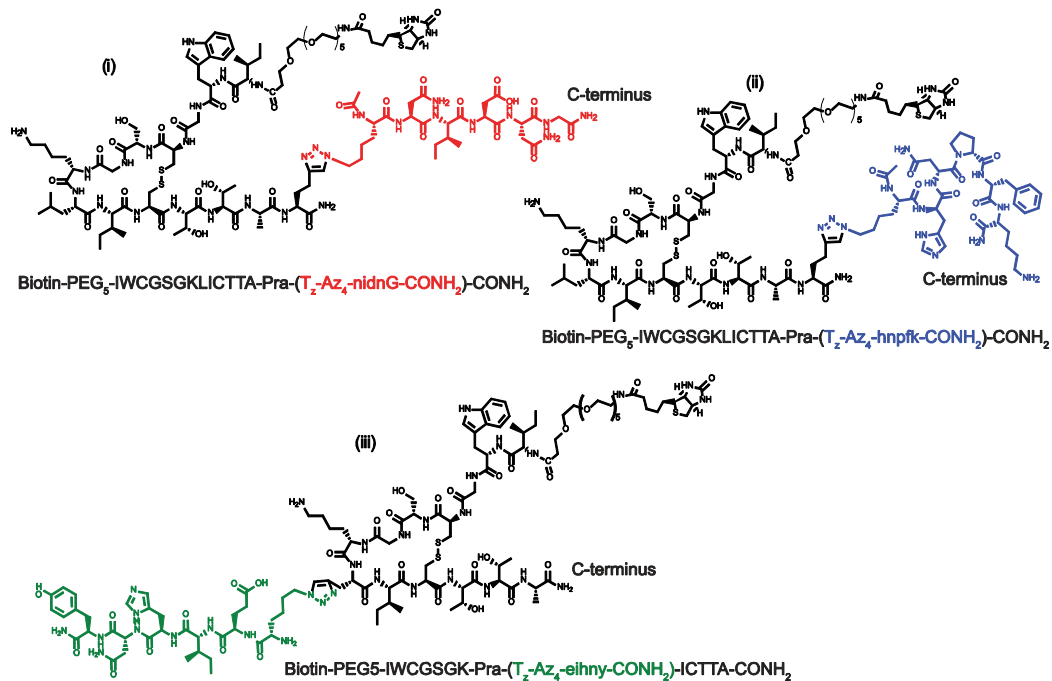


Figure 2.2. Structures of peptide ligands in PCC Agent cocktail. Acetylene-presenting anchor peptides (black) were derived from the immunogenic epitope of HIV-1 gp41 (residues 600-612). A22-nindG (i) and A21-hnpfk (ii) were evolved from the original epitope appended with Pra at the C-terminus whereas A22-eihny (iii) utilizes the “substituted” anchor where residue Leu-607 is replaced with Pra. Secondary ligand branches (colored) were identified from the *in situ* click screen of a 5-mer OBOC library presenting an azide functionality. Biligands (i) and (ii) were raised against the target anti-HIV antibody 3D6, and the biligand (iii) was raised against the antibody 4B3.

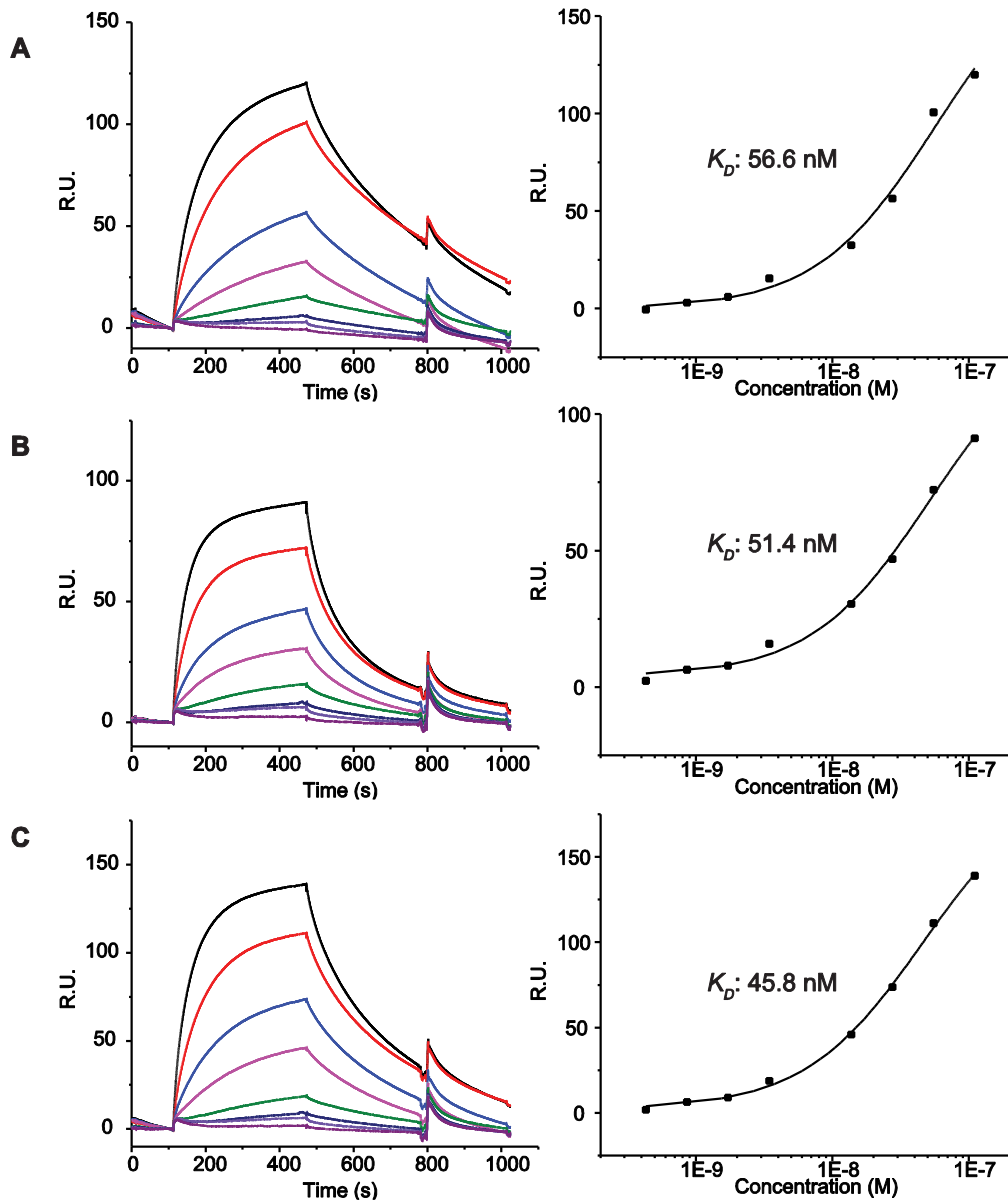


Figure 2.3. Apparent affinity of A21 and biligands directed against 3D6 as determined by SPR. **A.** Sensorgram and 1st order Hill fit to affinity data for A21. **B.** Sensorgram and 1st order Hill fit to affinity data for A21-nidnG (i). **C.** Sensorgram and 1st order Hill fit to affinity data for A21-hnpfk (ii).

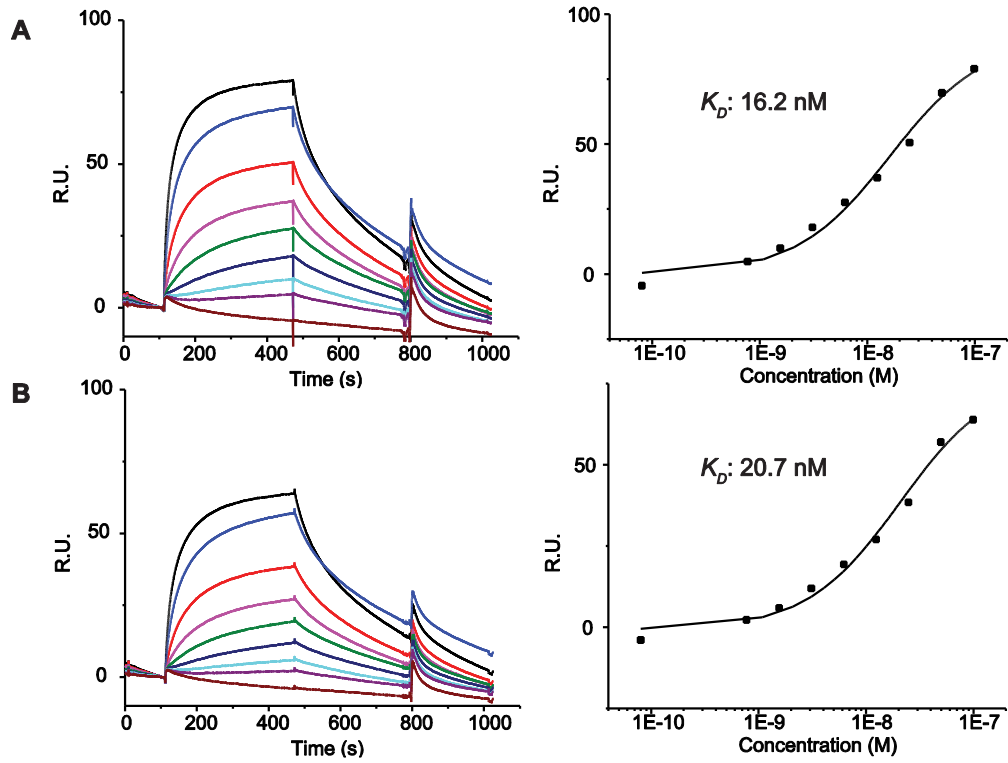


Figure 2.4. Apparent affinity of A22 and biligand directed against 4B3 as determined by SPR. **A.** Sensorgram and 1st order Hill fit to affinity data for A22. **B.** Sensorgram and 1st order Hill fit to affinity data for A22-eihny (iii).

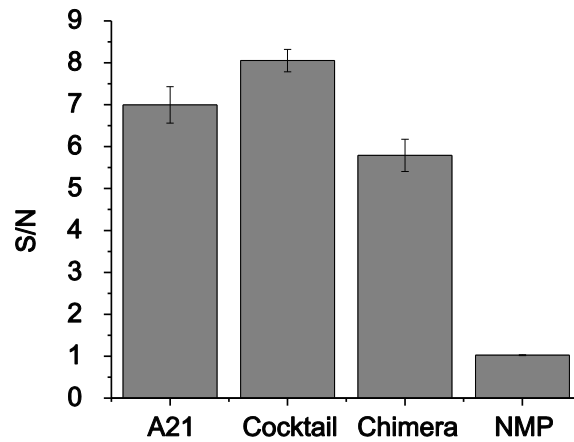


Figure 2.5. Performance of PCC agent cocktail to detect 3D6 and 4B3 from human serum. Comparative performance of the PCC Agent cocktail versus the original gp41 epitope A21 and the commercial chimeric protein antigen was tested by a sandwich ELISA. Target antibodies 3D6 and 4B3 (4 nM each) were both spiked into diluted, HIV-free human serum (1% v/v in TBS), and captured antibody was detected by peroxidase-conjugated anti-human IgG antibody.

2.6 MATERIALS AND METHODS

2.6.1 Anchor Synthesis

The anchor peptides A21 and A22 were synthesized C → N on 200-300 mgs of Rink amide resin (AnaSpec, Fremont, CA) with a Titan peptide synthesizer using standard Fmoc chemistry [17]. The synthesis used Fmoc and side chain protected L amino acids (Aaptec, Louisville, KY), Fmoc protected propargylglycine (Pra) (Aaptec, Louisville, KY), PEG₅ (EMD Millipore, Germany), and biotin (Sigma-Aldrich, St. Louis, MO). The finished peptides were side-chain deprotected and cleaved from resin in a mixture of 95% v/v trifluoroacetic acid (TFA) (Sigma-Aldrich, St. Louis, MO), 5% v/v dH₂O, and 5% triethylsilane (TES) (Sigma-Aldrich, St. Louis, MO), and precipitated in diethyl ether. Cu(Phen)₃ stock solution was prepared by mixing 150 mM Cu(II) sulfate pentahydrate (Sigma-Aldrich, St. Louis, MO) and 500 mM 1,10-phenanthroline (Sigma-Aldrich, St. Louis, MO) in 4:1 H₂O:Ethanol. The ether-precipitated ligands were cyclized by stirring the cleaved peptides dissolved in ~5 mL acetonitrile (ACN) overnight with 1 mL of the Cu(Phen)₃ stock solution. The cyclization mixtures were lyophilized, and the final peptide products were purified using reverse phase (RP) HPLC on a Kinetex 5μ XB-C18 250 x 4.6 mm prep column (Phenomenex, Torrance, CA). MALDI-TOF MS: A21: Expected mass [M+H]⁺ = 2006.96, Observed mass [M+H]⁺ = 2006.24. A22: Expected mass [M+H]⁺ = 1892.89, Observed mass [M+H]⁺ = 1892.85

2.6.2 OBOC Screens

All screens used naïve one-bead-one-compound (OBOC) D-pentapeptide libraries on TentaGel resin (TG) (Rapp Polymere, Tuebingen, Germany) of the form $\text{NH}_2\text{-Az}_4\text{-X}_1\text{X}_2\text{X}_3\text{X}_4\text{X}_5\text{-TG}$, excluding cysteine and methionine, where Az_4 is L-azidolycine. Libraries were synthesized on a Titan peptide synthesizer (Aaptec, Louisville, KY) using a split/mix method, and couplings were done using standard Fmoc SPPS chemistry in *N*-methylpyrrolidone (NMP).

A21 with 3D6

Screening against 3D6 was carried out in four main steps: pre-clear, target screen, anti-screen, and product screen. **Step 1 preclear:** 400 mg of OBOC library was blocked in 5% w/v dry milk in Tris buffered saline (TBS) (25 mM Tris-HCl, 150 mM NaCl, 10 mM MgCl_2 , pH 7.6) for 2 hr at room temperature, and then incubated with 1:10,000 phosphatase-conjugated streptavidin (SA-AP, Promega, Madison, WI) in 0.5% w/v dry milk in TBS for 1 hr. The beads were washed in high salt buffer (25 mM Tris-HCl, 750 mM NaCl, 10 mM MgCl_2 , pH 7.6) for 1 hr, and then developed with BCIP/NBT (Promega, Madison, WI) in BCIP buffer (100 mM Tris-HCl, 150 mM NaCl, 1 mM MgCl_2 , pH 9). After 20 minutes, the reaction was quenched with conc. HCl, and the purple beads were discarded. The remaining library was decolorized in NMP, dried with methanol (MeOH) and dichloromethane (DCM), and then swelled and blocked in 5% w/v dry milk in TBS for 2 hr at room temperature. **Step 2 target screen:** 4 mL of a solution containing 11.4 μM A21 and 147 nM 3D6 in 0.5% w/v dry milk in TBS was added to the precleared OBOC

library, and the *in situ* click reaction was allowed to proceed overnight at 4°C. Bound target was probed with 1:10,000 AP-conjugated rabbit anti-human IgG Fc (Thermo Scientific, Rockford, IL) in 0.5% w/v dry milk in TBS for 1 hr at room temperature. The beads were then washed in high salt buffer for 1 hr at room temperature, and developed with BCIP/NBT in BCIP buffer. The reaction was quenched after 20 minutes with conc. HCl, and the purple beads were retained and decolorized in NMP and dried with MeOH and DCM. The hit beads were then stripped of all bound protein by washing with 7.5 M Guanidine-HCl (pH 2) for 2 hr at room temperature, rinsed 10 times with water, and then blocked in 5% w/v dry milk in TBS for 2 hr at room temperature. **Step 3 anti-screen:** A solution of 1% v/v human serum (Omega Scientific, Tarzana, CA) in TBS was incubated with the hit beads from Step 2 for 1 hr at room temperature. Off-target human antibodies bound to the beads were probed with 1:10,000 AP-conjugated rabbit anti-human IgG Fc in 0.5% w/v dry milk in TBS for 1 hr at room temperature. The beads were then washed in high salt buffer for 1 hr, and developed with BCIP/NBT in BCIP buffer. The reaction was quenched after 20 minutes with conc. HCl, and the purple beads were discarded. The remaining beads were decolorized in NMP and dried with MeOH and DCM. The anti-screened beads were swelled in water and washed with Guanidine-HCl for 2 hr at room temperature, rinsed 10 times with water, and then blocked in 5% w/v dry milk in TBS for 2 hr at room temperature. **Step 4 product screen:** The beads were incubated for 1 hr at room temperature with 1:10,000 SA-AP in 0.5% w/v dry milk in TBS, washed for 1 hr with high salt buffer, and then developed with BCIP/NBT in BCIP buffer for 20 minutes. The reaction was quenched with conc. HCl, and

the purple beads were retained and sequenced using a Procise CLC Edman Degradation Protein Sequencing System (Applied Biosystems, Kingston, RI).

A22 with 4B3

Screening against 4B3 was carried out similarly to that described for 3D6, with two exceptions. In **Step 2**, the *in situ* click reaction solution contained 10 μ M A22 and 430 nM 4B3 in 0.5% w/v dry milk in TBS. In **Step 3**, the beads were anti-screened against 0.1% v/v human serum in TBS spiked with 430 nM 3D6.

2.6.3 Biligand Synthesis

Pra-OtBu

The C-terminally protected Pra molecule used in the synthesis of **(i)** and **(ii)** was made by refluxing Fmoc-L-Pra-OH (Aaptec, Louisville, KY) with tert-butyltrichloroacetamide (Sigma-Aldrich, St. Louis, MO) at 50°C for 3 hr in DCM. The formed product was separated from unreacted species on a silica flash column in DCM.

Peptides (i) and (ii)

The secondary ligands including N-terminal Az₄ for **(i)** and **(ii)** were synthesized C \rightarrow N on 200-300 mgs of Rink amide resin with a Titan peptide synthesizer using standard Fmoc chemistry. The synthesis used Fmoc and side chain protected D amino acids and L-Az₄ (Aaptec, Louisville, KY). Fmoc- and C-terminally protected Pra (Pra-OtBu) was clicked on-bead to the azide side chain of Az₄ by adding equal molar amounts of

Pra-OtBu, Cu(I) iodide (Sigma-Aldrich, St. Louis, MO), and L-ascorbic acid (Sigma-Aldrich, St. Louis, MO), in 2x excess to the azide on bead. The click mixture was agitated in 20% v/v piperidine in NMP for 3 hr at room temperature, and the copper was chelated by repeated washing with 10% w/v sodium diethyldithiocarbamate trihydrate (Sigma-Aldrich, St. Louis, MO) and 10% v/v *N,N*-diisopropylethylamine (DIEA) (Sigma-Aldrich, St. Louis, MO) in NMP until the beads were clear. The Fmoc deprotected Pra was then the starting point for the remainder of the anchor component of each ligand, including N-terminal PEG₅ and biotin. The anchor components were synthesized using standard Fmoc chemistry with protected L amino acids. The finished peptides were side-chain deprotected and cleaved from resin in 95:5:5 TFA:dH₂O:TES, then precipitated in diethyl ether. The ligands were cyclized by stirring the cleaved peptides dissolved in ~5 mL ACN overnight with 1 mL of the Cu(phen)₃ stock solution. The cyclization mixtures were lyophilized, and the final peptide products were purified using RP-HPLC on a Kinetex 5 μ XB-C18 250 x 4.6 mm prep column. MALDI-TOF MS: **(i)**: Expected mass [M+H]⁺ = 2733.30, Observed mass [M+H]⁺ = 2733.64. **(ii)**: Expected mass [M+H]⁺ = 2843.40, Observed mass [M+H]⁺ = 2843.60.

Peptide (iii)

A22 was synthesized, cyclized, and purified as described above. The secondary ligand component including N-terminal Az₄ for **(iii)** was synthesized C → N on Rink amide resin with a Titan peptide synthesizer using standard Fmoc chemistry. The synthesis used Fmoc and side chain protected D amino acids and L-Az₄. Resulting

secondary peptide was side-chain deprotected and cleaved from resin in 95:5:5 TFA:dH₂O:TES, precipitated in diethyl ether, and purified using RP-HPLC on a Kinetex 5 μ XB-C18 250 x 4.6 mm prep column. The purified secondary peptide was clicked to A22 in solution by mixing with 2x molar excess of A22, 10x Cu(I) iodide, 50x L-ascorbic acid, and 4x Tris[(1-benzyl-1*H*-1,2,3-triazol-4-yl)methyl]amine (TBTA) (Sigma-Aldrich, St. Louis, MO) in 5:1 NMP:dH₂O and stirring overnight at room temperature. The clicked biligand product was purified from the reaction mixture by RP-HPLC on a Kinetex 5 μ XB-C18 250 x 4.6 mm prep column. Expected mass [M+H]⁺ = 2720.31, observed mass [M+H]⁺ = 2720.5.

Scaling up (iii)

The secondary ligands including N-terminally Boc-protected Az₄ for (iii) was synthesized C \rightarrow N on Rink amide resin with a Titan peptide synthesizer using standard Fmoc chemistry. The synthesis used Fmoc and side chain protected D amino acids and L-Az₄ (AnaSpec, Fremont, CA). Truncated A22 (Pra-ICTTA) was synthesized C \rightarrow N on Sieber amide resin (ChemPep, Wellington, FL) with a Liberty 1 microwave peptide synthesizer (CEM, Matthews, NC) using standard Fmoc chemistry. The synthesis used Fmoc and side chain protected L amino acids and Fmoc-L-Pra. Fully protected truncated A22 was cleaved from the resin with 1% v/v TFA in DCM, and neutralized with DIEA. Solvent was removed using a rotary vacuum evaporator and the protected peptide was purified by RP-HPLC on a Kinetex 5 μ XB-C18 250 x 4.6 mm prep column. Resulting truncated A22 was clicked on-bead to the secondary peptide through the azide side

chain of Boc-Az₄ by adding equal molar amount of the protected truncated A22, 2x molar excess of Cu(I) iodide, and 2x excess of L-ascorbic acid to the azide on bead. The click mixture was agitated in 20% v/v piperidine in NMP overnight at room temperature, and then the copper was chelated by repeated washing with 10% w/v sodium diethyldithiocarbamate trihydrate and 10% v/v DIEA in NMP until the beads were clear. The Fmoc deprotected Pra was then the starting point for the remainder of the anchor component, including N-terminal PEG₅ and biotin (Biotin-PEG₅-IWGCSGK). The anchor components were synthesized using standard Fmoc chemistry with protected L amino acids. The finished peptide was N-terminal and side-chain deprotected and cleaved from resin in 95:5:5 TFA:dH₂O:TES, then precipitated in diethyl ether. The ligand was cyclized by stirring the cleaved peptide dissolved in ~5 mL ACN overnight with 1 mL of the Cu(phen)₃ stock solution. The cyclization mixtures were lyophilized, and the final peptide products were purified using RP-HPLC on a Kinetex 5μ XB-C18 250 x 4.6 mm prep column.

2.6.4 Assays

Anchor binding ELISA

Biotinylated anchor peptide was immobilized on streptavidin-coated 96-well plates (Thermo Scientific Pierce, Rockford, IL) at a concentration of 100 nM in TBS. The plates were blocked with 5% w/v dry milk in TBS, and then the anchor peptides were incubated with either 100 nM 3D6 or 4B3 in 0.5% w/v dry milk in TBS at room temperature for 1 hr. Bound antibody was probed with horseradish peroxidase (HRP)-

conjugated mouse monoclonal antibody to human IgG Fc (Abcam, Cambridge, MA), diluted 1:10,000 in 0.5% w/v dry milk in TBS for 1 hr at room temperature. The colorimetric assay was developed with TMB substrate (KPL, Gaithersburg, MD), then quenched with 1 M H₂SO₄ and read at 450 nm.

Surface Plasmon Resonance

SPR experiments were performed on a Biacore T200 instrument. Biotinylated peptides were immobilized on streptavidin-coated sensor chips (GE Healthcare Biosciences, Pittsburg, PA) at R.U. values ranging from 7-12. 4B3 or 3D6 was flowed at various concentrations in 1x HBS-EP buffer (GE Healthcare Biosciences, Pittsburgh, PA), and affinity curves were fit using the default settings of the Biacore evaluation software.

Cocktail binding ELISA

Recombinant multi-epitope chimeric HIV antigen ("chimera") (BioLink International, Lisle, IL) was chemically biotinylated using ChromaLink Biotin Labeling Kit (Solulink, San Diego, CA) according to the manufacturer's instructions, using 10x molar excess of the ChromaLink biotinylation reagent to the buffer-exchanged protein. Streptavidin-coated 96-well plates were saturated with the biotinylated biligand cocktail or chimera using 1 μ M solutions in TBS. The plates were blocked with 5% w/v dry milk in TBS, and then the capture reagents were incubated with either 1% v/v human serum or a mixture of 4 nM each 3D6 and 4B3 spiked in 1% v/v human serum in TBS at room temperature for 1 hr. Bound antibody was probed with HRP-conjugated mouse

monoclonal antibody to human IgG Fc, diluted 1:15,000 in 0.5% w/v dry milk in TBS for 1 hr at room temperature. The colorimetric assay was developed with TMB substrate, then quenched with 1 M H₂SO₄ and read at 450 nm (A450). The A450 for each sample is normalized against the A450 for the serum control, to yield a measurement of the signal-to-noise ratio of the assay.

2.7 CONCLUSION

Described in this chapter is a method for developing a PCC Agent cocktail to capture the diversity of human antibodies generated in response to an infectious agent, with specific application to HIV. The components of the cocktail were raised against 4B3 and 3D6, two representative anti-HIV antibodies, and individual and collective binding of the capture agents to the target antibodies was characterized. The cocktail displayed a moderately enhanced performance compared to the original gp 41 epitope (A21) and the gold standard chimeric antigen when used to detect 4B3 and 3D6 from human serum.

2.8 ACKNOWLEDGEMENTS

This work was done in collaboration with Aiko Umeda, Blake Farrow, Connie L. Hseuh, and Kaycie M. Deyle. It was funded primarily by a grant from the Bill and Melinda Gates Foundation. Additional funding for the development of screening approaches, and for certain capture agent characterization methods, was provided by

the Institute for Collaborative Biotechnologies through grant W911NF-09-0001 from the U.S. Army Research Office. The content of the information does not necessarily reflect the position or the policy of the Government, and no official endorsement should be inferred.

2.9 REFERENCES

1. (1996) In: Baron S, editor. Medical Microbiology. 4th ed. Galveston (TX).
2. Fanales-Belasio E, Raimondo M, Suligo B, Butto S (2010) HIV virology and pathogenetic mechanisms of infection: a brief overview. *Ann Ist Super Sanita* 46: 5-14.
3. Alvarez M, Chueca N, Guillot V, Bernal Mdel C, Garcia F (2012) Improving Clinical Laboratory Efficiency: Introduction of Systems for the Diagnosis and Monitoring of HIV Infection. *Open Virol J* 6: 135-143.
4. Tebourski F, Slim A, Elgaaied A (2004) The significance of combining World Health Organization and Center for Disease Control criteria to resolve indeterminate human immunodeficiency virus type-1 Western blot results. *Diagn Microbiol Infect Dis* 48: 59-61.
5. Daskalakis D (2011) HIV diagnostic testing: evolving technology and testing strategies. *Top Antivir Med* 19: 18-22.
6. Butto S, Suligo B, Fanales-Belasio E, Raimondo M (2010) Laboratory diagnostics for HIV infection. *Ann Ist Super Sanita* 46: 24-33.
7. Ginocchio CC, Carman WF, Arens MQ (2011) Update on HIV diagnostic testing algorithms. Editors' introduction. *J Clin Virol* 52 Suppl 1: S1.
8. Agnew HD, Rohde RD, Millward SW, Nag A, Yeo WS, et al. (2009) Iterative in situ click chemistry creates antibody-like protein-capture agents. *Angew Chem Int Ed Engl* 48: 4944-4948.
9. Millward SW, Henning RK, Kwong GA, Pitram S, Agnew HD, et al. (2011) Iterative in Situ Click Chemistry Assembles a Branched Capture Agent and Allosteric Inhibitor for Akt1. *Journal of the American Chemical Society* 133: 18280-18288.

10. Huisgen R (1984) 1,3-Dipolar cycloaddition – introduction, survey, mechanism. In: Padwa A, editor. 1,3-Dipolar Cycloaddition Chemistry Wiley. pp. 1-176.
11. Thirumurugan P, Matosiuk D, Jozwiak K (2013) Click Chemistry for Drug Development and Diverse Chemical-Biology Applications. Chem Rev.
12. Finn MG, Fokin VV (2010) Click chemistry: function follows form. Chem Soc Rev 39: 1231-1232.
13. Lam KS, Lebl M, Krchnak V (1997) The "One-Bead-One-Compound" Combinatorial Library Method. Chem Rev 97: 411-448.
14. Du AP, Limal D, Semetey V, Dali H, Jolivet M, et al. (2002) Structural and immunological characterisation of heteroclitic peptide analogues corresponding to the 600-612 region of the HIV envelope gp41 glycoprotein. J Mol Biol 323: 503-521.
15. Xu JY, Gorny MK, Palker T, Karwowska S, Zolla-Pazner S (1991) Epitope mapping of two immunodominant domains of gp41, the transmembrane protein of human immunodeficiency virus type 1, using ten human monoclonal antibodies. J Virol 65: 4832-4838.
16. Millward SW, Henning RK, Kwong GA, Pitram S, Agnew HD, et al. (2011) Iterative in situ click chemistry assembles a branched capture agent and allosteric inhibitor for Akt1. J Am Chem Soc 133: 18280-18288.
17. Fields GB, Noble RL (1990) Solid phase peptide synthesis utilizing 9-fluorenylmethoxycarbonyl amino acids. International journal of peptide and protein research 35: 161-214.

Chapter 3

PCC Agent Based Assay for the Detection of Anti-HIV Antibodies from Human Sera

3.1 INTRODUCTION

HIV diagnostic assays typically use chimeric proteins comprised of immunogenic and conserved antigens from the HIV to capture specific anti-HIV antibodies from the body fluid of potentially infected patients. However, the biologically produced chimeric recombinant proteins are susceptible to thermal, chemical, and biological degradation, as well as batch to batch variability. These limitations can adversely influence the performance of a diagnostic test [1,2,3], especially when used outside of controlled laboratory settings.

This chapter explores the ability of the PCC Agent cocktail described in Chapter 2 to detect anti-HIV antibodies from human sera as compared to that of a standard recombinant chimeric antigen like those typically used in anti-HIV antibody detection assays. The chimeric protein used contained a fragment of HIV-1 gp41 (residues 546-692), the “O” group HIV-1 gp41 immunodominant region (residues 580-623), and a fragment of HIV-2 gp36 (residues 591-617). A good performance of this chimeric antigen has been reported elsewhere [4]. Two sets of samples were assayed, one clinical and one commercial. In both cases the PCC Agent cocktail showed increased average signal to noise compared to the chimeric antigen.

3.2 PATIENT SAMPLE ASSAY

The PCC Agent cocktail and the standard antigen were co-evaluated against a panel of clinical samples using sandwich ELISAs. Serum samples were collected from nine HIV-1-positive patients in Southern California. For the comparison assays,

streptavidin-coated 96-well plates were saturated with the PCC Agent cocktail or chemically biotinylated chimera in triplicates. Serum samples were diluted to 1% v/v in Tris-buffered saline (TBS) supplemented with 0.1% w/v bovine serum albumin (BSA), and incubated in the wells for 1 hr at room temperature. Unbound proteins were washed off and captured IgG was detected with a peroxidase-conjugated mouse monoclonal anti-human IgG-Fc antibody. The comparison assay results for the patient serum samples along with a healthy control are shown in Figure 3.1. The signal-to-noise (S/N) ratio in these assays is defined as the measured ELISA signal for a given patient sample, divided by that for the healthy control. The PCC Agent cocktail performed at least as well, and typically much better, than the standard chimeric protein antigen. The average S/N improvement by the cocktail PCC agent over the chimeric antigen was a factor of 2.5.

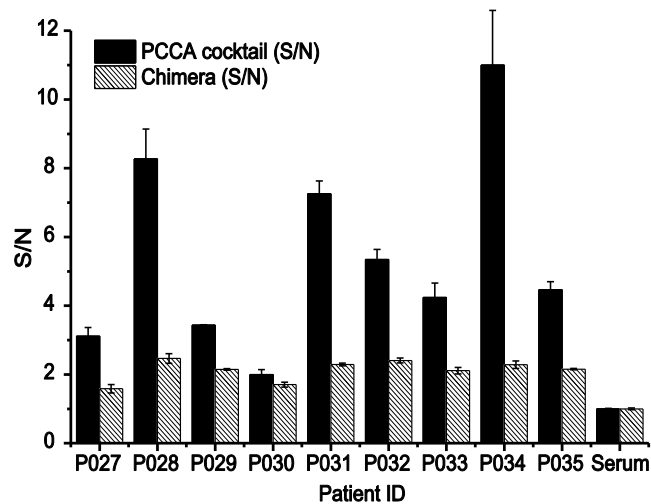


Figure 3.1. Comparative performance of the PCC Agent cocktail versus the commercial chimeric protein, using sandwich ELISAs to detect anti-HIV-1 IgGs from a panel of sera samples collected from nine HIV-positive patients. The absorbance at 450 nm (A_{450}) for each sample is normalized against the A_{450} for the healthy control, to yield a measurement of the signal-to-noise ratio of the assay. The PCC Agent cocktail, which is designed to capture a subset of anti-gp41 IgGs, exhibits superior performance for every sample, even though the chimeric protein is designed to capture antibodies against multiple HIV-1-associated epitopes (those containing fragments of HIV-1 gp41, “O” group HIV-1 gp41 immunodominant region, and HIV-2 gp39). For the assays, the PCC agent cocktail and the biotinylated chimeric antigen were immobilized on a streptavidin-coated 96-well plate and incubated with diluted patient serum (1% v/v). Captured anti-HIV antibodies were detected using peroxidase-conjugated anti-human IgG antibody.

3.3 PATH SAMPLE ASSAY

The PCC Agent cocktail and the standard antigen were also co-evaluated against a panel of commercial samples. Serum samples from individual patients containing high, medium, or low titers of anti-HIV antibodies were obtained from SeraCare, through PATH of POC diagnostics program funded by the Bill and Melinda Gates Foundation. For the comparison assays, streptavidin-coated 96-well plates were saturated with the PCC Agent cocktail or chemically biotinylated chimera in triplicates. Serum samples were diluted to 1% v/v in Tris-buffered saline (TBS) supplemented with 0.1% w/v bovine serum albumin (BSA), and incubated in the wells for 1 hr at room temperature. Unbound proteins were washed off and captured IgG was detected with a peroxidase-conjugated mouse monoclonal anti-human IgG-Fc antibody. The comparison assay results for the serum samples are shown in Figure 3.2. The signal-to-noise (S/N) ratio in these assays is defined as the measured ELISA signal for a given high, medium, or low titer sample, divided by that for the respective healthy control. The PCC Agent cocktail generally outperformed the standard chimeric protein antigen, with the exception of the low titer samples. The reasons for this are not entirely clear. However, the average S/N improvement by the cocktail PCC agent over the chimeric antigen was a factor of 2.8.

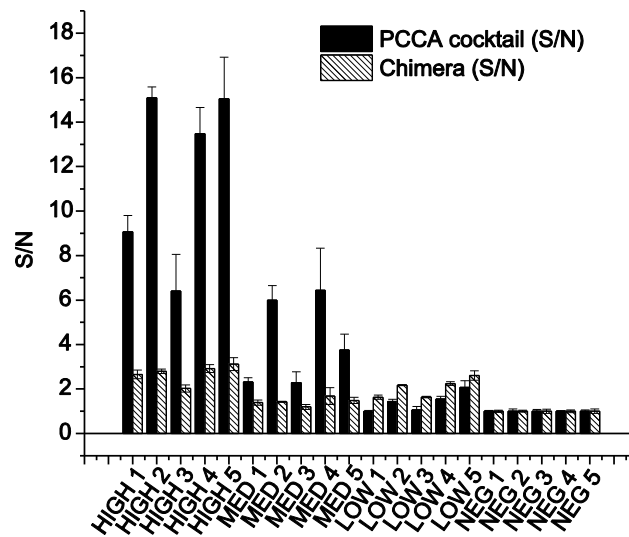


Figure 3.2. Comparative performance of the PCC Agent cocktail versus the commercial chimeric protein, using sandwich ELISAs to detect anti-HIV-1 IgGs from a panel of HIV-1 specific IgG containing plasma samples provided by PATH. The samples were rated HIGH, MED, or LOW in accordance with the titer of anti-HIV antibodies, and pooled HIV negative sera samples were used as a control (NEG). The absorbance at 450 nm (A450) for each sample is normalized against the A450 for the healthy control, to yield a measurement of the signal-to-noise ratio of the assay. The PCC Agent cocktail, which is designed to capture a subset of anti-gp41 IgGs, exhibits superior performance for every sample, even though the chimeric protein is designed to capture antibodies against multiple HIV-1-associated epitopes (those containing fragments of HIV-1 gp41, “O” group HIV-1 gp41 immunodominant region, and HIV-2 gp39). For the assays, the PCC agent cocktail and the biotinylated chimeric antigen were immobilized on a streptavidin-coated 96-well plate and incubated with diluted patient serum (1% v/v). Captured anti-HIV antibodies were detected using peroxidase-conjugated anti-human IgG antibody.

3.4 STABILITY ASSAY

We then tested the PCC Agents for thermal stability. The PCC Agent cocktail component **(iii)** were synthesized at a large scale for an academic setting (~7 mg, Figure 3.3) and the lyophilized samples were stored under N₂ at 25°C, 37°C, or 57°C for 58 days. The samples were then analyzed by HPLC to determine the presence of any degradation product. The traces of the peptide at each temperature are nearly identical, indicating little to no degeneration at these temperatures (Figure 3.3). The performance of these stored PCC Agents was then also tested in an ELISA, with no detectable loss of performance (Figure 3.3).

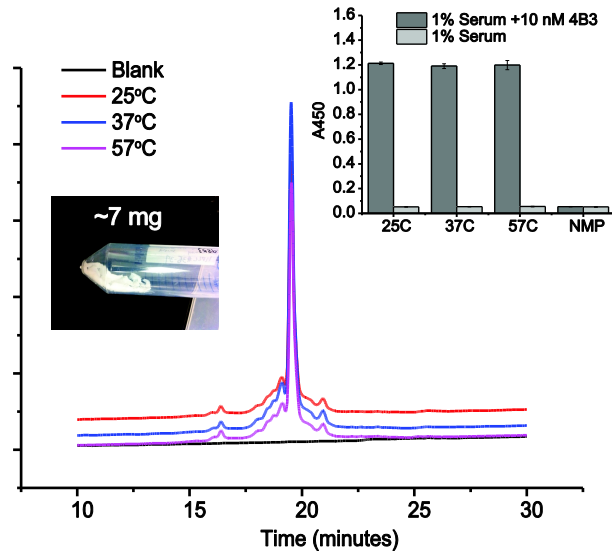


Figure 3.3. Samples of (iii) were stored as a powder (inset photo), under N_2 at temperatures up to $57^\circ C$ for ~ 2 months, and resolved by analytical HPLC to determine the presence of any degradation product. The HPLC traces reveal that the fingerprint of the PCC Agent is unchanged. The inset shows that the assay performance of the PCC Agent is also unaffected.

3.5 MATERIALS AND METHODS

3.5.1 Patient serum ELISA

Peripheral blood was obtained from HIV-1 infected patients at the University of California, Los Angeles (UCLA) Medical Center between July and August of 2012. Sera were stored at -80°C before subsequent analysis. Streptavidin-coated 96-well plates were saturated with the biotinylated biligand cocktail or chimera using 1 μM solutions in TBS. The plates were blocked with 5% w/v dry milk in TBS, and then the capture reagents were incubated with patient serum samples diluted to 1% v/v in TBS containing 0.1% w/v bovine serum albumin (BSA). Additionally, both cocktail and chimera capture reagents were incubated with 1% v/v commercial healthy human serum in TBS. Bound antibody was probed with HRP-conjugated mouse monoclonal antibody to human IgG Fc, diluted 1:10,000 in TBS with 0.1% w/v BSA. The colorimetric assay was developed with TMB substrate, then quenched with 1 M H_2SO_4 and read at 450 nm (A450). The A450 for each sample is normalized against the A450 for the healthy control, to yield a measurement of the signal-to-noise ratio of the assay.

3.5.2 PATH samples ELISA

Serum samples were obtained from SeraCare, through PATH of POC diagnostics program funded by the Bill and Melinda Gates foundation. Five groups of four samples were tested, where each group contained high, medium, and low titer samples, along with a negative sample that did not contain anti-HIV antibodies. Sera were stored at -80°C before subsequent analysis. Streptavidin-coated 96-well plates were saturated

with the biotinylated biligand cocktail or chimera using 1 μM solutions in TBS. The plates were blocked with 5% w/v dry milk in TBS, and then the capture reagents were incubated with patient serum samples diluted to 1% v/v in TBS containing 0.1% w/v bovine serum albumin (BSA). Additionally, both cocktail and chimera capture reagents were incubated with 1% v/v commercial healthy human serum in TBS. Bound antibody was probed with HRP-conjugated mouse monoclonal antibody to human IgG Fc, diluted 1:10,000 in TBS with 0.1% w/v BSA. The colorimetric assay was developed with TMB substrate, then quenched with 1 M H_2SO_4 and read at 450 nm (A450). The A450 for the samples in each group are normalized against the A450 for the negative sample in that group.

3.5.3 Stability assay

Small amounts of **(iii)** were stored under N_2 at 25°C, 37°C, or 57°C for 58 days. Samples were diluted in 1:1 ACN/ H_2O with 0.1% v/v TFA to an equal concentration determined by measuring the absorbance values at 280 nm using NanoDrop spectrophotometer (Thermo Scientific, Waltham, MA) and resolved by analytical RP-HPLC. The remaining samples were lyophilized and used in a single point sandwich ELISA. Streptavidin-coated 96-well plates were saturated with the samples of **(iii)** recovered from the storage experiments using 1 μM solutions in TBS. The plates were blocked with 5% w/v dry milk in TBS, then incubated with either 1% v/v human serum or 10 nM 4B3 spiked in 1% v/v human serum in 0.5% w/v dry milk in TBS at room temperature for 1 hr. Bound antibody was probed with HRP-conjugated mouse

monoclonal antibody to human IgG Fc diluted 1:15,000 in 0.5% w/v dry milk in TBS. The colorimetric assay was developed with TMB substrate, then quenched with 1 M H₂SO₄ and read at 450 nm.

3.6 CONCLUSION

This thesis demonstrated the successful application of this method for HIV-1 diagnostics by producing a cocktail of three PCC Agents that detected the presence of anti-HIV antibodies in clinical samples with a significantly enhanced signal-to-noise relative to the standard, recombinant protein-based chimeric antigen. In a recent report, an antigenic peptide cocktail comprised of synthetic peptides derived directly from gp120/V3-I (HIV-1 Indian isolate), gp41 (HIV-1), and gp36 (HIV-2), as well as the recombinant protein rp24 (HIV-1) was shown to also provide superior performance relative to the chimeric antigen [5]. This points to the possibility that expanding the current approach by developing multiple cocktails of PCC Agents, each directed against a distinct HIV epitope, would likely provide superior performance to that reported here. The strategy presented provides a promising approach for developing assays for detecting the immune response to other infectious agents, especially where challenges associated with the polyclonal nature of a humoral immune response can compromise assay sensitivity.

3.7 ACKNOWLEDGEMENTS

This work was done in collaboration with Aiko Umeda, Jocelyn T. Kim, and Bert T. Lai. It was funded primarily by a grant from the Bill and Melinda Gates Foundation. Additional funding for the development of screening approaches, and for certain capture agent characterization methods, was provided by the Institute for Collaborative Biotechnologies through grant W911NF-09-0001 from the U.S. Army Research Office. The content of the information does not necessarily reflect the position or the policy of the Government, and no official endorsement should be inferred.

3.8 REFERENCES

1. Daskalakis D (2011) HIV diagnostic testing: evolving technology and testing strategies. *Top Antivir Med* 19: 18-22.
2. Ginocchio CC, Carman WF, Arens MQ (2011) Update on HIV diagnostic testing algorithms. Editors' introduction. *J Clin Virol* 52 Suppl 1: S1.
3. Alvarez M, Chueca N, Guillot V, Bernal Mdel C, Garcia F (2012) Improving Clinical Laboratory Efficiency: Introduction of Systems for the Diagnosis and Monitoring of HIV Infection. *Open Virol J* 6: 135-143.
4. Chin CD, Laksanasopin T, Cheung YK, Steinmiller D, Linder V, et al. (2011) Microfluidics-based diagnostics of infectious diseases in the developing world. *Nat Med* 17: 1015-1019.
5. Tiwari RP, Jain A, Khan Z, Kumar P, Bhriugu V, et al. (2012) Designing of novel antigenic peptides cocktail for the detection of antibodies to HIV-1/2 by ELISA. *Journal of immunological methods*.

Chapter 4

A Selective ^{15}N -to- ^1H Polarization Transfer Sequence for More Sensitive Detection
of ^{15}N -Choline

4.1 ABSTRACT

This chapter discusses selective polarization transfer from ^{15}N to methyl ^1H spins in ^{15}N -choline. The sensitivity and information content of heteronuclear nuclear magnetic resonance is frequently optimized by transferring spin order of spectroscopic interest to the isotope of highest detection sensitivity prior to observation. This strategy was extended to ^{15}N -choline using the scalar couplings to transfer polarization from ^{15}N to choline's nine methyl ^1H spins in high field. A theoretical analysis of a sequence using nonselective pulses showed that the optimal efficiency of this transfer is decreased by 62% as the result of competing ^{15}N - ^1H couplings involving choline's four methylene protons. A frequency-selective pulse was therefore incorporated to support evolution of only the ^{15}N -methyl ^1H coupling during the transfer period. This sequence provided a 52% sensitivity enhancement over the nonselective version in *in vitro* experiments on a sample of thermally polarized ^{15}N -choline in D_2O . Further, the ^{15}N T_1 of choline in D_2O was measured to be 217 ± 38 s, the ^{15}N -methyl ^1H coupling constant was found to be 0.817 ± 0.001 Hz, and the larger of choline's two ^{15}N -methylene ^1H coupling constants was found to be 3.64 ± 0.01 Hz. Possible improvements and applications to *in vivo* experiments using long-lived hyperpolarized heteronuclear spin order are discussed.

4.2 INTRODUCTION

It is now possible to routinely generate samples of certain small biomolecules with nuclear polarizations on the order of ten percent using PASADENA (parahydrogen and synthesis allow dramatically enhanced nuclear alignment) [1] or DNP (dynamic nuclear polarization) [2; 3]. These technologies show promise for clinical applications based on the *in vivo* characterization of metabolic processes on the seconds timescale. Experiments of this nature, rely on storage of the polarization on heteronuclei with long population relaxation times, such as carbonyl ^{13}C or quaternary ^{15}N nuclei, in order to minimize relaxation losses during sample delivery and to provide time for transport, binding, and metabolism. However, the sensitivity enhancement afforded by this strategy is partly lost if the final signal is also detected on a low- γ heteronucleus. Chekmenev *et al.* [4] have proposed that optimal sensitivity can be obtained by storing polarization on a slowly-relaxing heteronuclear spin and then using an INEPT[5] sequence to coherently transfer magnetization to nearby ^1H nuclei for detection, and have demonstrated the method with two hyperpolarized reagents, $1\text{-}^{13}\text{C}$ -succinate- d_2 and 2,2,3,3-tetrafluoropropyl $1\text{-}^{13}\text{C}$ -propionate- d_3 (TFPP). Those experiments were designed assuming that the relevant ^1H and ^{13}C sites were 3-spin ABX systems.

Here we demonstrate an extension of this polarization transfer strategy to hyperpolarized ^{15}N -choline, an $\text{A}_9\text{BB}'\text{CC}'\text{X}$ system of 14 spin $\frac{1}{2}$ nuclei. Choline is a useful biomarker, showing significantly altered uptake and metabolism in diseased brain tissue [6] and in malignant tumor cells in the breast and prostate [7; 8]. Hyperpolarization of

^{15}N -choline to $(4.6 \pm 1)\%$ has been reported after two hours of DNP at 1.4 K [3]. The ^{15}N longitudinal relaxation time of $T_1 = 120$ s in blood [3] is promising for metabolic studies.

We have investigated two INEPT-based pulse sequences for ^{15}N -to- ^1H polarization transfer in ^{15}N -choline. The first is a nonselective refocused INEPT sequence similar to that used by Chekmenev *et al.* to transfer polarization from ^{13}C to multiple ^1H sites in succinate and TFPP [4]. While this sequence is effective, a product operator analysis shows that significantly greater sensitivity can be obtained by using a selective sequence targeting choline's nine degenerate methyl ^1H spins. We therefore also present a selective refocused INEPT transfer that uses a REBURP pulse to support coherence transfer from ^{15}N to choline's methyl ^1H spins while suppressing competing transfer pathways to methylene ^1H nuclei. These pulse sequences are experimentally demonstrated *in vitro* using a thermally polarized sample of ^{15}N -choline in aqueous solution.

4.3 THEORY

At a given spin polarization and probe efficiency, the sensitivity of detection in an NMR experiment scales as the square of the gyromagnetic ratio of the nuclide being observed. In the case of ^{15}N hyperpolarization, therefore, a sensitivity enhancement of $(\gamma_{^1\text{H}} / \gamma_{^{15}\text{N}})^2 = 97$ can be obtained by transferring to ^1H for detection rather than directly observing a ^{15}N signal, assuming unity transfer of spin angular momentum, as is closely

approached within an isolated ^{15}N - ^1H spin pair with a resolved scalar coupling. Such a transfer can be achieved using refocused INEPT (Figure 4.1), the standard pulse sequence for polarization transfer between spins with a direct scalar coupling. The effect of this sequence when applied to ^{15}N -choline can be determined using a product operator analysis. In the following discussion the relevant ^{15}N - ^1H scalar coupling constants will be labeled J_m , J_a , and J_b as indicated in Figure 4.2. Couplings between the methyl and methylene ^1H spins will be unimportant and are neglected.

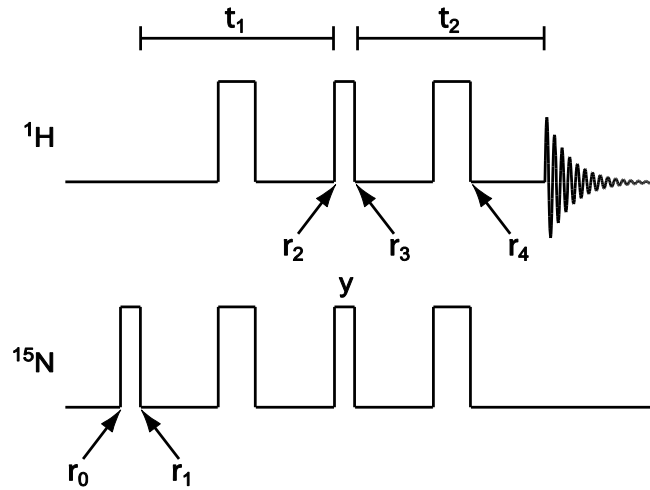


Figure 4.1. A refocused INEPT pulse sequence for polarization transfer from ^{15}N to ^1H for detection. Narrow (wide) rectangles denote radiofrequency pulses with a tip angle of $\pi/2$ (π). All pulses are applied along the x axis except where indicated.

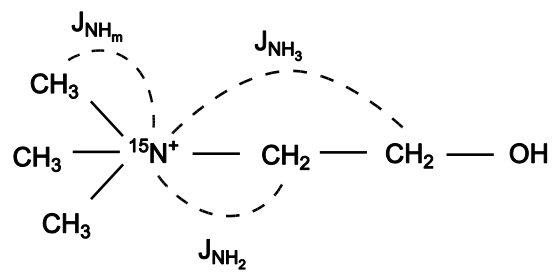


Figure 4.2. The structure of ^{15}N -choline. Labels indicate the relevant ^{15}N - ^1H scalar couplings.

First, consider the effect of the sequence on the spin system of Figure 4.2, while initially neglecting the effects of the ^{15}N -methylene ^1H couplings J_a and J_b . The system's magnetization is proportional to the dimensionless ^{15}N spin angular momentum, with initial value normalized to $\rho_0 = S_z$. This is converted to in-phase ^{15}N single-quantum coherence by the first ^{15}N $(\pi/2)_x$ pulse to obtain $\rho_1 = -S_y$. This coherence evolves under the ^{15}N -methyl ^1H scalar couplings during the INEPT transfer period τ_1 to produce terms that are antiphase with respect to the methyl ^1H spins. The simultaneous π pulses in the middle of τ_1 refocus chemical shift evolution, leaving only the effects of couplings between ^{15}N and each of the nine methyl ^1H spins. At the end of τ_1 the system's state is given by:

$$\begin{aligned} \rho_2 = & -S_y \cos^9(\pi J_m \tau_1) + \sum_{i=1}^9 2S_x I_{iz} \cos^8(\pi J_m \tau_1) \sin(\pi J_m \tau_1) \\ & + \sum_{i=1}^8 \sum_{j=i+1}^9 4S_y I_{iz} I_{jz} \cos^7(\pi J_m \tau_1) \sin^2(\pi J_m \tau_1) + HO. \end{aligned}$$

Here, *HO* indicates higher-order terms, specifically single-quantum ^{15}N coherence that is antiphase with respect to three or more ^1H spins. After the transfer delay, simultaneous ^1H $(\pi/2)_x$ and ^{15}N $(\pi/2)_y$ pulses are applied:

$$\begin{aligned} \rho_3 = & -S_y \cos^9(\pi {}^2J_{N-CH_3} \tau_1) + \sum_{i=1}^9 2S_z I_{iy} \cos^8(\pi {}^2J_{N-CH_3} \tau_1) \sin(\pi {}^2J_{N-CH_3} \tau_1) \\ & + \sum_{i=1}^8 \sum_{j=i+1}^9 4S_y I_{iy} I_{jy} \cos^7(\pi {}^2J_{N-CH_3} \tau_1) \sin^2(\pi {}^2J_{N-CH_3} \tau_1) + HQ. \end{aligned}$$

The pulses convert the terms HO to high-order multiple-quantum coherences, which have been abbreviated as HQ . At this point, ^{15}N coherences and multiple-quantum ^1H coherences, which will not lead to observable signals at the end of the experiment, can be dropped from the density operator. This leaves only single-quantum ^1H coherences that are antiphase with respect to ^{15}N :

$$\rho_3 = \sum_{i=1}^9 2S_z I_{iy} \cos^8(\pi J_m \tau_1) \sin(\pi J_m \tau_1).$$

The next part of the sequence is a refocusing period of duration $\tau_2 = 1/(2J_m)$ during which the antiphase single-quantum ^1H terms evolve into in-phase ^1H coherence:

$$\rho_4 = -\sum_{i=1}^9 I_{ix} \cos^8(\pi J_m \tau_1) \sin(\pi J_m \tau_1).$$

The detected ^1H signal is proportional to the total magnetization of the nine methyl protons, so the dependence of the initial signal amplitude on τ_1 is:

$$S_{sel} = A_{sel} 9 \cos^8(\pi J_m \tau_1) \sin(\pi J_m \tau_1) + C. \quad (1)$$

This expression includes a hardware-dependent proportionality constant A_{sel} and a constant C accounting for any DC offset in the observed signal. Equation 1 is similar to the expression derived by Doddrell *et al.* for a coherence transfer in the opposite direction, from n equivalent ^1H spins to a heteronucleus [9]. The value of τ_1 that maximizes S_{sel} is given by:

$$\tau_1 = \frac{1}{\pi J_m} \tan^{-1} \left(\frac{1}{2\sqrt{2}} \right).$$

For the value $J_m = 0.82$ Hz measured experimentally for ^{15}N -choline, the optimal transfer delay is $\tau_1 = 0.132$ s, yielding $S_{sel} = 1.873 A_{sel} + C$. The transfer function of the angular momentum from ^{15}N to ^1H or vice versa (Eq. 1) can exceed unity. The conserved quantity is the sum of the squares of the coefficients of the normalized product operators expressing the density operator. Contributions to the observable signal from choline's nine methyl ^1H spins combine linearly and constructively at the optimized value of τ_1 .

The above calculation is readily generalized to include the effects of scalar coupling between the ^{15}N spin and the four methylene protons (J_a and J_b in Fig. 2), yielding an analogous relative signal function:

$$S_{non} = A_{non} 9 \cos^8(\pi J_m \tau_1) \sin(\pi J_m \tau_1) \cos^2(\pi J_a \tau_1) \cos^2(\pi J_b \tau_1) + C \quad (2)$$

A proportionality constant A_{non} and a DC offset constant C have again been included. Maximizing this function numerically for the best known values of the three coupling constants for choline, $J_m = 0.82$ Hz, $J_a = -0.57$ Hz, $J_b = 3.64$ Hz, gives an optimal transfer delay $\tau_1 = 0.233$ s, which yields a signal of $S_{non} = 0.721 A_{non} + C$.

Comparing the maximum values of S_{sel} and S_{non} , it is apparent that the ^{15}N -methylene ^1H couplings have the effect of reducing the observable ^1H signal by 62% in

the idealized case of an experiment for which $A_{sel} = A_{non}$ and $C = 0$. It would clearly be advantageous to suppress these couplings. This can be achieved by replacing the ^1H pulse in the middle of τ_1 with a selective pulse tailored to invert the methyl ^1H spins without affecting the methylene ^1H spins.

4.4 EXPERIMENTAL

Data was collected on a Varian ^{UNITY}INOVA spectrometer operating at a ^1H resonance frequency of 500 MHz. The sample was prepared by dissolving 20 mg ^{15}N -choline chloride (ISOTEC, Miamisburg, Ohio) in 700 μl D_2O . Refocused INEPT experiments were performed using the pulse sequence shown in Figure 4.3, which implements the selective ^{15}N -methyl ^1H transfer described in the theory section using a 6.695 ms ^1H REBURP pulse [10] centered at the methyl ^1H frequency. A time $\tau_{reb} = 6.4$ ms, equal to the effective evolution time of the ^{15}N -methyl ^1H coupling during the REBURP pulse, was subtracted from the transfer delay as indicated in Fig. 3. For nonselective INEPT experiments, the REBURP was replaced with a nonselective π pulse and τ_{reb} was set to zero.

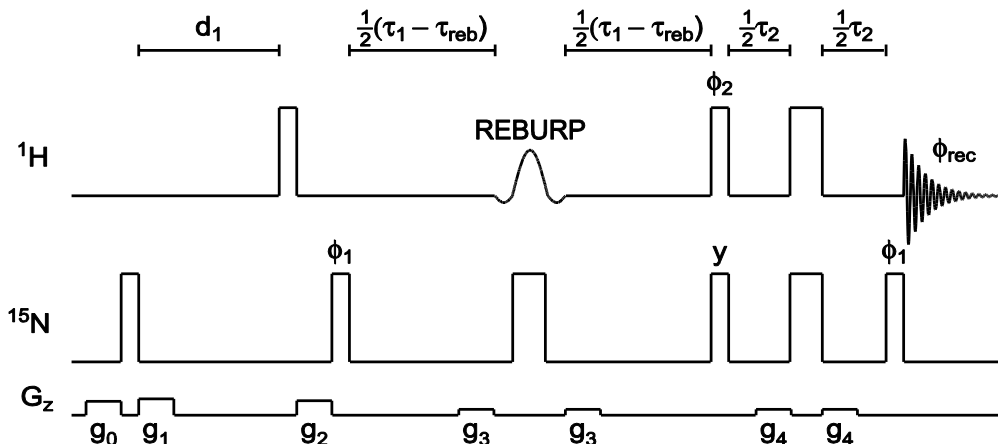


Figure 4.3. Selective refocused INEPT pulse sequence for coherent polarization transfer from ^{15}N to methyl ^1H in ^{15}N -choline. Narrow (wide) rectangles denote radiofrequency pulses with a tip angle of $\pi/2$ (π), applied with B_1 field strengths of 23.9 kHz for ^1H and 15.6 kHz for ^{15}N . The shaped ^1H pulse is a 6.695 ms REBURP [10] centered on the methyl ^1H frequency. A four step phase cycle ($\phi_1 = x, x, x, x$; $\phi_2 = x, y, x, y$; $\phi_{\text{rec}} = x, y, x, y$) was used to suppress signals originating from ^1H magnetization and to prevent carry over of signal from one transient to the next. A recycle delay d_1 of 60 s ($\sim 0.25 T_1$) was used. Since it is impractical to make this delay long enough to allow full relaxation of the choline ^{15}N spin, a purge element consisting of a ^{15}N $\pi/2$ pulse sandwiched by gradients g_0 and g_1 is used to eliminate ^{15}N magnetization at the start of d_1 , ensuring a consistent starting magnetization for all experiments. A ^1H purge element comprising a ^1H $\pi/2$ pulse and gradient g_2 is used at the start of each transient. Gradients g_3 and g_4 are used to suppress coherence transfer pathways created by imperfect π pulses.

To allow efficient testing in the absence of hyperpolarization, the sequence includes a ^{15}N purge element before the recycle delay d_1 to ensure that the system reaches a consistent state at the start of each transient. This measure is necessary because it is impractical to allow full relaxation of the choline ^{15}N spin after each transient owing to its very long T_1 . The sequence includes a ^{15}N $\pi/2$ pulse immediately prior to acquisition in order to purge any ^1H coherence that remains antiphase with respect to ^{15}N after the refocusing period. In the absence of this pulse, intermittent phase aberrations were observed in the methyl ^1H resonance.

For ^{15}N T_1 measurements by inversion-recovery, the pulse sequence of Figure 4.3 was modified by adding a ^{15}N π pulse and a variable recovery delay immediately before the ^1H purge pulse. For these experiments, the ^{15}N purge element before d_1 was removed and d_1 was increased to 600 s.

Data analysis was performed in MATLAB (The MathWorks, Natick, MA) using scripts developed in house. Spectral data was quantified by fitting the methyl ^1H resonance to a complex Lorentzian lineshape function, except for inversion-recovery data, which was quantified by integration. A downhill simplex algorithm was used for least-squares data fitting, and uncertainties in the extracted parameters were estimated using a bootstrap Monte Carlo method [11].

The value of τ_{reb} , which is subtracted from the INEPT transfer delay in order to account for evolution of the ^{15}N -methyl ^1H scalar coupling during the long REBURP

pulse, was determined using a numerical simulation of the pulse sequence. Calculations were performed in GAMMA v4.1.2 [12] in Hilbert space using a spin system of practical size, consisting of one ^{15}N and six methyl ^1H spins, with $J_m = 0.82$ Hz. The ^1H resonance frequency was set to 500 MHz, and the carrier frequencies were set on resonance with the ^{15}N and methyl ^1H spins. The REBURP and the nonselective pulses were simulated with finite widths corresponding to the experimental values, and relaxation and phase cycling were neglected. The pulse sequence shown in Figure 4.3 was simulated, and the methyl ^1H signal amplitude was calculated, for each of a series of values of the INEPT transfer delay ($\tau_1 - \tau_{reb}$). The signal data, shown in Figure 4.4, was then subjected to least-squares fit to a version of Eq. 1 appropriate for a system containing six methyl ^1H spins and including τ_{reb} as an adjustable parameter, resulting in the value of $\tau_{reb} = 6.4$ ms used experimentally.

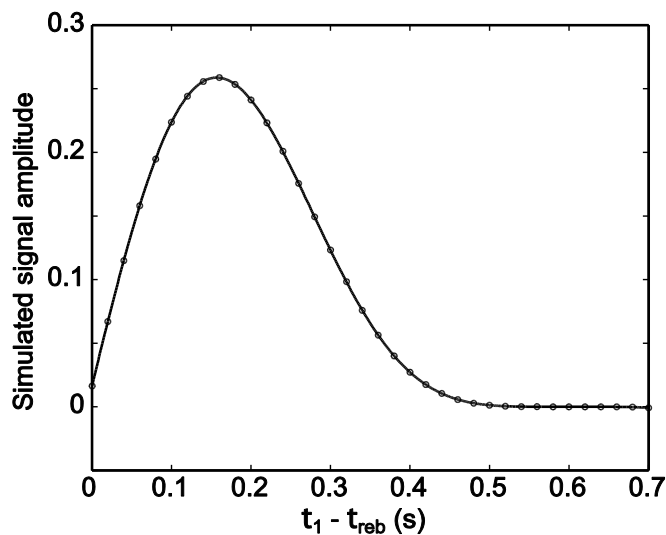


Figure 4.4. Numerical simulation of the selective ^{15}N -to- ^1H INEPT pulse sequence acting on a simplified spin system. Circles are simulated methyl ^1H signal amplitudes for different values of the INEPT transfer delay ($\tau_1 - \tau_{reb}$). The line was calculated using a modified form of Eq. 1 with parameter values from a least-squares fit to the data. This fit was used to determine τ_{reb} , the effective evolution time of the ^{15}N -methyl ^1H coupling during the sequence's REBURP pulse.

4.5 RESULTS AND DISCUSSION

Figure 4.5 shows a spectrum of ^{15}N -choline recorded using the selective ^{15}N -to- ^1H INEPT sequence of Figure 4.3, alongside a ^{15}N -detected spectrum of the same sample recorded in a similar measurement time. It is not meaningful to compare these spectra quantitatively because they were both recorded using a probe that is optimized for direct heteronuclear observation, a factor which diminishes the sensitivity advantage of ^1H detection. However, even under these unfavorable circumstances the signal-to-noise ratio is clearly much higher in the selective INEPT spectrum (Figure 4.5a) than in the ^{15}N -detected spectrum (Figure 4.5b).

A modified version of the selective ^{15}N -to- ^1H INEPT experiment was used to measure the ^{15}N longitudinal relaxation time of ^{15}N -choline in D_2O solution, and a value of $T_1 = (217 \pm 38)$ s was obtained (Figure 4.6). This is comparable to the value $T_1 = (285 \pm 12)$ s previously reported by Gabellieri *et al.* [3] for ^{15}N -choline in 90% H_2O / 10% D_2O .

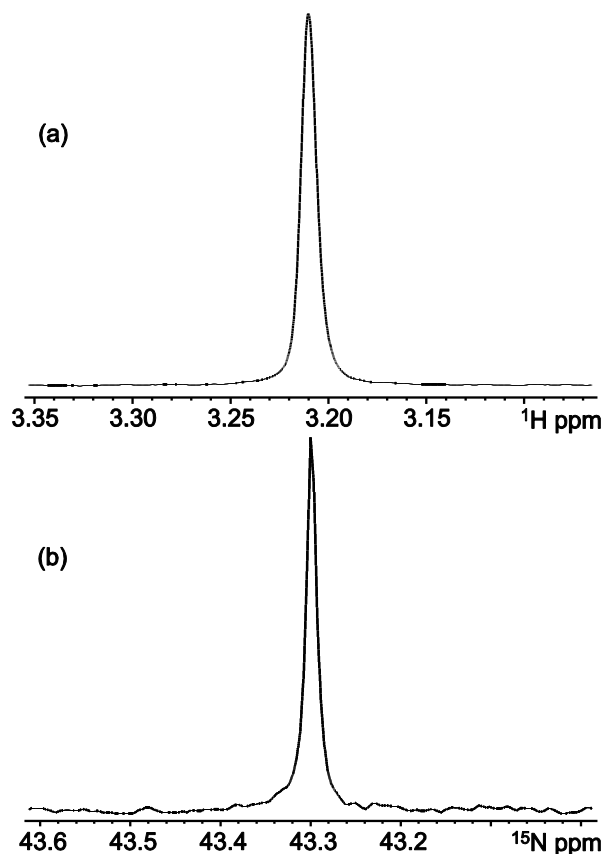


Figure 4.5. (a) ^1H spectrum of ^{15}N -choline recorded using the selective ^{15}N -to- ^1H INEPT sequence of Fig. 3. Only the methyl resonance is shown. (b) Single-pulse ^{15}N spectrum of ^{15}N -choline, recorded with tip angle $\pi/2$. Spectra (a) and (b) were each collected on the same Varian AutoX Dual Broadband probe, taking the sum of four transients with a recycle delay of 60 s. An enhancement factor of 11.0 greater sensitivity when using selective ^{15}N -to- ^1H INEPT sequence was estimated from Monte Carlo fits of (a) and (b) to Lorentzian lineshapes. The peak amplitudes were used as “signals” and the standard deviations as “noise” to construct pseudo “SNR” values for each spectrum to take into account differences in the linewidths of ^1H and ^{15}N peaks. The ratio $\frac{\text{"SNR"}_{^1\text{H}}}{\text{"SNR"}_{^{15}\text{N}}}$ gave the calculated enhancement factor.

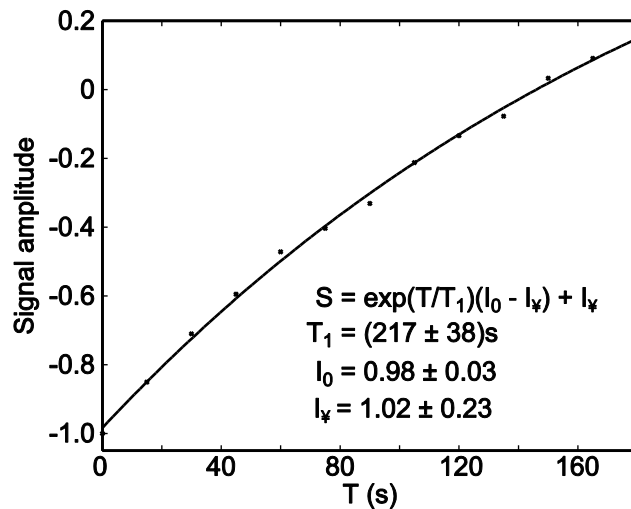


Figure 4.6. Measurement of the ^{15}N longitudinal relaxation time of ^{15}N -choline in D_2O solution using a modified version of the pulse sequence shown in Figure 3. The experiment was repeated for 13 values of the inversion-recovery delay $T = 0.001, 15, 30, 45, \dots, 180$ s. Crosses are experimental methyl ^1H signal amplitudes obtained by integrating the spectral data. The line was calculated using the indicated equation and parameter values from a least-squares fit to the data.

A series of ^{15}N -choline ^{15}N -to- ^1H INEPT spectra were recorded using both selective and nonselective versions of the pulse sequence of Figure 3 with values of the transfer delay τ_1 ranging from 6.4 ms to 700 ms. The methyl ^1H signal amplitudes observed in these experiments are plotted in Figure 7. The selective INEPT sequence allows ^{15}N -choline to be detected with 52% greater sensitivity than the nonselective sequence, comparing the maximum signal amplitude observed in each case. In the Theory section, the amplitude of the methyl ^1H signal was predicted as a function of the transfer delay for the selective (Eq. 1) and nonselective (Eq. 2) experiments using a product operator analysis. By fitting the observed signal amplitudes to Eqs. 1 and 2, the optimal length of τ_1 for each experiment can be determined, as well as precise values of choline's ^{15}N - ^1H coupling constants.

A simultaneous least-squares fit to both datasets yields parameter values $A_{sel} = 0.632 \pm 0.001$, $A_{non} = 1.000 \pm 0.005$, $J_m = (0.817 \pm 0.001)$ Hz, $J_b = (3.64 \pm 0.01)$ Hz, and $C = 0.000 \pm 0.001$. These values for the coupling constants agree well with ones derived from previously published ^1H - ^{14}N values: $J_m = 0.80$ Hz and $J_b = 3.61$ Hz [13]. The value of the smaller ^{15}N -methylene ^1H coupling constant was found to have a negligible effect on the fitting process, so this parameter was fixed at a reasonable value of $J_a = -0.57$ Hz.

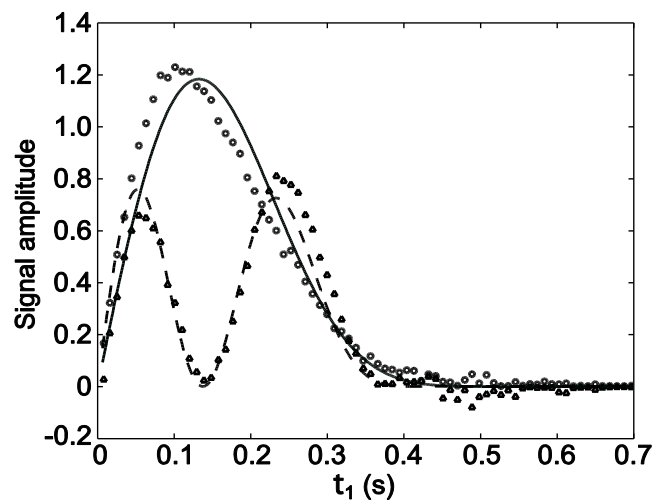


Figure 4.7. Amplitude of the methyl ^1H signal observed in ^{15}N -to- ^1H INEPT spectra of ^{15}N -choline using selective (circles) and nonselective (triangles) versions of the pulse sequence shown in Figure 3, as a function of the INEPT transfer period τ_1 . The lines were calculated using Eq. 1 (solid line) and Eq. 2 (dashed line) with parameter values from a least-squares fit to the data.

Note that, for experiments using the selective and nonselective versions of the pulse sequence of Figure 3 on the same spectrometer hardware and sample, the constants C in Eqs. 1 and 2 should be the same, but A_{sel} may be smaller than A_{non} due to signal losses during the selective sequence's REBURP pulse. Comparing the values of A_{sel} and A_{non} from the least squares fit it appears that 36% of the signal is lost in this way. This can be attributed in part to miscalibration of the REBURP pulse. A three pulse sequence ($\pi/2$ - REBURP - $\pi/2$) was used to calibrate the REBURP pulse by seeking pulse width and power parameters that gave the best null signal. It would be more appropriate to choose a calibration sequence that uses the REBURP pulse for inversion, as it is used in the selective INEPT sequence, rather than for refocusing. Also, a sequence with a larger number of pulses would be preferable, so that the cumulative effects of B_1 inhomogeneity would be comparable in the calibration sequence and the selective INEPT sequence.

We have presented a pulse sequence that suppresses the effects of the four methylene protons on the INEPT transfer from ^{15}N to methyl ^1H in ^{15}N -choline. Note that the same result can be achieved by selective deuteration of ^{15}N -choline. This approach might provide the additional benefit of increasing the molecule's ^{15}N longitudinal relaxation time and would be an option for DNP experiments. However, the present selective recoupling strategy is clearly advantageous for ^{15}N -choline hyperpolarization using PASADENA. In these experiments, two of the methylene ^1H spins derive from a parahydrogen molecule which reacts with an unsaturated precursor to initiate the hyperpolarization process. Although deuteration of the alkene precursor

can remove two of the methylene ^1H spins, those which supply the spin order cannot be eliminated.

The success of this selective coherence transfer strategy in ^{15}N -choline has clear implications for studies of other hyperpolarized small biomolecules. By directing the spin order to a subset of the possible detection spins, sensitivity is improved. The recoupling strategy demonstrated here accomplishes this by way of a frequency selective π pulse, which simplifies, and often shortens, the polarization transfer step. Similar selective INEPT sequences could be used to improve the sensitivity of the ^{13}C -to- ^1H polarization transfer experiments demonstrated by Chekmenev *et al.* in hyperpolarized TFPP [4] by directing the spin order to one of the resolved ^1H sites.

The selective ^{15}N -choline transfer presented here also has potentially useful applications to thermally polarized *in vivo* ^{15}N spectroscopy. Pulse sequences can be devised to transfer methyl ^1H polarization to ^{15}N for an encoding period and then back to methyl ^1H for detection. Such sequences would benefit from choline's long ^{15}N T_1 while making use of the strong thermal polarization of the nine methyl ^1H spins. This strategy could be used to resolve species such as choline and phosphocholine by ^{15}N - ^1H correlation spectroscopy, or even to study the metabolic interconversion of choline and related compounds using a sequence with a longitudinal ^{15}N period for chemical exchange.

4.6 CONCLUSION

As part of a strategy to improve the sensitivity of *in vivo* experiments on hyperpolarized small biomolecules, we have investigated INEPT pulse sequences for the transfer of magnetization from ^{15}N to the methyl ^1H spins in ^{15}N -choline. Product operator analysis of a simple refocused INEPT sequence shows that the optimized efficiency of this transfer is diminished by 62% by the action of competing couplings between ^{15}N and choline's methylene ^1H spins. A selective INEPT sequence, using a ^1H REBURP pulse to suppress undesired couplings during the transfer period, was devised and tested *in vitro* on a thermally polarized ^{15}N -choline sample. It was demonstrated that the selective INEPT sequence leads to a 52% stronger methyl ^1H signal than the nonselective version.

4.7 ACKNOWLEDGEMENTS

This work was done in collaboration with Jason E. Ollerenshaw, Valerie A. Norton, and Daniel P. Weitekamp. It was supported by the Beckman Institute pilot program, "Spin-Polarized Molecules for Structural and Systems Biology." JEO was supported by a Postdoctoral Fellowship from the Natural Sciences and Engineering Research Council of Canada.

4.8 REFERENCES

- [1] E.Y. Chekmenev, J. Hovener, V.A. Norton, K. Harris, L.S. Batchelder, P. Bhattacharya, B.D. Ross, and D.P. Weitekamp, PASADENA Hyperpolarization of Succinic Acid for MRI and NMR Spectroscopy. *Journal of the American Chemical Society* 130 (2008) 4212-4213.
- [2] K. Golman, Metabolic imaging by hyperpolarized ^{13}C magnetic resonance imaging for in vivo tumor diagnosis. *Cancer Research* 66 (2006) 10855.
- [3] C. Gabellieri, S. Reynolds, A. Lavie, G.S. Payne, M.O. Leach, and T.R. Eykyn, Therapeutic target metabolism observed using hyperpolarized ^{15}N choline. *J. Am. Chem. Soc.* 130 (2008) 4598-4599.
- [4] E.Y. Chekmenev, V.A. Norton, D.P. Weitekamp, and P. Bhattacharya, Hyperpolarized ^1H NMR employing low g nucleus for spin polarization storage. *J. Am. Chem. Soc.* 131 (2009) 3164-3165.
- [5] R.F. Gareth A. Morris, Enhancement of Nuclear Magnetic Resonance Signals by Polarization Transfer. *Journal of the American Chemical Society* 101 (1979) 763-762.
- [6] Y. Boulanger, M. Labelle, and A. Khiat, Role of phospholipase A_2 on the variations of the choline signal intensity observed by ^1H magnetic resonance spectroscopy in brain diseases. *Brain Res. Rev.* 33 (2000) 380-389.
- [7] R. Katz-Brull, D. Seger, D. Rivenson-Segal, E. Rushkin, and H. Degani, Metabolic markers of breast cancer: enhanced choline metabolism and reduced choline-ether-phospholipid synthesis. *Cancer Res.* 62 (2002) 1966-1970.
- [8] E. Sutinen, M. Nurmi, A. Roivainen, M. Varpula, T. Tolvanen, P. Lehtikainen, and H. Minn, Kinetics of $[^{11}\text{C}]$ choline uptake in prostate cancer: a PET study. *Eur. J. Nucl. Med. Mol. Imaging* 31 (2004) 317-324.

- [9] D.M. Doddrell, D.T. Pegg, W. Brooks, and M.R. Bendall, Enhancement of ^{29}Si or ^{119}Sn NMR signals in the compounds $\text{M}(\text{CH}_3)_n\text{Cl}_{4-n}$ ($\text{M} = \text{Si}$ or Sn , $R = 4, 3, 2$) using proton polarization transfer. Dependence of the enhancement on the number of scalar coupled protons. *J. Am. Chem. Soc.* 103 (1981) 727-728.
- [10] H. Geen, and R. Freeman, Band-selective radiofrequency pulses. *J. Magn. Reson.* 93 (1991) 93-141.
- [11] W.H. Press, S.A. Teukolsky, W.T. Vetterling, and B.P. Flannery, *Numerical Recipes in C: The Art of Scientific Computing* 2nd edition, Cambridge University Press, Cambridge, UK, 1992.
- [12] S.A. Smith, T.O. Levante, B.H. Meier, and R.R. Ernst, Computer simulations in magnetic resonance. An object-oriented programming approach. *J. Magn. Reson.* A106 (1994) 75-105.
- [13] V. Govindaraju, K. Young, and A.A. Maudsley, Proton NMR chemical shifts and coupling constants for brain metabolites. *NMR Biomed.* 13 (2000).

Appendix A

Understanding PCC Agent Binding to Single Point Mutation E17K of Akt1 Pleckstrin

Homology Domain through Molecular Dynamics

A.1 INTRODUCTION

The Akt kinase is a critical molecular router that mediates cell growth, apoptosis, and translation [1], and Akt overexpression and/or hyperactivation has been observed in many cancer types [2]. The Akt1 activation mechanism includes binding to the PIP3 lipid on the cell membrane with a domain called the Pleckstrin Homology Domain (PHD). Mutations in the PHD of Akt1 that increase its affinity for binding with PIP3 will cause the upregulation of downstream pathways, thereby promoting the formation of cancerous cells [3].

Recent experiments performed on mice have revealed that a single amino acid point mutation to the PHD of Akt1, called the E17K mutation, was sufficient to cause cancer [4]. This same mutation has been found in certain human ovarian, colorectal and breast cancers. The E17K mutation exchanges a negatively charged glutamate for a positively charged lysine, causing the formation of an additional hydrogen bond between the PHD and PIP3 on the cell membrane. This induces a conformational change that causes Akt1(E17K) to bind to the plasma membrane four times stronger than it would in its wild-type form [4]. This strengthened binding is believed to be the underlying mechanism for the creation of a type of cancerous cells in mice.

It is hypothesized that blocking the binding between PIP3 and Akt1(E17K) could reduce or terminate the growth of cancerous cells derived from the E17K mutation in humans, thus serving as a less invasive and less toxic means of chemotherapy. Previous work has shown that peptide capture agents can be raised against Akt that are epitope targeted and/or inhibitory [5,6,7]. Specifically, a 5mer peptide capture agent (yleaf) has

been developed to bind to the E17K mutation of the PH domain of Akt1 [7]. Molecular dynamics (MD) trajectories of the peptide/protein complex are constructed for the anchor with both the mutant and wild type (WT) Akt1 PH domains, and used to calculate the free energy of binding for each system.

A.2 PEPTIDE CAPTURE AGENT AGAINST E17K MUTATION OF AKT1 PHD

Work in the Heath group has yielded a 5mer anchor peptide that differentiates the E17K mutated Akt1 PHD from the wild type domain [7]. The epitope targeted one-bead-one-compound screening method used to identify the ligand provides an anchor point for the C-terminus location of peptide binding. Additionally, biotin labeling experiments done using a variant of the peptide with an N-terminal tosyl-biotin labeling arm indicate a general region of N-terminal peptide interaction with the target around the residue Y26 [8]. These data were used in choosing the initial configuration of the yleaf-tosyl-biotin ligand in relation to either the E17K or WT target.

A.3 CONSTRUCTION OF E17K AND WT SYSTEMS

A.3.1 yleaf-tosyl-biotin

The N-terminal tosyl-biotin labeling arm was constructed in ChemDraw, then imported into Maestro. The bond lengths were manually doubled, and then the B3LYP/6-31G** optimized structure and Mulliken charges were obtained using Jaguar. Unknown bond length, bond angle, and torsion parameters for the tosyl group were

optimized using B3LYP/6-31G** in Jaguar. The yleaf peptide was grown onto the minimized tosyl structure using (D) amino acids to form the complete ligand. yleaf-tosyl-biotin was equilibrated in explicit water at 300 K for 1 ns to obtain the ligand conformation (Figure A.1) used to construct the ligand/protein complexes.

A.3.2 Ligand/Protein Complexes

Crystal structures for E17K (2UZR) and wild type (1UNP) Akt1 PH domains were obtained from the Protein Data Bank. ZDOCK was used to determine an initial relative configuration of the ligand shown in Figure A.1 to the E17K PHD. The anchor peptide was initially screened against the 32mer fragment corresponding to residues 1-32 of the E17K PHD, and ZDOCK predictions were restricted to only include relative conformations that allowed for interaction of the ligand with this fragment. The selected ligand configuration was also used for the wild type PH domain. Figure A.2 shows the top three ZDOCK output structures, and Figure A.3 shows the chosen structure for both E17K and WT systems.

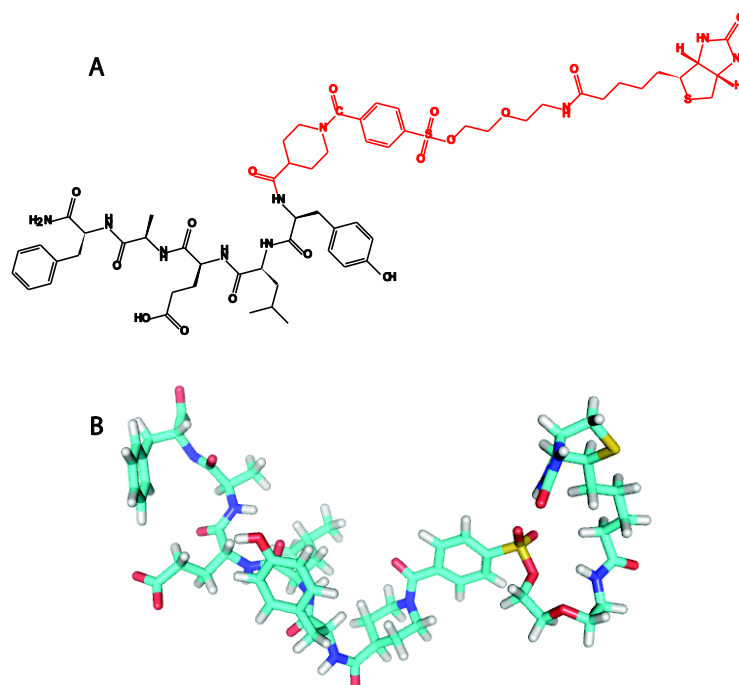


Figure A.1. **A.** ChemBioDraw structure of yleaf-tosyl-biotin. **B.** Equilibrated structure of yleaf-tosyl-biotin used to construct WT and E17K complexes.

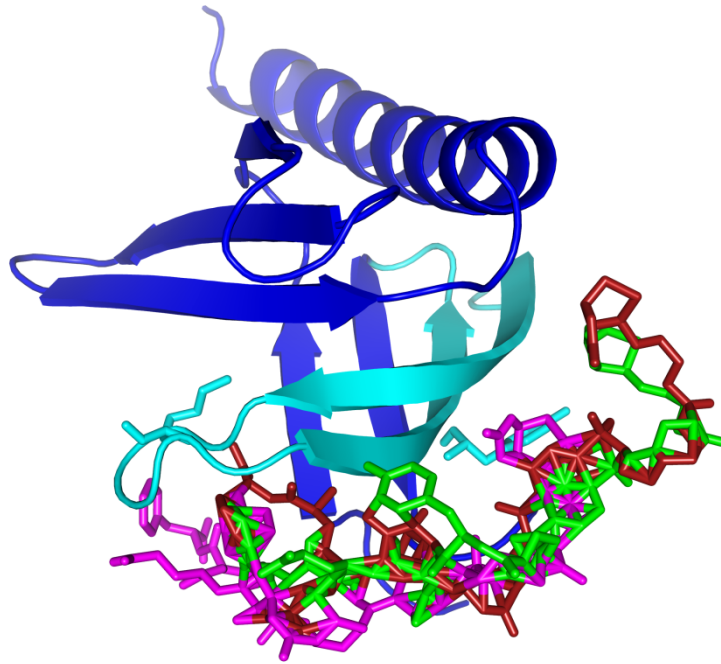


Figure A.2. Top three ZDOCK predicted conformations of yleaf-tosyl-biotin/E17K PH domain complex. Interaction was constrained to occur only with the first 32 residues of the protein (highlighted) that represent the fragment against which the peptide ligand was raised. The two amino acids of interest from experimental binding assays, E17K and Y26, are shown as sticks.

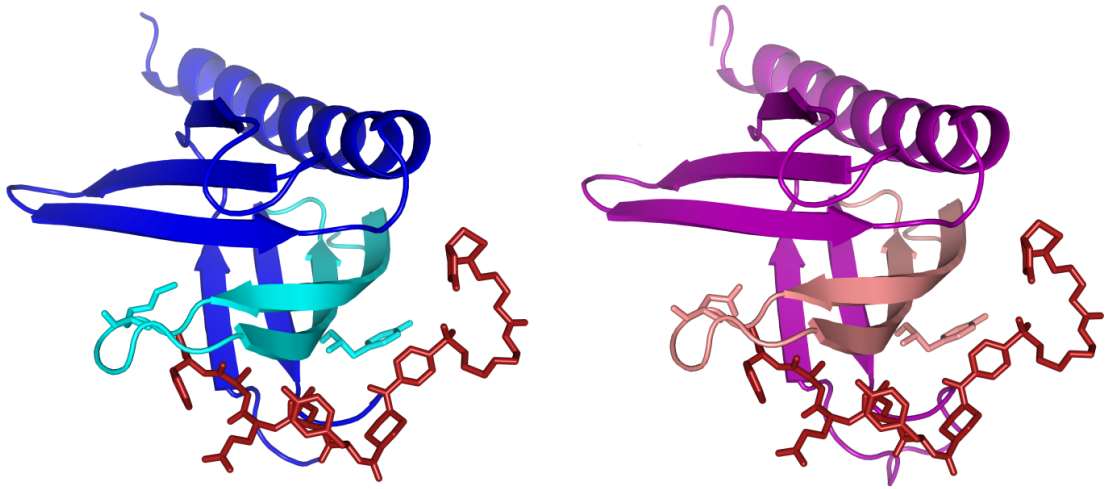


Figure A.3. Selected ligand conformation complexed with the mutant (blue) and wild type (purple) PH domains. This structure was chosen because the ligand most closely spans the two amino acids of interest (E17 or E17K, and Y26).

A.4 MOLECULAR DYNAMICS

The systems were neutralized by adding Cl⁻ or Na⁺ counterions as necessary, and were fully solvated in TIP3P water boxes. Each system was first subjected to a minimization of 10,000 steps. Then the solvent molecules, ligand, and binding fragment were equilibrated for 200 ps at 300 K while the remaining protein coordinates were fixed. The full systems were then minimized for 5,000 steps. Finally, both systems were equilibrated for a total of 5 ns at 300 K. The MD simulations were carried out with the NAMD 2.6 program [9]. Plots of the root mean squared deviation (rmsd) from the initial configuration of the trajectories and restarted trajectories from both systems are shown in Figure A.4.

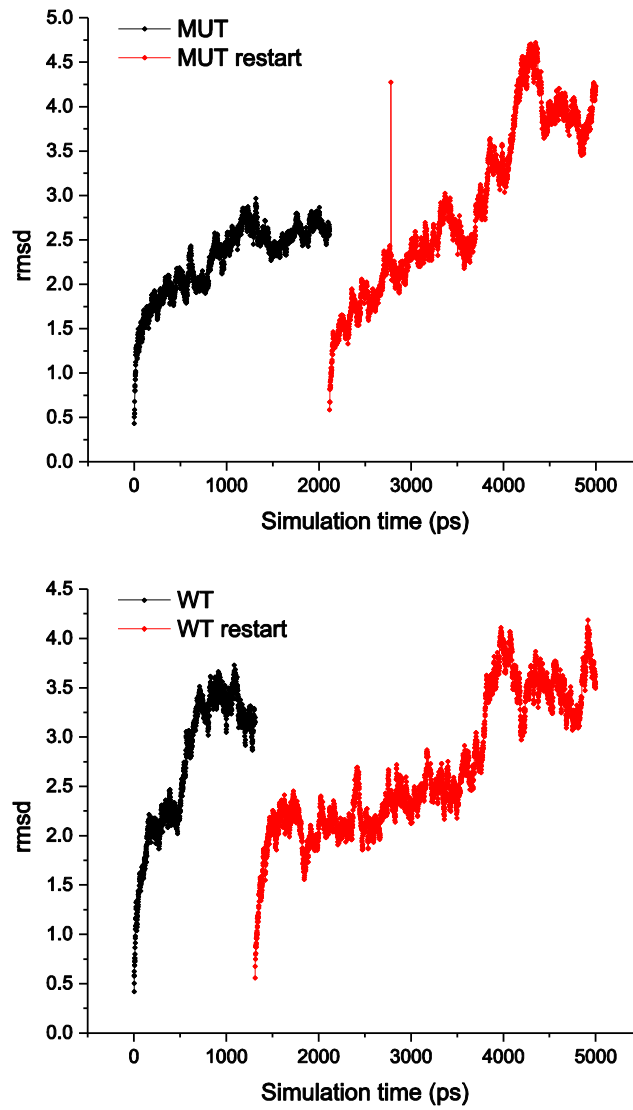


Figure A.4. Rmsd plots for the MD trajectories and restarted trajectories of the E17K and WT complexes.

A.5 BINDING ENERGY

To obtain a good comparison of free binding energy between the two systems, energy landscapes were constructed for E17K and WT by plotting the free energy of binding of conformations representing local macrostates vs. their rmsd from the lowest energy conformation, similar to the approach taken by [10]. If the reference structure is truly the lowest energy, the landscape will be smoothly funnel shaped. If there is an alternative lowest energy structure, the landscape will be non-funnel shaped. Figure A.5 shows examples of this type of landscape, where each dot represents one of 200,000–400,000 independent Rosetta *ab initio* structure prediction simulations [10]. For the purpose of this work, the rmsd of each trajectory is like a partition function, where each point represents a microstate. Plateaus in the rmsd represent macrostates, and given an infinite amount of simulation time, the system will spend a Boltzmann weighted percentage of time in each macrostate. Binding energies were calculated for a number of 100 ps plateaus in each trajectory using a Generalized Born implicit solvent model. After identifying the conformation with the lowest calculated binding energy REF, the energies of the other conformations were plotted against the rmsd of those conformations relative to REF. The energy vs. rmsd plot for the E17K and WT systems are shown in Figures A.6 and A.7, and the structure of the chosen reference structures are shown in Figure A.8. Significantly fewer data points were able to be obtained for the E17K and WT systems than the *ab initio* structure prediction simulations, but the plots suggest the funnel shape described by [10], indicating that the correct lowest energy reference structure had been selected.

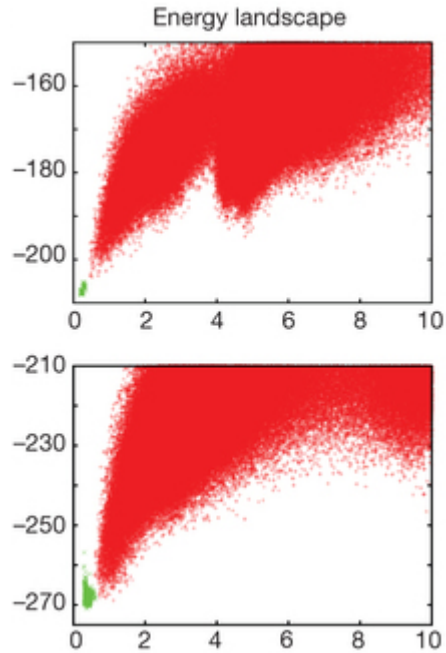


Figure A.5. Energy landscapes obtained from Rosetta *ab initio* structure prediction simulations on Rosetta@home. Red points represent the lowest-energy structures obtained in independent Monte Carlo structure prediction trajectories starting from an extended chain for each sequence; the y axis shows the Rosetta all-atom energy and the x axis shows the C α root mean squared deviation from the design model. Green points represent the lowest-energy structures obtained in trajectories starting from the design model. The bottom figure shows a landscape that is funnel shaped, and the top shows one that is non funnel shaped. Adapted from [10].

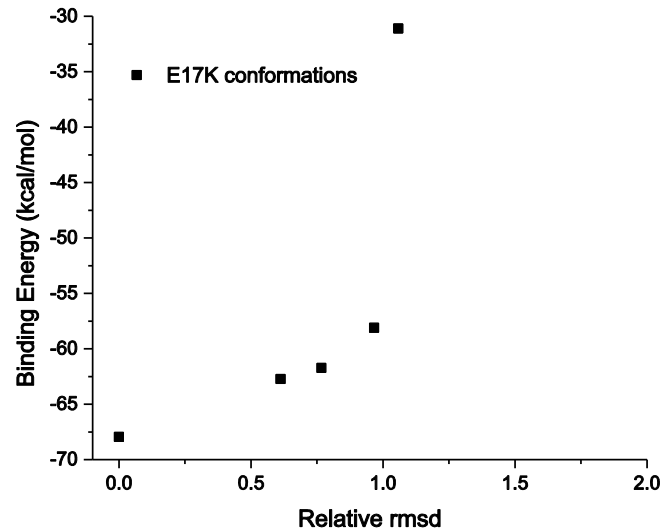


Figure A.6. Energy landscape for E17K complex. The y-axis is the Generalized Born calculation of binding energy, and the x-axis is the rmsd relative to the lowest energy structure. Each point is a plateau in the trajectory rmsd, representing a macrostate of the system. The binding energy of the reference state calculated without including entropy contribution is -67.95 kcal/mol.

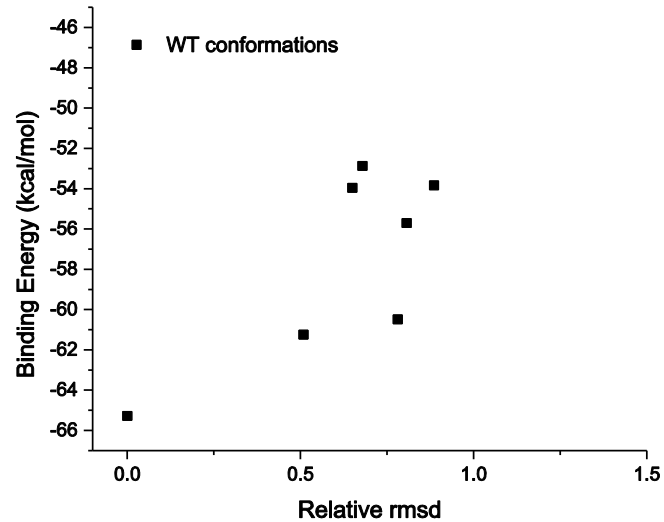


Figure A.7. Energy landscape for WT complex. The y-axis is the Generalized Born calculation of binding energy, and the x-axis is the rmsd relative to the lowest energy structure. Each point is a plateau in the trajectory rmsd, representing a macrostate of the system. The binding energy of the reference state calculated without including entropy contribution is -65.28 kcal/mol.

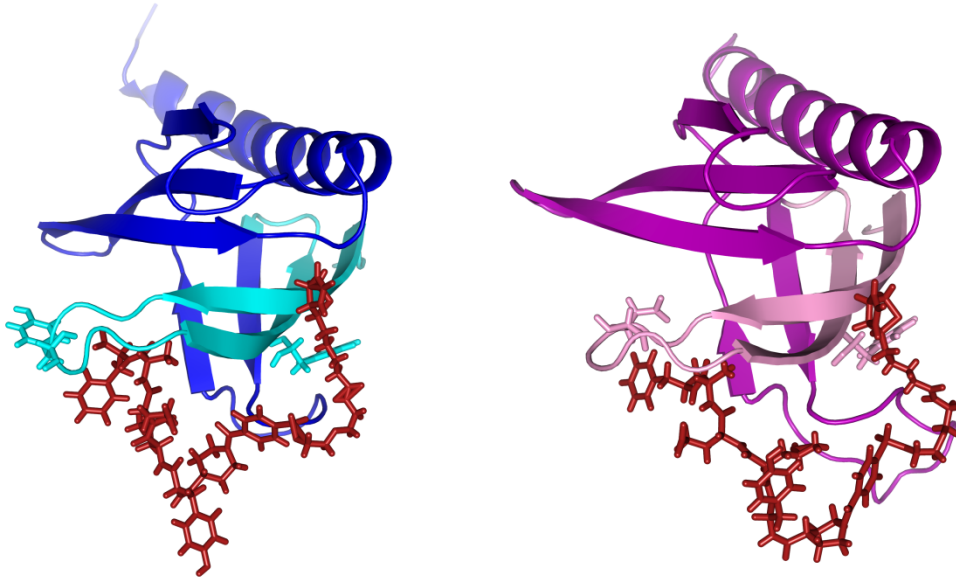


Figure A.8. Structures of the E17K and WT reference states. There are distinct differences in the conformation of the peptide around the E17K mutation site between the two systems.

A.6 CONCLUSION

This appendix explored the use of MD calculations to understand the selectivity of the peptide ligand yleaf-tosyl-biotin for the E17K mutant of Akt1 PH domain over the wild type domain. The structure of the ligand was constructed and minimized, then complexed with both the E17K and wild type structures of Akt1 PHD. Trajectories were run, and the energies of macrostates of the system were calculated and plotted against their rmsd relative to a reference state to determine if the lowest energy state had been identified. The binding energy of the E17K reference state was found to be 2.67 kcal/mol lower than that of the WT reference state. This corresponds to a factor of ~90 difference in K_d , which is within the error of experimental measurements.

A.7 ACKNOWLEDGEMENTS

This work was done in collaboration with William Goddard III, Kaycie Deyle, and Blake Farrow.

A.8 REFERENCES

1. Vivanco I, Sawyers CL (2002) The phosphatidylinositol 3-kinase–AKT pathway in human cancer. *Nature Reviews Cancer* 2: 489-501.
2. Altomare DA, Testa JR (2005) Perturbations of the AKT signaling pathway in human cancer. *Oncogene* 24: 7455-7464.
3. Rebecchi M, Scarlata S (1998) Pleckstrin homology domains: a common fold with diverse functions. *Annual review of biophysics and biomolecular structure* 27: 503-528.
4. Carpten JD, Faber AL, Horn C, Donoho GP, Briggs SL, et al. (2007) A transforming mutation in the pleckstrin homology domain of AKT1 in cancer. *Nature* 448: 439-444.
5. Millward SW, Henning RK, Kwong GA, Pitram S, Agnew HD, et al. (2011) Iterative in Situ Click Chemistry Assembles a Branched Capture Agent and Allosteric Inhibitor for Akt1. *Journal of the American Chemical Society* 133: 18280-18288.
6. Nag A, Das S, Yu MB, Deyle KM, Millward SW, Heath JR (2013) A Chemical Epitope-Targeting Strategy for Protein Capture Agents: The Serine 474 Epitope of the Kinase Akt2. *Angewandte Chemie International Edition* In press.
7. Deyle K et al., Submitted.
8. Tamura T, Tsukiji S, Hamachi I (2012) Native FKBP12 Engineering by Ligand-Directed Tosyl Chemistry: Labeling Properties and Application to Photo-Cross-Linking of Protein Complexes in Vitro and in Living Cells. *Journal of the American Chemical Society* 134: 2216-2226.
9. Phillips JC, Braun R, Wang W, Gumbart J, Tajkhorshid E, et al. (2005) Scalable molecular dynamics with NAMD. *Journal of computational chemistry* 26: 1781-1802.
10. Koga N, Tatsumi-Koga R, Liu G, Xiao R, Acton TB, et al. (2012) Principles for designing ideal protein structures. *Nature* 491: 222-227.

Appendix B

Peptide-Based General Antibody Detection Agent

B.1 INTRODUCTION

Detecting the immune response to an infectious agent can provide useful *in vitro* diagnostic information. Assays of this nature require a general antibody detection agent, often a conjugated anti-Fc antibody or protein substrate, i.e., Protein A. However, most biological reagents have inherent variability, which can adversely influence the performance of the diagnostic test. Peptide capture agents have been shown to be highly robust and inexpensive to produce, and to have similar affinities and selectivities as antibodies. DeLano *et al.* reported the discovery of a cyclic 13-amino acid peptide (Fc-III) that bound the “consensus region” of IgG Fc by phage display affinity screening [1]. We explored possible improvements to the Fc-III peptide in terms of affinity and selectivity by employing *in situ* click screening to obtain a biligand, and in terms of stability by replacing the disulfide bridge of Fc-III, with the goal of using the modified peptide as a detection agent in diagnostic assays.

B.2 WELLS PEPTIDE

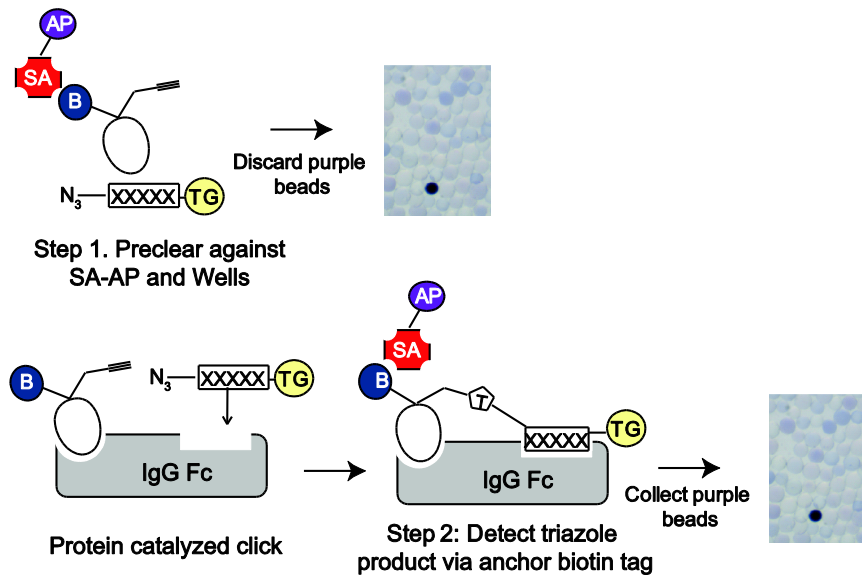
Using a cyclic phage display library of the form $X_iCX_jCX_k$ (where C is cysteine, X is a random amino acid, and $i + j + k = 18$), DeLano *et al.* found the 13-residue Fc binding sequence Fc-III (DCAWHLGELVWCT) [1,2]. When synthesized, this peptide was found to inhibit the binding of Protein A Z-domain to Fc with a K_i of 25 nM, which is 200 fold greater affinity than an earlier, longer consensus sequence found by the group. The increased affinity with shorter length implied that the final sequence very efficiently

interacts with the Fc binding pocket. We added a propargyl glycine (Pra) residue at the N-terminus of Fc-III and tested the ability of this modified cyclic peptide to bind IgG Fc. The anchor peptide, monikered Wells peptide, was also C-terminally tagged with a polyethylene glycol (PEG) oligomer bridge and a biotin label.

B.3 BILIGAND SCREEN

The *in situ* click screen is illustrated in Scheme 2.1. The target IgG Fc is incubated with an excess of the selected anchor peptide and a large OBOC library at 4°C for 6 hrs (see Materials and Methods). The OBOC library is synthesized on TentaGel resin (Rapp Polymere, Tuebingen, Germany), and is a comprehensive library of 5-mers with a 6th amino acid at the C-terminus presenting an azide functionality. The OBOC library is comprised of non-natural (D) stereoisomers of the natural amino acids, excluding cysteine and methionine. The *in situ* screen is designed to identify a secondary (2^o) peptide that, when coupled to the anchor, forms a biligand with increased selectivity and/or affinity for the target IgG Fc.

In Step 1 of the screen, the OBOC library is cleared of beads that exhibit non-specific binding to Wells peptide and alkaline phosphatase-conjugated streptavidin (SA-AP), which is used as a detection reagent in the next step. Step 2 is called a product screen, and is unique to sequential *in situ* click screens [3]. This screen detects the presence of *in situ* clicked reaction products, which are those hit beads containing the triazole-linked anchor peptide. A complete list of screen hits is given in Table B.1.



Scheme B.1. Screening strategy for selecting capture agents against human IgG Fc. The flow chart represents the use of the cyclic Wells peptide as an anchor ligand for in situ click screening against a large OBOC azide-presenting peptide library.

k	e	r	i	g
a	h	r	i	G
d	G	r	i	G
r	r	i	G	p
G	e	h	n	i
y	l	h	n	i
G	a	h	G	i
e	i	r	v	k
k	w	l	r	v
y	k	l	a	i
i	q	f	k	l
p	i	l	i	p
r	f	q	a	p
r	y	a	a	k
n	k	G	h	i

Table B.1. Biligand screen results. List of pentapeptide “hits” from OBOC biligand screens performed with Wells peptide and human IgG Fc. The selected secondary ligands corresponding to WA and WG are shown in blue and red respectively (shown in Figure B.1).

B.4 1,4 TRIAZOLE LINKED BILIGAND CHARACTERIZATION

The performance of these biligands was then characterized using an in-house developed on-bead ELISA assay (data not shown). Sandwich ELISAs were used for affinity estimations of the two best performing biligands (Figure B.1) from the on-bead experiments. The affinity increase of the biligands over Wells is marginal. Hill fits to the ELISA data give K_d values of 18 nM for WA, 21 nM for WG, and 25 nM for Wells (Figure B.2).

B.5 1,5 TRIAZOLE LINKED BILIGAND CHARACTERIZATION

The in situ click process does not yield a stereospecific triazole product, and it is impossible to measure which click product variant the protein “catalyzed” during a screen. Therefore it can be useful to test the 1,5 triazole linked versions of potential biligands. Here, the biligand WA was synthesized using a 1,5 triazole small molecule linker and its performance compared to that of Wells by sandwich ELISA (Figures B.2 - B.3). The difference in affinity between the 1,5 triazole linked biligand and Wells was negligible.

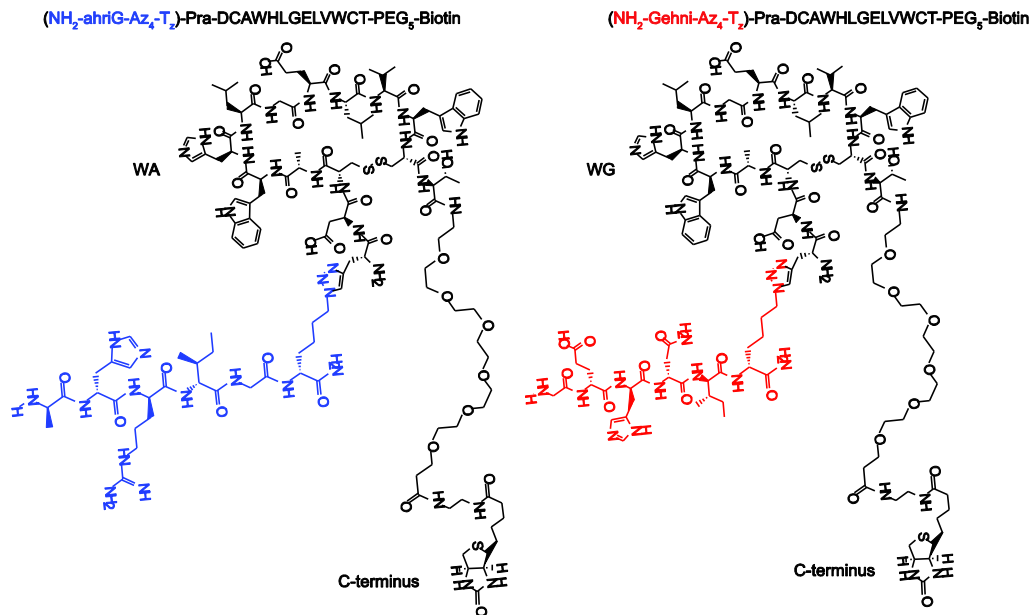


Figure B.1. Structures of peptide biligands identified in screen against IgG Fc. Acetylene-presenting anchor peptides (black) were derived from Fc-III. Wells-ahriG (WA) and Wells-Gehni (WG) were evolved from the original peptide appended with Pra at the N-terminus, and secondary ligand branches (colored) were identified from the *in situ* click screen of a 5-mer OBOC library presenting an azide functionality.

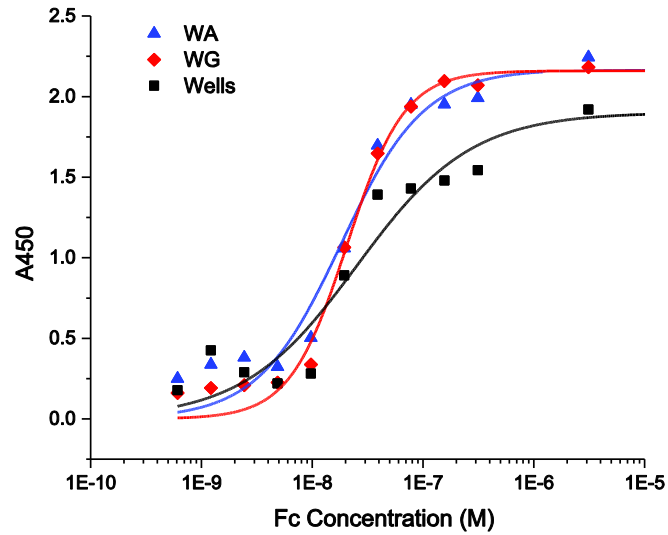


Figure B.2. Apparent affinity of Wells and biligands directed against Fc as determined by sandwich ELISA. Lines represent 1st order Hill fits to the affinity data. Wells: $K_d = 25$ nM, WA: $K_d = 18$ nM, WG: $K_d = 21$ nM.

(NH₂-ahriG-Az₄-1,5T₂)-Pra-DCAWHLGELVWCT-PEG₅-Biotin

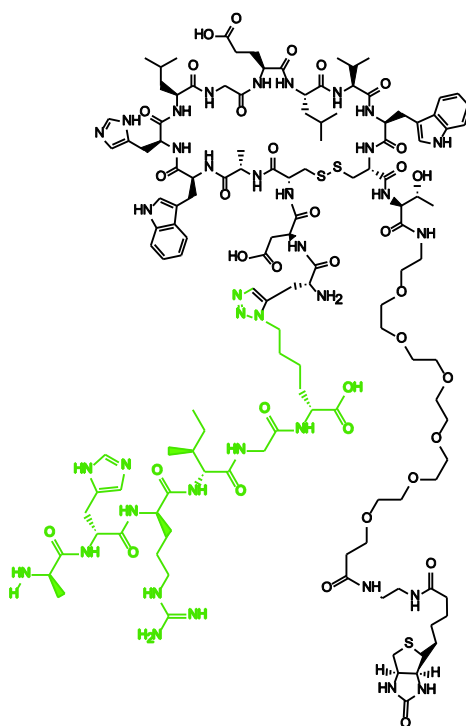


Figure B.3. Structure of 1,5 triazole linked biligand. Biligand peptide WA was synthesized with a 1,5 triazole linker.

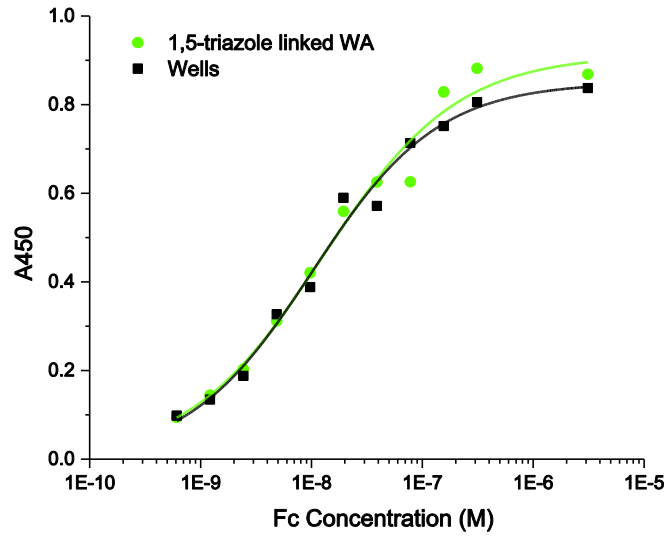


Figure B.4. Apparent affinity of Wells and 1,5 triazole linked WA directed against Fc as determined by sandwich ELISA. Lines represent 1st order Hill fits to the affinity data.

B.6 CLICK CYCLIZED WELLS

To enhance the stability of the Wells anchor peptide, we attempted to replace the disulphide bridge with a Cu(I) catalyzed click triazole. (D) or (L) azidoalanine (Az1) was substituted for Cys2, and Pra was substituted for Cys12, then the peptide was cyclized using Cu(I) catalyzed click chemistry (Figure B.5). Single point ELISAs showed that this approach to cyclization removed all affinity to IgG Fc (Figure B.6). This could be due to the change in confirmation of the peptide cycle when constrained by an alternative cyclization moiety. The use of both (D) and (L) Az1 was an attempt to circumvent that, but was unsuccessful.

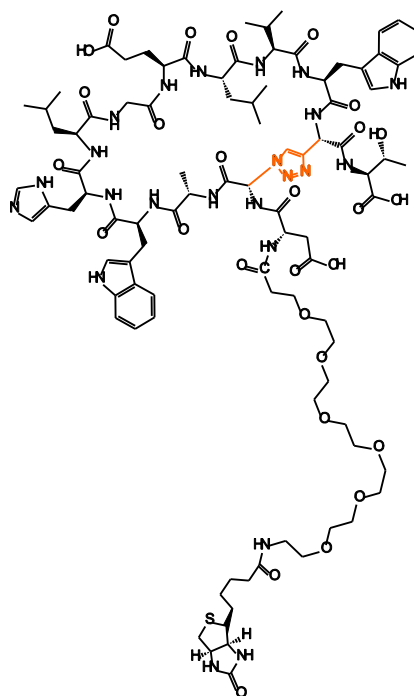


Figure B.5. Structure of Cu(I) click cyclized Wells peptide. The disulfide bond in Wells peptide was replaced with a Cu(I) catalyzed triazole formed from substitutions of Az1 and Pra for Cys2 and Cys12 respectively.

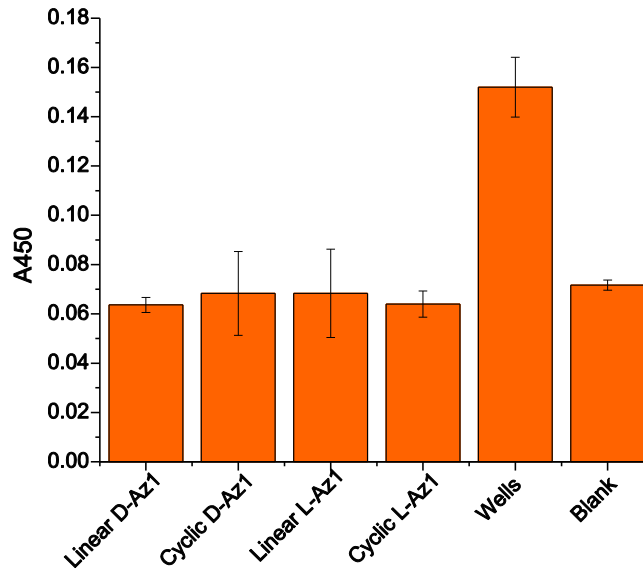


Figure B.6. Performance of click cyclized Wells peptide variants compared to Wells peptide tested by sandwich ELISA. Fc (500 nM) was spiked into TBS, and captured antibody was detected by peroxidase-conjugated anti-human IgG antibody.

B.7 MATERIALS AND METHODS

B.7.1 Anchor Synthesis

The anchor Wells peptide was synthesized C → N on 200-300 mgs of Biotin NovaTag resin (EMD Biosciences, San Diego, CA) with a Titan peptide synthesizer using standard Fmoc chemistry [4]. The synthesis used Fmoc and side chain protected L amino acids (Aaptec, Louisville, KY), Fmoc protected propargylglycine (Pra) (Aaptec, Louisville, KY) and PEG₅ (EMD Millipore, Germany). The finished peptide was side-chain deprotected and cleaved from resin in a mixture of 95% v/v trifluoroacetic acid (TFA) (Sigma-Aldrich, St. Louis, MO), 5% v/v dH₂O, and 5% triethylsilane (TES) (Sigma-Aldrich, St. Louis, MO), and precipitated in diethyl ether. Cu(Phen)₃ stock solution was prepared by mixing 150 mM Cu(II) sulfate pentahydrate (Sigma-Aldrich, St. Louis, MO) and 500 mM 1,10-phenanthroline (Sigma-Aldrich, St. Louis, MO) in 4:1 H₂O:Ethanol. The ether-precipitated ligand was cyclized by stirring the cleaved peptides dissolved in ~5 mL acetonitrile (ACN) overnight with 1 mL of the Cu(Phen)₃ stock solution. The cyclization mixture was lyophilized, and the final peptide product was purified using reverse phase (RP) HPLC on a Kinetex 5 μ XB-C18 250 x 4.6 mm prep column (Phenomenex, Torrance, CA).

B.7.2 OBOC Screen

The screen used naïve one-bead-one-compound (OBOC) D-pentapeptide libraries on TentaGel resin (TG) (Rapp Polymere, Tuebingen, Germany) of the form NH₂-

X₁X₂X₃X₄X₅-Az₄-TG, excluding cysteine and methionine, where Az₄ is L-azidolysine. Libraries were synthesized on a Titan peptide synthesizer (Aaptec, Louisville, KY) using a split/mix method, and couplings were done using standard Fmoc SPPS chemistry in *N*-methylpyrrolidone (NMP).

Screening against Fc was carried out in two main steps: pre-clear, and product screen. **Step 1 preclear:** 200 mg of OBOC library was blocked in 5% w/v dry milk in Tris buffered saline (TBS) (25 mM Tris-HCl, 150 mM NaCl, 10 mM MgCl₂, pH 7.6) for 2 hr at room temperature, and then incubated with 1:10,000 phosphatase-conjugated streptavidin (SA-AP, Promega, Madison, WI) and 25 μM Wells peptide in 0.5% w/v dry milk in TBS for 1 hr. The beads were washed in high salt buffer (25 mM Tris-HCl, 750 mM NaCl, 10 mM MgCl₂, pH 7.6) for 1 hr, and then developed with BCIP/NBT (Promega, Madison, WI) in BCIP buffer (100 mM Tris-HCl, 150 mM NaCl, 1 mM MgCl₂, pH 9). After 1 hour, the reaction was quenched with conc. HCl, and the purple beads were discarded. The remaining library was decolorized in NMP, dried with methanol (MeOH) and dichloromethane (DCM), and then swelled and blocked in 5% w/v dry milk in TBS for 2 hr at room temperature. **Step 2 product screen:** 4 mL of a solution containing 25 μM A21 and 23 nM Fc in 0.5% w/v dry milk in TBS was added to the precleared OBOC library, and the *in situ* click reaction was allowed to proceed for 6 hours at 4°C. Click solution was drained and the beads were washed for 1 hr in high salt buffer. The beads were incubated for 1 hr at room temperature with 1:10,000 SA-AP in 0.5% w/v dry milk in TBS, washed for 1 hr with high salt buffer, and then developed with BCIP/NBT in BCIP buffer for 1 hour. The reaction was quenched with conc. HCl, and the purple beads

were retained and sequenced using a Procise CLC Edman Degradation Protein Sequencing System (Applied Biosystems, Kingston, RI).

B.7.3 Biligand Synthesis

1,4 Triazole linked WA and WG

The secondary ligands including C-terminal Az₄ for WA and WG were synthesized C → N on 200-300 mgs of Rink amide resin with a Titan peptide synthesizer using standard Fmoc chemistry. The synthesis used Fmoc and side chain protected D amino acids and L-Az₄ (Aaptec, Louisville, KY). The ligands were side-chain deprotected and cleaved from resin in 95:5:5 TFA:dH₂O:TES, then precipitated in diethyl ether and purified using RP-HPLC on a Kinetex 5μ XB-C18 250 x 4.6 mm prep column. The purified secondary ligands were clicked to cyclized Wells peptide in solution using 2x molar excess of secondary, 10x Cu(I) iodide, 50x L-ascorbic acid, and 4x Tris[(1-benzyl-1*H*-1,2,3-triazol-4-yl)methyl]amine (TBTA) (Sigma-Aldrich, St. Louis, MO) in 5:1 NMP:dH₂O and stirring overnight at room temperature. The clicked biligand products were purified from the reaction mixture by RP-HPLC on a C18 semi prep column.

1,5 Triazole linked WA

The anchor peptide was synthesized C → N omitting Pra on 200-300 mgs of Biotin NovaTag resin (EMD Biosciences, San Diego, CA) with a Titan peptide synthesizer using standard Fmoc chemistry [4]. A pre-clicked Fmoc protected 1,5 triazole Pra-Az₄ small molecule linker (InDi Molecular) was amide coupled to the N-terminal Asp of Wells

peptide, which after Fmoc deprotection served as the starting point for the synthesis of the secondary ligand. The finished peptide was side-chain deprotected and cleaved from resin in a mixture of 95% v/v trifluoroacetic acid (TFA) (Sigma-Aldrich, St. Louis, MO), 5% v/v dH₂O, and 5% triethylsilane (TES) (Sigma-Aldrich, St. Louis, MO), and precipitated in diethyl ether. Cu(Phen)₃ stock solution was prepared by mixing 150 mM Cu(II) sulfate pentahydrate (Sigma-Aldrich, St. Louis, MO) and 500 mM 1,10-phenanthroline (Sigma-Aldrich, St. Louis, MO) in 4:1 H₂O:Ethanol. The ether-precipitated ligand was cyclized by stirring the cleaved peptides dissolved in ~5 mL acetonitrile (ACN) overnight with 1 mL of the Cu(Phen)₃ stock solution. The cyclization mixtures were lyophilized, and the final peptide product was purified using reverse phase (RP) HPLC on a C18 prep column (Phenomenex, Torrance, CA).

B.7.4 Click Cyclized Wells Synthesis

The anchor Wells peptide was synthesized C → N, including N-terminal PEG and biotin, on 200-300 mgs of Rink amid resin (AnaSpec, Fremont, CA) with a Titan peptide synthesizer using standard Fmoc chemistry [4]. The synthesis used Fmoc and side chain protected L amino acids (Aaptec, Louisville, KY), Fmoc protected propargylglycine (Pra) (Aaptec, Louisville, KY), Fmoc protected (D) and (L) azidoalanine (Iris Biotech, Germany), PEG₅ (EMD Millipore, Germany), and biotin (Sigma-Aldrich, St. Louis, MO). The finished peptide was side-chain deprotected and cleaved from resin in a mixture of 95% v/v trifluoroacetic acid (TFA) (Sigma-Aldrich, St. Louis, MO), 5% v/v dH₂O, and 5%

triethylsilane (TES) (Sigma-Aldrich, St. Louis, MO), and precipitated in diethyl ether. A Cu(I) click cyclization solution was prepared by mixing 10x Cu(I) iodide, 50x L-ascorbic acid, and 4x Tris[(1-benzyl-1*H*-1,2,3-triazol-4-yl)methyl]amine (TBTA) (Sigma-Aldrich, St. Louis, MO) in 5:1 NMP:dH₂O. The ether-precipitated ligands were cyclized by stirring the cleaved peptides dissolved in ~2 mL Cu(I) click solution. The clicked biligand products were purified from the reaction mixture by RP-HPLC on a C18 semi prep column.

B.7.5 Assays

Biligand binding ELISA

Biotinylated WA, WG, and Wells peptides were immobilized on streptavidin-coated 96-well plates (Thermo Scientific Pierce, Rockford, IL) at a concentration of 400 nM in TBS. The plates were blocked with 5% w/v dry milk in TBS, and then the anchor peptides were incubated with varying concentrations of Fc in 0.5% w/v dry milk in TBS at room temperature for 1 hr. Bound antibody was probed with horseradish peroxidase (HRP)-conjugated mouse monoclonal antibody to human IgG Fc (Abcam, Cambridge, MA), diluted 1:10,000 in 0.5% w/v dry milk in TBS for 1 hr at room temperature. The colorimetric assay was developed with TMB substrate (KPL, Gaithersburg, MD), then quenched with 1 M H₂SO₄ and read at 450 nm.

1,5 triazole linked biligand binding ELISA

Biotinylated 1,5 triazole linked WA peptide was immobilized on streptavidin-coated 96-well plates (Thermo Scientific Pierce, Rockford, IL) at a concentration of 300

nM in TBS. The plates were blocked with 5% w/v dry milk in TBS, and then the anchor peptides were incubated with varying concentrations of Fc in 0.5% w/v dry milk in TBS at room temperature for 1 hr. Bound antibody was probed with horseradish peroxidase (HRP)-conjugated mouse monoclonal antibody to human IgG Fc (Abcam, Cambridge, MA), diluted 1:10,000 in 0.5% w/v dry milk in TBS for 1 hr at room temperature. The colorimetric assay was developed with TMB substrate (KPL, Gaithersburg, MD), then quenched with 1 M H₂SO₄ and read at 450 nm.

Click cyclized Wells ELISA

Biotinylated Cu(I) click cyclized Wells peptide was immobilized on streptavidin-coated 96-well plates (Thermo Scientific Pierce, Rockford, IL) at a concentration of 1 μM in TBS. The plates were blocked with 5% w/v dry milk in TBS, and then the anchor peptides were incubated with 500 nM of Fc in 0.5% w/v dry milk in TBS at room temperature for 1 hr. Bound antibody was probed with horseradish peroxidase (HRP)-conjugated mouse monoclonal antibody to human IgG Fc (Abcam, Cambridge, MA), diluted 1:10,000 in 0.5% w/v dry milk in TBS for 1 hr at room temperature. The colorimetric assay was developed with TMB substrate (KPL, Gaithersburg, MD), then quenched with 1 M H₂SO₄ and read at 450 nm.

B.8 CONCLUSION

Described in this appendix is an attempt to improve the previously discovered Fc binding peptide Fc-III in terms of affinity, selectivity, and stability. While a number of approaches were taken, the performance of the original Wells anchor peptide was not significantly improved. Preliminary immunoprecipitation data (not shown) indicated possible selectivity enhancement, but was not verified. The lack of improvement of Wells peptide with the addition of a secondary ligand may reflect the increased dwell time that such a strong binder has with its target during a screen; there are less significant constraints on the nature of the secondary ligand that clicks to the anchor in the *in situ* process due to the relatively constant presence of the anchor ligand at the target binding site.

B.9 ACKNOWLEDGEMENTS

This work was done in collaboration with Steven Millward, Kaycie M. Deyle, Errika Romero.

B.10 REFERENCES

1. DeLano WL, Ultsch MH, Wells JA (2000) Convergent solutions to binding at a protein-protein interface. *Science* 287: 1279-1283.
2. Lowman HB, Chen YM, Skelton NJ, Mortensen DL, Tomlinson EE, et al. (1998) Molecular mimics of insulin-like growth factor 1 (IGF-1) for inhibiting IGF-1: IGF-binding protein interactions. *Biochemistry* 37: 8870-8878.
3. Millward SW, Henning RK, Kwong GA, Pitram S, Agnew HD, et al. (2011) Iterative in situ click chemistry assembles a branched capture agent and allosteric inhibitor for Akt1. *J Am Chem Soc* 133: 18280-18288.
4. Fields GB, Noble RL (1990) Solid phase peptide synthesis utilizing 9-fluorenylmethoxycarbonyl amino acids. *International journal of peptide and protein research* 35: 161-214.

Appendix C

Algorithm for Peptide Clustering

C.1 INTRODUCTION

The one-bead-one-compound *in situ* click screening approach often yields a number of peptide “hits.” Rather than synthesizing and vetting each individual sequence, it can be useful to group the results into clusters of peptides based on physical properties, and then to choose a representative peptide from each cluster to scale up and test. This appendix provides an example clustering algorithm that uses the concept of persistence homology to group peptides by hydrophobicity, isoelectric point, and residue weight. The grouping is amino acid order dependent.

C.2 PERSISTENCE CLUSTERING

Persistence states that structures that persist at multiple scales are most likely to be real. For example, if an image is sampled by using a small number of points, persistence can be used to determine properties of the original shape. The points are grouped by drawing a disc of radius ϵ around each point. Each collection of overlapping discs is considered a cluster. These clusters provide one possible interpretation of the original data.

To obtain a more complete analysis of the data, ϵ is continuously varied and the clusters tracked as the discs grow around the points. As discs from one cluster begin to overlap with discs from another cluster, the two initial clusters “die” and a new merged cluster is “born.” The lifetime of a cluster is the time between a cluster’s birth and death. Thus, groups of points that are far from other points will have a long lifetime, which indicates that they are more meaningful clusters.

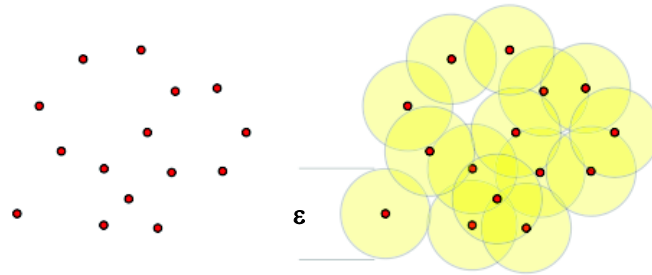


Figure C.1. Discs formed around points with growing radius ε . As the discs around points overlap, new clusters form that include points rooting the newly touching discs. Eventually all the discs will touch, and the cluster containing all points will continue for infinite “time.” Adapted from [1].

C.3 ALGORITHM DESCRIPTION

The MatLab function BasicParam takes as input text files that contain a list of sequences and the number n of amino acids per sequence. It then uses hydrophobicity, isoelectric point, and residue weight to construct a point in $3n$ dimensional for each sequence. To prevent any of the physical parameters from overly contributing to the clustering based on their absolute amounts, they are all scaled by the inverse of their average. Once each sequence is represented by a point, the Euclidian pair wise distances between the points are computed. Initially, each point is its own cluster. Then, the two points with the smallest pair wise distance are merged. The time of death of the initial point clusters, and the time of birth of the new merged cluster, is set to the distance between those two points (see Figure B.2). Clusters containing points with the next least distance continue to iteratively merge until all points in the data set exist as a single cluster. Additionally, a covariance matrix was constructed and diagonalized to find the eigenvectors and eigenvalues that characterize the sequence space.

C.4 OUTPUT

The function outputs a list of clusters and their associated lifetimes, along with a plot of the input sequences projected onto the top two eigenvectors. The complete list of eigenvectors is also plotted against the associated eigenvalues, and the top four eigenvectors are decomposed into their individual components as charts. The output from clustering the hits obtained in the A22/4B3 screen described in Chapter 2 is shown in Table B.1 and Figures B.3 – B.5.

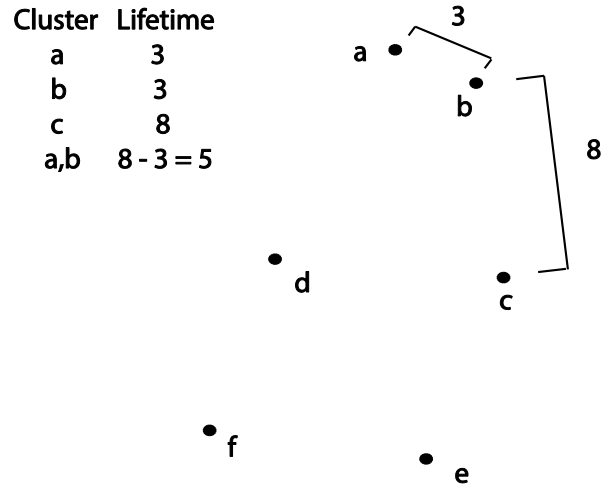


Figure C.2. Illustrative example of how lifetimes of clusters are computed. The lifetimes of clusters “a” and “b” are 3, because they are closer to each other than any other point and that is the distance between them. 3 then becomes the birth time for cluster “ab,” and the lifetime of “ab” is 5 because it dies at time 8, when the cluster “abc” is born.

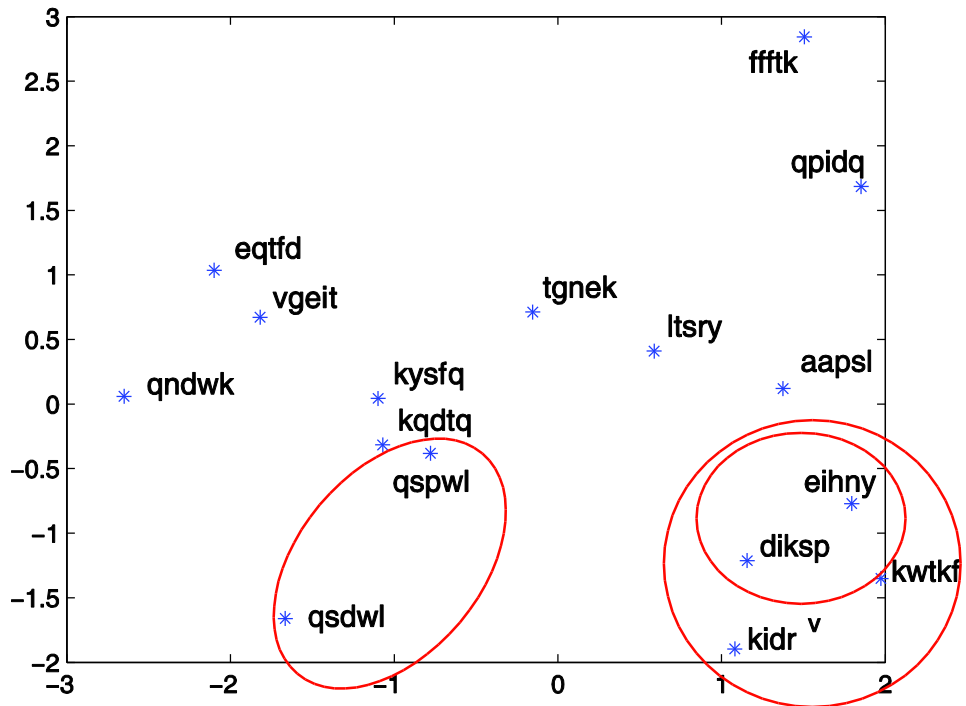


Figure C.3. Projection of the peptide “points” onto the top two eigenvectors taken from the diagonalization of the covariance matrix. The clusters containing more than one point with the three longest lifetimes from Table B.1 are circled.

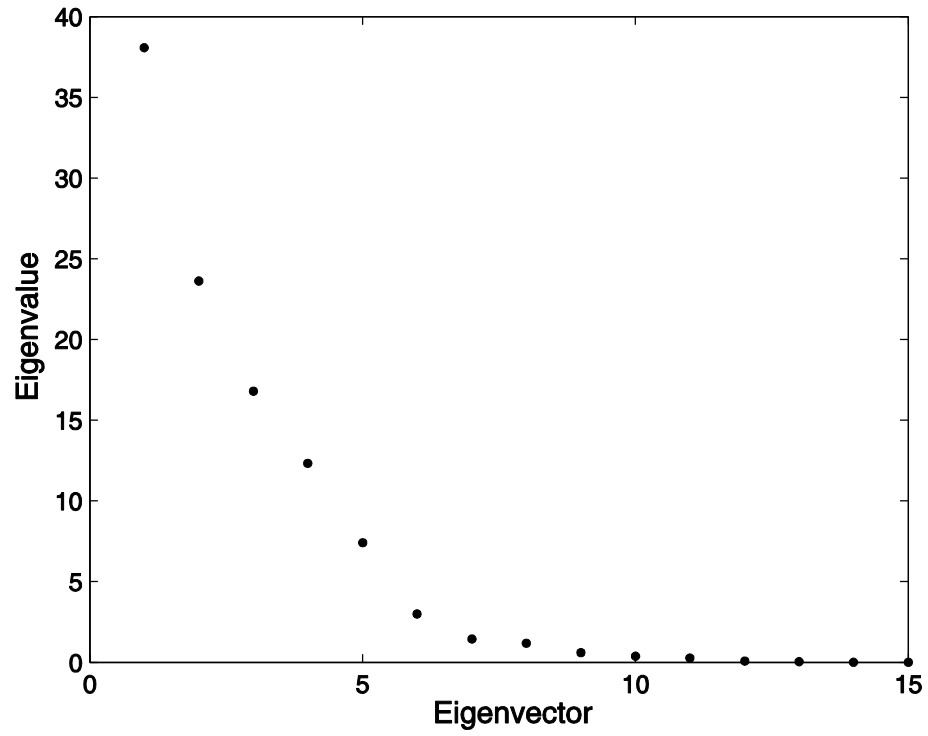


Figure C.4. Plot of eigenvectors vs. their associated eigenvalues. This allows users to know how many relevant eigenvectors describe the set of input peptides.

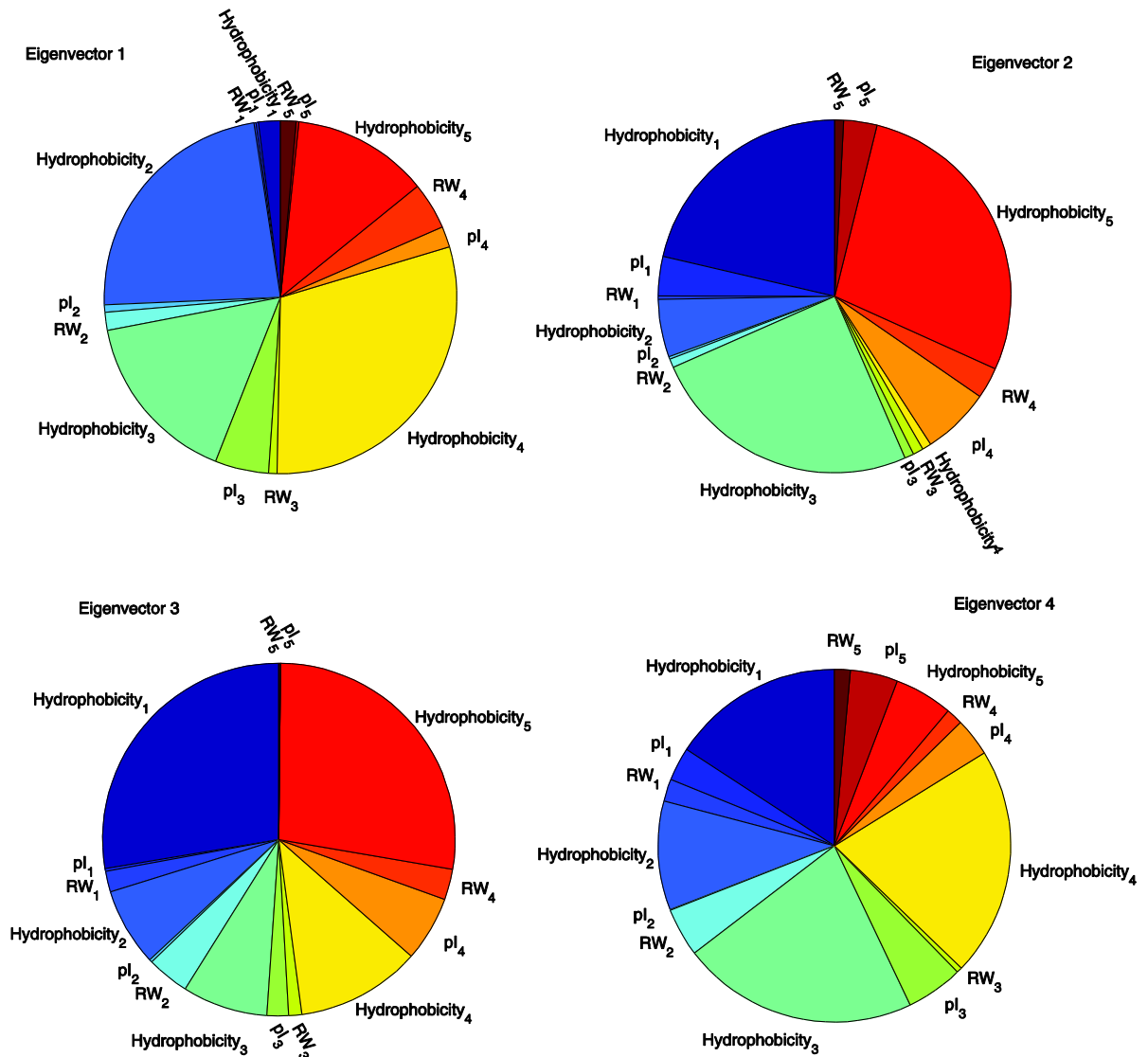


Figure C.5. Visual representation of the components of the top four eigenvectors. This shows what physical characteristics are dominant when describing the list of input peptides. The order of the amino acids is preserved during clustering, so Hydrophobicity₁ refers to the hydrophobicity of the N-terminal amino acid of the peptides. For this set, the top four eigenvectors have large hydrophobicity components, though not all from the same amino acid index.

C.5 FUNCTION CODE

```

function BasicParam(filename, pepLength)

%Feb 8, 2013
%Physical parameters come from the wwHydrophobicity scale, Sigma PI
values,
%and residue weight.
%Note: hydrophobicities are at pH 7 except for proline, which was
estimated
%from an InDi (or AN SD) measurement
%Note: the number of traits is hard coded in, so that has to be changed
%every time you mess with the parameters.

%http://www.sigmaaldrich.com/life-science/metabolomics/learning-
center/amin
%o-acid-reference-chart.html

Hydr =
1/((41+49+55+31+100+0+8+99+23+97+74+28+50+10+14+5+13+76+97+63)/20);
PI =
1/((6+5.07+2.77+3.22+5.48+5.97+7.59+6.02+9.74+5.98+5.74+5.41+6.3+5.56+1
0.76+5.68+5.6+5.96+5.89+5.66)/20);
RW =
1/((71.08+103.15+115.09+129.12+147.18+57.05+137.14+113.16+128.18+113.16
+131.2+114.11+97.12+128.13+156.19+87.07+101.11+99.13+186.22+163.18)/20)
;
scaling = [Hydr PI RW];
%scaling = 1;

%[Hydrophobicity pI ResidueWeight]

A = [41 6.00 71.08].*scaling;
C = [49 5.07 103.15].*scaling;
D = [-55 2.77 115.09].*scaling;
E = [-31 3.22 129.12].*scaling;
F = [100 5.48 147.18].*scaling;
G = [0 5.97 57.05].*scaling;
H = [8 7.59 137.14].*scaling;
I = [99 6.02 113.16].*scaling;
K = [-23 9.74 128.18].*scaling;
L = [97 5.98 113.16].*scaling;
M = [74 5.74 131.20].*scaling;
N = [-28 5.41 114.11].*scaling;
P = [50 6.30 97.12].*scaling;
Q = [-10 5.56 128.13].*scaling;
R = [-14 10.76 156.19].*scaling;
S = [-5 5.68 87.07].*scaling;
T = [13 5.60 101.11].*scaling;
V = [76 5.96 99.13].*scaling;
W = [97 5.89 186.22].*scaling;
Y = [63 5.66 163.18].*scaling;

%Read in sequences from text file function argument, and determine the

```

```

%numberof sequences
sequences = textread(filename, '%s', -1);
nseq = length(sequences);

%Initialize matrix to hold each sequence vector
ntrait = 3;
Z=zeros(nseq,pepLength*ntrait);

%For each individual sequence assign a vector based on Grantham Values
for j = 1:nseq
    seq = sequences{j};
    o = [];

    for i=1:length(seq)

        switch seq(i)
            case 's'
                o = [o S];
            case 'r'
                o = [o R];
            case 'l'
                o = [o L];
            case 'p'
                o = [o P];
            case 't'
                o = [o T];
            case 'a'
                o = [o A];
            case 'v'
                o = [o V];
            case 'g'
                o = [o G];
            case 'i'
                o = [o I];
            case 'f'
                o = [o F];
            case 'y'
                o = [o Y];
            case 'c'
                o = [o C];
            case 'h'
                o = [o H];
            case 'q'
                o = [o Q];
            case 'n'
                o = [o N];
            case 'k'
                o = [o K];
            case 'd'
                o = [o D];
            case 'e'
                o = [o E];
            case 'm'
                o = [o M];
            case 'w'
                o = [o W];
        end
    end
end

```

```

    end

    end
    Z(j,:) = 0;
end

%Compute pairwise distances between each "sequence point" given by
%a row in the Z matrix and put in array n. Also, create a 2x#pairs
matrix
%cataloging pair indices to go along with distances.
n=[];
Idx=[];
k=1;
for i = 1:nseq
    for j = i+1:nseq
        n(k) = norm(Z(i,:)-Z(j,:));
        Idx(1,k) = i;
        Idx(2,k) = j;
        k=k+1;
    end
end

%Sort the array of distances from smallest to largest and use returned
%permutation to analogously sort pair indices.
[N,O] = sort(n);
Idx = Idx(:,O);

%Create array of parents of "sequence points"
p = [1:nseq];

%Create an array of cluster birth
tb = zeros(1,nseq);

% %Union the points with distance smaller than 200
% for k = 1:length(N)
%     if(N(k)>= 200)
%         %sprintf('stopping at distance %f\n', N(k))
%         break;
%     end
%     %sprintf('Unioning %f and %f with distance
%f\n',Idx(1,k),Idx(2,k),N(k))
%     p = Union(Idx(1,k),Idx(2,k),p);
% end

% '%Find' all points to see which ones share a root after Union and put
into
% %array 'root'
% for i = 1:nseq
%     j = Find(i,p);
%     root(i) = j;
% end

% [R,O_r] = sort(root);
% sequences(O_r);

```

```

%Iteratively 'Union' clusters containing the points with the next
%least distance

sets = {};
ages = [];
birth = [];
death = [];
for i = 1:length(N)

    %Find roots of the two sets being joined
    r1 = Find(Idx(1,i),p);
    r2 = Find(Idx(2,i),p);

    %Set the current time to the distance between the two merging
clusters
    t = N(i);

    %Check if the two sequences are already in the same cluster
    if r1 ~= r2

        %Save the sequences in the two merging clusters
        %disp('=====');
        set1 = MkSet(r1,nseq,p,sequences);
        set2 = MkSet(r2,nseq,p,sequences);

        sets(end+1) = {set1};
        sets(end+1) = {set2};

        %Compute and save the ages of the merging clusters
        age1 = t - tb(r1);
        age2 = t - tb(r2);

        ages = [ages age1];
        ages = [ages age2];

        %Keep running tally of birth/death times for persistence barcode
        birth = [birth tb(r1)];
        birth = [birth tb(r2)];

        death = [birth t];
        death = [birth t];

        %Union the two clusters
        p = Union(Idx(1,i),Idx(2,i),p);

        %Save birth time for new cluster
        tb(r2) = t;

    end
end
birth;
death;
%Sort ages from largest to smallest, accordingly rearrange sets of
%sequence names

```

```

[Ages,O_A] = sort(ages, 'descend');
Sets = sets(O_A);

%Read out vectors of ages and sets
disp('-----')
%DispSet(sets, ages);
% disp('-----')
DispSet(Sets, Ages);
disp('-----')

%Plot "persistence barcode" to see if any clustering is actually
present

%Do PCA analysis to see if there exist any major axes along which the
%sequence data falls.

m = size(Z);

%Center data
center = zeros(1,m(2));
for i = 1:nseq
center = center + Z(i,:);
end
center = center/nseq;
Zc = zeros(m);
for i = 1:nseq
Zc(i,:) = Z(i,:) - center;
end

%Create covariance matrix
covar = zeros(m(2), m(2));
CoVar = zeros(m(2), m(2));
for i = 1:nseq
    covar = Zc(i,:)'*Zc(i,:);
    CoVar = CoVar + covar;
end

%Diagonalize covariance matrix to find largest eigenvalues and
%corresponding eigenvectors
[vec,val] = eig(CoVar);
CoVar*vec - vec*val;

%Plot eigenvalues and display eigenvectors associated with two largest
%values. Also label eigenvectors with next two largest eigenvalues to
%decompose into pie charts to examine components.
Diagval = diag(val);
[Val,O_val] = sort(Diagval, 'descend');
Vec = vec(:,O_val);
plot(Val, '.k', 'MarkerSize',10);
eig1 = Vec(:,1); eig2 = Vec(:,2); eig3 = Vec(:,3); eig4 = Vec(:,4);

%Project sequence points onto the two largest eigenvectors and plot
Projection(Vec(:,1), Vec(:,2), Zc, sequences, nseq);

```

```

%Create pie chart to examine the components of the four eigenvectors
with
%the largest eigenvalues
labels = {'Hydrophobicity_1', 'pI_1', 'RW_1', 'Hydrophobicity_2',
'pI_2', ...
        'RW_2', 'Hydrophobicity_3', 'pI_3', 'RW_3', 'Hydrophobicity_4',
'pI_4', ...
        'RW_4', 'Hydrophobicity_5', 'pI_5', 'RW_5'};
figure
pie(abs(eig1), labels)
title('Eigenvector 1')

figure
pie(abs(eig2), labels)
title('Eigenvector 2')

figure
pie(abs(eig3), labels)
title('Eigenvector 3')

figure
pie(abs(eig4), labels)
title('Eigenvector 4')

end

%-----
--%

function y = Find(x,p)
    y = x;
    while(p(y)~=y)
        y = p(y);
    end
end

function p = Union(x1,x2,p)
    r1 = Find(x1,p);
    r2 = Find(x2,p);
    p(r1) = r2;
end

function Set = MkSet(r1,nseq,p,seq)
    Set = {};
    for i = 1:nseq
        r = Find(i,p);
        if r == r1
            Set(end+1) = seq(i);
        end
    end
end

function DispSet(Sets, Ages)

```

```

for i = 1:length(Sets)
    Si = Sets{i};
    str = sprintf('%f\t', Ages(i));
    for j=1:length(Si)
        str = sprintf('%s %s\t', str, char(Si{j}));
    end
    disp(str);
end
end

function Projection(eig1, eig2, Zc, sequences, nseq)
x = [];
y = [];
for i = 1:nseq
    x = [x Zc(i, :)*eig1];
    y = [y Zc(i, :)*eig2];
end
figure;
plot(x, y, '*')
dx = .2; dy = 0.2;
text(x+dx, y+dy, sequences);
end

```

C.6 CONCLUSION

This appendix describes a clustering algorithm designed to help characterize groups of peptide hits from *in situ* click screens. The objective is to provide guidance about which peptides are useful to scale up and assay, and give information about the physical characteristics that predominately describe the differences between input peptides.

C.7 ACKNOWLEDGEMENTS

I would like to thank Keenan Crane for introducing me to the concept of persistent homology, and for his incredibly helpful guidance while developing this algorithm.

C.8 REFERENCES

1. Ghrist R (2008) Barcodes: the persistent topology of data. *Bulletin of the American Mathematical Society* 45: 61-75.

Appendix D

A cocktail of thermally stable, chemically synthesized capture agents for the efficient detection of anti-gp41 antibodies from human sera

A Cocktail of Thermally Stable, Chemically Synthesized Capture Agents for the Efficient Detection of Anti-Gp41 Antibodies from Human Sera

Jessica A. Pfeilsticker^{1,3}, Aiko Umeda^{1,3}, Blake Farrow², Connie L. Hsueh¹, Kaycie M. Deyle¹, Jocelyn T. Kim³, Bert T. Lai⁴, James R. Heath^{1*}

1 Division of Chemistry and Chemical Engineering, California Institute of Technology, Pasadena, California, United States of America, **2** Division of Engineering and Applied Sciences, Division of Biology, California Institute of Technology, Pasadena, California, United States of America, **3** Division of Biology, California Institute of Technology, Pasadena, California, United States of America, **4** Indi Molecular, Culver City, California, United States of America

Abstract

We report on a method to improve *in vitro* diagnostic assays that detect immune response, with specific application to HIV-1. The inherent polyclonal diversity of the humoral immune response was addressed by using sequential *in situ* click chemistry to develop a cocktail of peptide-based capture agents, the components of which were raised against different, representative anti-HIV antibodies that bind to a conserved epitope of the HIV-1 envelope protein gp41. The cocktail was used to detect anti-HIV-1 antibodies from a panel of sera collected from HIV-positive patients, with improved signal-to-noise ratio relative to the gold standard commercial recombinant protein antigen. The capture agents were stable when stored as a powder for two months at temperatures close to 60°C.

Citation: Pfeilsticker JA, Umeda A, Farrow B, Hsueh CL, Deyle KM, et al. (2013) A Cocktail of Thermally Stable, Chemically Synthesized Capture Agents for the Efficient Detection of Anti-Gp41 Antibodies from Human Sera. PLoS ONE 8(10): e76224. doi:10.1371/journal.pone.0076224

Editor: William R. Abrams, New York University, United States of America

Received: June 14, 2013; **Accepted:** August 13, 2013; **Published:** October 7, 2013

Copyright: © 2013 Pfeilsticker et al. This is an open-access article distributed under the terms of the Creative Commons Attribution License, which permits unrestricted use, distribution, and reproduction in any medium, provided the original author and source are credited.

Funding: This work was funded primarily by a grant from the Bill and Melinda Gates Foundation. Additional funding for the development of screening approaches, and for certain capture agent characterization methods, was provided by the Institute for Collaborative Biotechnologies through grant W911NF-09-0001 from the U.S. Army Research Office. The content of the information does not necessarily reflect the position or the policy of the Government, and no official endorsement should be inferred. The funders had no role in study design, data collection and analysis, decision to publish, or preparation of the manuscript.

Competing Interests: James R Heath is a founder and board member of Indi Molecular - Indi molecular was spun out of Integrated diagnostics recently, so a declaration of a competing interest with Indi Molecular is now more appropriate. Indi Molecular is seeking to commercialize the PCC Agent technology. Bert T.Lai is an employee of Indi Molecular. Associated patents are pending. A patent has been filed (not issued) that is related to the capture agent development approach utilized in this paper (PCT/US09/47799/WO2009155420). This does not alter the authors' adherence to all the PLOS ONE policies on sharing data and materials, as detailed online in our guide for authors.

* E-mail: heath@caltech.edu

These authors contributed equally to this work.

Introduction

Detecting the immune response to an infectious agent can provide a useful *in vitro* diagnostic surrogate relative to direct pathogen detection [1]. Such assays are commonly used for detecting HIV infection because of its characteristic immunopathology [2]. Direct detection of HIV viral RNA and p24 antigen is only effective at an early stage of infection, approximately 2–6 weeks of initial exposure [3,4]. Antibodies against HIV envelope proteins emerge in patients' blood around 3–4 weeks of infection [2,5] as the viral RNA and p24 levels decline as a result of immunocomplex formation [6]. The high serum level of anti-HIV IgG is maintained throughout the course of clinical latency (2–20+ years), during which time viral antigens are under detection limits until the onset of acquired immunodeficiency syndrome (AIDS) [2,5]. Viral load and CD4⁺ cell counts are mainly used for prognostic purposes to monitor the efficacy of treatments; however viral load is sometimes used for the diagnosis of infant HIV infections where antibody-based assays are not applicable [3,7]. Assays for anti-HIV antibodies are the most widely used diagnostic test both in cases where infection is presumed to have occurred more than 6 weeks prior to testing, and for epidemiological

reasons, to estimate the incidence of HIV in a population [8], since, with the exception of infant HIV, virtually 100% of the infected individuals express these antibodies [3]. Typically in these assays, immunogenic and conserved antigens from the HIV are expressed as regions of a single chimeric protein. That chimeric protein is then used to capture specific antibodies from the body fluid (e.g. blood, saliva or urine) of potentially infected patients; a positive assay result implies infection. However, the polyclonal diversity of antibodies across a patient population can translate into large variations in assay performance from patient to patient. In addition, the chimeric recombinant proteins are biological reagents, and so may have limitations related to shelf life and batch-to-batch variability. These limitations can adversely influence the performance of a diagnostic test [3,5,9], especially one that is deployed in harsh physical environments.

Here we report on the use of iterative *in situ* click chemistry [10,11] to prepare a cocktail of chemically synthesized capture agents (called protein-catalyzed capture agents, or PCC Agents) that is designed to sample the polyclonal diversity of an antibody-based immune response. We demonstrate the concept by developing a PCC Agent-based assay designed to detect human antibodies that bind to a conserved region of the HIV-1 envelope

glycoprotein gp41. The performance of that assay is compared against the gold standard chimeric protein antigen using sera collected from a cohort of HIV-1-positive human subjects, plus controls. We also report on the thermal stability of the capture agent cocktail, with an eye towards point-of-care HIV diagnostics assays that are needed in environments where refrigeration chains may not exist.

Materials and Methods

For detailed protocols see **Materials and Methods S1**.

Ethics Statement

All study documents and procedures regarding the patient serum assays were approved by the UCLA and Caltech Institutional Review Boards. All subjects provided written informed consent prior to initiation of study procedures.

Results and Discussion

The development of a PCC Agent against a protein target utilizes the target itself to promote the 1,3-dipolar cycloaddition between an acetylene and an azide group to form a triazole linkage (the *in situ* ‘click’ reaction) [12]. The protein effectively plays the role of an extremely selective, but much less efficient, variant of the Cu(I) catalyst that is commonly used for such couplings [13,14]. For the present work, the two reacting species are peptides – one peptide (the anchor) is a chemically modified variant of a conserved, immunogenic epitope on the HIV-1 gp41 protein, and the second peptide is selected via an *in situ* click screen from a large (10^6 element) one-bead-one-compound (OBOC) [15] peptide library. The protein targets are human monoclonal antibodies raised against variants of the gp41 epitope represented by the anchor peptide.

The PCC Agents developed here were designed to capture antibodies that are selective for residues 600–612 (IWCGSGK-LICTTA) of gp41. Previous studies have shown that a large fraction of HIV-1-positive patients develop antibodies against this epitope [16,17]. Our strategy for sampling the polyclonal diversity of such antibodies was to develop PCC Agents that exhibited both differential, as well as similar avidities for human monoclonal antibodies (mAbs) raised against different parts of this epitope. A key decision in this regard involves the selection of the anchor peptides from which the PCC Agents are developed. For this task, we modified the polypeptide fragment corresponding to residues 600–612 of gp41 with artificial amino acids at multiple locations, and tested the ability of these modified peptides to detect two different monoclonal anti-gp41 antibodies 3D6 and 4B3 (Polymun, Klosterneuburg, Austria). The 3D6 mAb was raised against the epitope SGKLIIC, whereas the 4B3 mAb was raised against SGKLICTTA. One anchor peptide, A21, was synthesized by adding a propargyl glycine (Pra) residue at the C-terminus of the residues 600–612 of gp41. This anchor peptide was also N-terminally tagged with a polyethylene glycol (PEG) oligomer bridge and a biotin label. For a second anchor peptide (A22), Leu-607 was substituted with Pra. A22 also included an N-terminal PEG-biotin label. A21 equally detected 3D6 and 4B3 with an estimated dissociation constant (K_d) of 1–50 nM, while A22 differentially detected 3D6 ($K_d > 10 \mu\text{M}$) and 4B3 ($K_d = 1–50 \text{ nM}$) (**Figure S1** in Supporting Information). A21 and A22 were then separately developed into PCC agents against 3D6 and 4B3, respectively.

The *in situ* click screens are illustrated in **Figure 1**. The target IgG is incubated with an excess of the selected anchor peptide and

a large OBOC library at 4°C overnight (see **Materials and Methods S1**). The OBOC library is synthesized on TentGel resin (Rapp Polymere, Tuebingen, Germany), and is a comprehensive library of 5-mers with a 6th amino acid at the N-terminus presenting an azide functionality. To help ensure chemical and biochemical stability, the OBOC library is comprised of non-natural (D) stereoisomers of the 20 natural amino acids, excluding cysteine and methionine. The *in situ* screen is designed to identify a secondary (2°) peptide that, when coupled to the anchor, forms a biligand with increased selectivity and/or affinity for the target IgG. The screen proceeds stepwise. In the first step (not shown in **Figure 1**) the OBOC library is cleared of beads that exhibit non-specific binding to alkaline phosphatase-conjugated streptavidin (SA-AP), which is used as a detection reagent in a later step. Step 2 is a target screen, and so is designed to detect the presence of the bound IgG target to specific beads, and defines possible hits. The step 3 screen is designed to remove those beads from the pool of potential hits that also exhibit binding to off-target serum proteins. Step 4 is called a product screen, and is unique to sequential *in situ* click screens [11]. This screen is designed to detect for the presence of *in situ* clicked reaction products, which are those hit beads containing the triazole-linked anchor peptide. Typically, Step 2 yields a few hundred hits (~0.05% of the OBOC library). Step 3 reduces that pool by a factor of 2 or 3 to about 100 hits, and Step 4 further reduces the number of hits to around 10. This is a manageable number, meaning that each hit can be separately synthesized as a biligand using Cu(I) catalyzed click chemistry to couple the anchor and 2° peptides. The performance of these biligands is then characterized using immunoprecipitation (pull-down) assays detected by Western blotting from spiked serum samples for specificity (data not shown), and sandwich ELISAs and surface plasmon resonance (SPR) assays for affinity estimations (**Figure S2**, **Figure S3**). A complete list of the hits for the A21/3D6 and A22/4B3 screens is given in **Table S1**. This approach yielded two equivalently performing biligands against 3D6, and one biligand against 4B3 (**Figures S2**, **Figure S3**). These three PCC agents (**Figure 2**) were combined, in equal parts, to form a capture agent cocktail. The cocktail slightly outperformed both the standard commercial chimeric antigen and A21, when tested against healthy human serum spiked with both 3D6 and 4B3 (**Figure S4**). A21 is the equivalent of the original antigenic epitope of gp41.

The PCC Agent cocktail and the standard antigen were co-evaluated against a panel of clinical samples using sandwich ELISAs. Serum samples were collected from nine HIV-1-positive patients in Southern California. The standard antigen is a recombinant chimeric protein containing a fragment of HIV-1 gp41 (residues 546–692), the ‘O’ group HIV-1 gp41 immunodominant region (residues 580–623), and a fragment of HIV-2 gp36 (residues 591–617). A good performance of this chimeric antigen has been reported elsewhere [18]. For the comparison assays, streptavidin-coated 96-well plates were saturated with the PCC Agent cocktail or chemically biotinylated chimera in triplicates. Serum samples were diluted to 1% v/v in Tris-buffered saline (TBS) supplemented with 0.1% w/v bovine serum albumin (BSA), and incubated in the wells for 1 hr at room temperature. Unbound proteins were washed off and captured IgG was detected with a peroxidase-conjugated mouse monoclonal anti-human IgG-Fc antibody. The comparison assay results for the patient serum samples along with a healthy control are shown in **Figure 3A**. The signal-to-noise (S/N) ratio in these assays is defined as the measured ELISA signal for a given patient sample, divided by that for the healthy control. The PCC Agent cocktail performed at least as well, and typically much better, than the standard chimeric

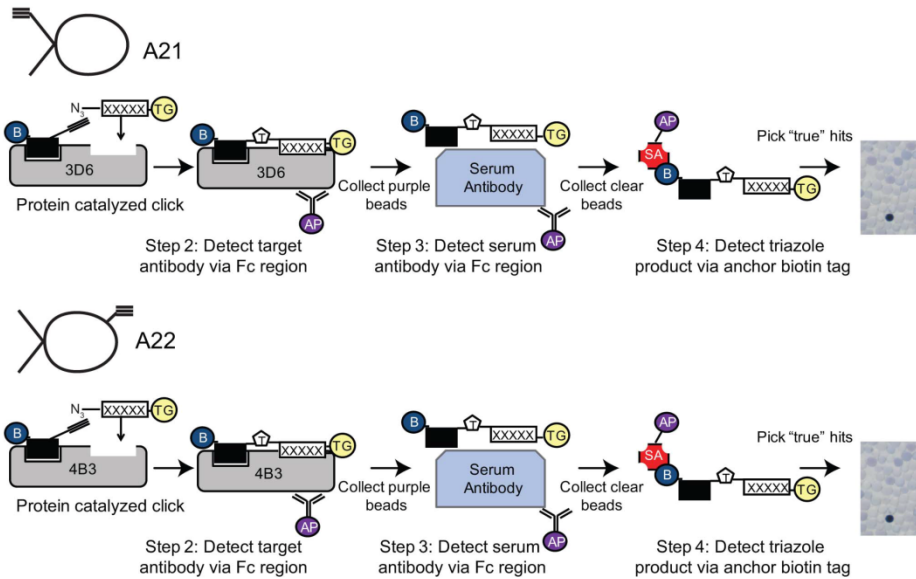


Figure 1. Screening strategy for selecting capture agents against anti-HIV antibodies 3D6 and 4B3. The flow chart represents the use of the A21 and A22 cyclic peptides as anchor ligands for separate *in situ* click screens against a large OBOC azide-presenting peptide library. doi:10.1371/journal.pone.0076224.g001

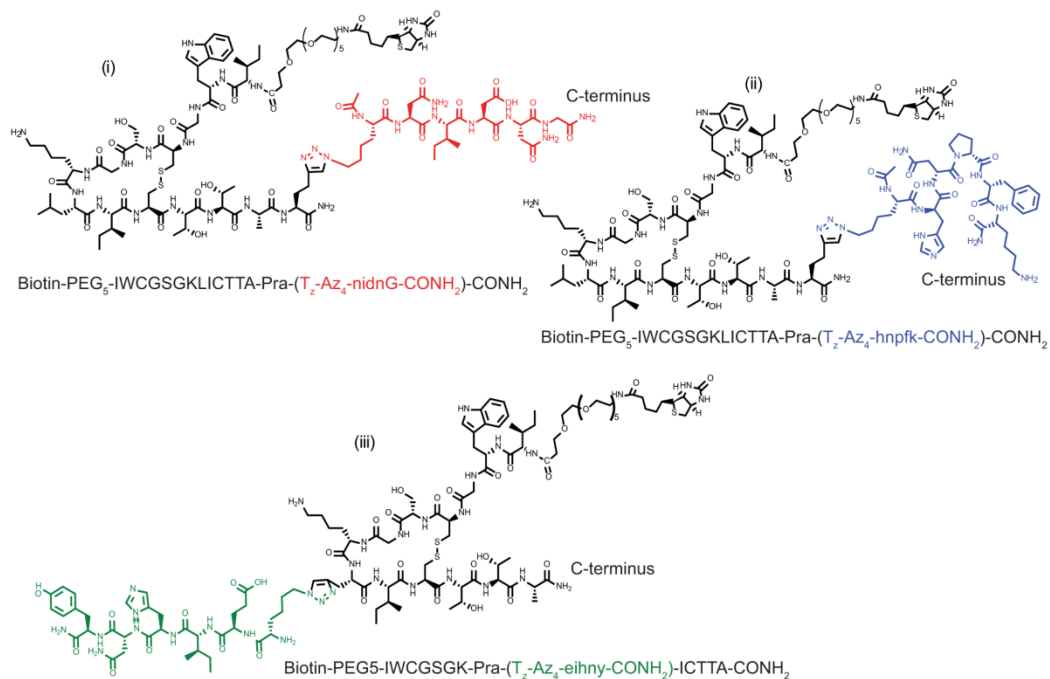


Figure 2. Structures of peptide ligands in PCC Agent cocktail. Acetylene-presenting anchor peptides (black) were derived from the immunogenic epitope of HIV-1 gp41 (residues 600–612). A22-nidnG (i) and A21-hnpfk (ii) were evolved from the original epitope appended with Pra at the C-terminus whereas A22-eihny (iii) utilizes the “substituted” anchor where residue Leu-607 is replaced with Pra. Secondary ligand branches (colored) were identified from the *in situ* click screen of a 5-mer OBOC library presenting an azide functionality. Biligands (i) and (ii) were raised against the target anti-HIV antibody 3D6, and the biligand (iii) was raised against the antibody 4B3. doi:10.1371/journal.pone.0076224.g002

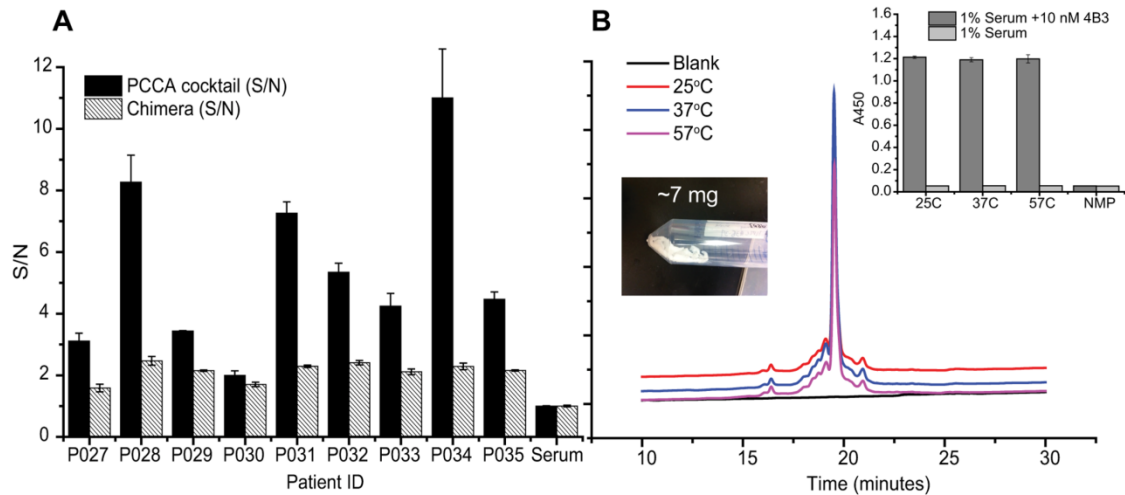


Figure 3. Performance of the PCC Agent cocktail, and thermal stability and scale up of a cocktail component. **A.** Comparative performance of the PCC Agent cocktail versus the commercial chimeric protein, using sandwich ELISAs to detect anti-HIV-1 IgGs from a panel of sera samples collected from nine HIV-positive patients. The absorbance at 450 nm (A450) for each sample is normalized against the A450 for the healthy control, to yield a measurement of the signal-to-noise ratio of the assay. The PCC Agent cocktail, which is designed to capture a subset of anti-gp41 IgGs, exhibits superior performance for every sample, even though the chimeric protein is designed to capture antibodies against multiple HIV-1-associated epitopes (those containing fragments of HIV-1 gp41, "O" group HIV-1 gp41 immunodominant region, and HIV-2 gp39). For the assays, the PCC agent cocktail and the biotinylated chimeric antigen were immobilized on a streptavidin-coated 96-well plate and incubated with diluted patient serum (1% v/v). Captured anti-HIV antibodies were detected using peroxidase-conjugated anti-human IgG antibody. **B.** Samples of (iii) were stored as a powder (inset photo), under N_2 at temperatures up to 57°C for ~2 months, and resolved by analytical HPLC to determine the presence of any degradation product. The HPLC traces reveal that the fingerprint of the PCC Agent is unchanged. The inset shows that the assay performance of the PCC Agent is also unaffected.
doi:10.1371/journal.pone.0076224.g003

protein antigen. The average S/N improvement by the cocktail PCC agent over the chimeric antigen was a factor of 2.5.

We then tested the PCC Agents for thermal stability. The PCC Agent cocktail component (iii) were synthesized at a large scale for an academic setting (~7 mg, Figure 3B) and the lyophilized samples were stored under N_2 at 25°C, 37°C, or 57°C for 58 days. The samples were then analyzed by HPLC to determine the presence of any degradation product. The traces of the peptide at each temperature are nearly identical, indicating little to no degeneration at these temperatures (Figure 3B). The performance of these stored PCC Agents was then also tested in an ELISA, with no detectable loss of performance (Figure 3B).

Conclusion

We describe here a method for developing a PCC Agent cocktail to capture the diversity of human antibodies generated in response to an infectious agent. We demonstrated the successful application of this method for HIV-1 diagnostics by producing a cocktail of three PCC Agents that detected the presence of anti-HIV antibodies in clinical samples with a significantly enhanced signal-to-noise relative to the standard, recombinant protein-based chimeric antigen. In a recent report, an antigenic peptide cocktail comprised of synthetic peptides derived directly from gp120/V3-I (HIV-1 Indian isolate), gp41 (HIV-1), and gp36 (HIV-2), as well as the recombinant protein rp24 (HIV-1) was shown to also provide superior performance relative to the chimeric antigen [19]. This points to the possibility that expanding the current approach by developing multiple cocktails of PCC Agents, each directed against a distinct HIV epitope, would likely provide superior performance to that reported here. The strategy presented provides a promising

approach for developing assays for detecting the immune response to other infectious agents, especially where challenges associated with the polyclonal nature of a humoral immune response can compromise assay sensitivity.

Supporting Information

Materials and Methods S1 Detailed experimental protocols. (DOCX)

Figure S1 Differential detection of 3D6 and 4B3 by anchor ligands. Relative affinities of A21 and A22 for 3D6 and 4B3 were determined by sandwich ELISA. Biotinylated anchor ligands A21 and A22 were immobilized on streptavidin-coated 96-well plated at a concentration of 100 nM, and incubated with the solutions of target anti-HIV antibodies 3D6 and 4B3 at 100 nM in TBS. Captured antibody was detected by peroxidase-conjugated anti-human IgG antibody. (TIFF)

Figure S2 Apparent affinity of A21 and biligands directed against 3D6 as determined by SPR. **A.** Sensorgram and 1st order Hill fit to affinity data for A21. **B.** Sensorgram and 1st order Hill fit to affinity data for A21-nidnG (i). **C.** Sensorgram and 1st order Hill fit to affinity data for A21-hnpfK (ii). (TIFF)

Figure S3 Apparent affinity of A22 and biligand directed against 4B3 as determined by SPR. **A.** Sensorgram and 1st order Hill fit to affinity data for A22. **B.** Sensorgram and 1st order Hill fit to affinity data for A22-eihny (iii). (TIFF)

(TIF)

Figure S4 Performance of PCC agent cocktail to detect 3D6 and 4B3 from human serum. Comparative performance of the PCC Agent cocktail versus the original gp41 epitope A21 and the commercial chimeric protein antigen was tested by a sandwich ELISA. Target antibodies 3D6 and 4B3 (4 nM each) were both spiked into diluted, HIV-free human serum (1% v/v in TBS), and captured antibody was detected by peroxidase-conjugated anti-human IgG antibody.

(TIF)

Table S1 Biligand screen results. List of pentapeptide “hits” from OBOC biligand screens performed with A21/3D6 and A22/4B3. The selected secondary ligands corresponding to (i), (ii), and (iii) are in bold.

References

1. Brachman PS (1996) In: Baron S, editor. *Medical Microbiology*. 4th ed. Galveston (TX).
2. Fanales-Belasio E, Raimondo M, Suligoi B, Butto S (2010) HIV virology and pathogenetic mechanisms of infection: a brief overview. *Ann Ist Super Sanita* 46: 5–14.
3. Alvarez M, Chueca N, Guillot V, Bernal Mdel C, Garcia F (2012) Improving Clinical Laboratory Efficiency: Introduction of Systems for the Diagnosis and Monitoring of HIV Infection. *Open Virol J* 6: 135–143.
4. Tebourski F, Slim A, Elgaaied A (2004) The significance of combining World Health Organization and Center for Disease Control criteria to resolve indeterminate human immunodeficiency virus type-1 Western blot results. *Diagn Microbiol Infect Dis* 48: 59–61.
5. Daskalakis D (2011) HIV diagnostic testing: evolving technology and testing strategies. *Top Antivir Med* 19: 18–22.
6. Butto S, Suligoi B, Fanales-Belasio E, Raimondo M (2010) Laboratory diagnostics for HIV infection. *Ann Ist Super Sanita* 46: 24–33.
7. Korenromp EL, Williams BG, Schmid GP, Dye C (2009) Clinical prognostic value of RNA viral load and CD4 cell counts during untreated HIV-1 infection—a quantitative review. *PLoS One* 4: e5950.
8. Iweala OI (2004) HIV diagnostic tests: an overview. *Contraception* 70: 141–147.
9. Ginocchio CC, Carman WF, Arens MQ (2011) Update on HIV diagnostic testing algorithms. Editors' introduction. *J Clin Virol* 52 Suppl 1: S1.
10. Agnew HD, Rohde RD, Millward SW, Nag A, Yeo WS, et al. (2009) Iterative in situ click chemistry creates antibody-like protein-capture agents. *Angew Chem Int Ed Engl* 48: 4944–4948.
11. Millward SW, Henning RK, Kwong GA, Pitram S, Agnew HD, et al. (2011) Iterative in situ click chemistry assembles a branched capture agent and allosteric inhibitor for Akt1. *J Am Chem Soc* 133: 18280–18288.
12. Huisgen R (1984) 1,3-Dipolar cycloaddition – introduction, survey, mechanism. In: Padwa A, editor. *1,3-Dipolar Cycloaddition Chemistry* Wiley. 1–176.
13. Thirumurugan P, Matosiuk D, Jozwiak K (2013) Click Chemistry for Drug Development and Diverse Chemical-Biology Applications. *Chem Rev*.
14. Finn MG, Fokin VV (2010) Click chemistry: function follows form. *Chem Soc Rev* 39: 1231–1232.
15. Lam KS, Lebl M, Krchnak V (1997) The “One-Bead-One-Compound” Combinatorial Library Method. *Chem Rev* 97: 411–448.
16. Du AP, Limal D, Semetey V, Dali H, Jolivet M, et al. (2002) Structural and immunological characterisation of heteroclitic peptide analogues corresponding to the 600–612 region of the HIV envelope gp41 glycoprotein. *J Mol Biol* 323: 503–521.
17. Xu JY, Gorny MK, Palker T, Karwowska S, Zolla-Pazner S (1991) Epitope mapping of two immunodominant domains of gp41, the transmembrane protein of human immunodeficiency virus type 1, using ten human monoclonal antibodies. *J Virol* 65: 4832–4838.
18. Chin CD, Laksanasopin T, Cheung YK, Steinmiller D, Linder V, et al. (2011) Microfluidics-based diagnostics of infectious diseases in the developing world. *Nat Med* 17: 1015–1019.
19. Tiwari RP, Jain A, Khan Z, Kumar P, Bhriju V, Bisen PS (2013) Designing of novel antigenic peptide cocktail for the detection of antibodies to HIV-1/2 by ELISA. *J Immun Meth* 387: 157–166.

(TIF)

Acknowledgments

We thank Prof. David Baltimore (California Institute of Technology) for the generous gift of HIV positive serum samples and the use of the HIV facility. We also thank Stella Ouyang for training and assistance with the serum samples. Additionally we thank Alex Sutherland for his helpful graphics software guidance.

Author Contributions

Conceived and designed the experiments: JAP AU BF JRH. Performed the experiments: JAP AU CLH KMD BF BTL. Analyzed the data: JAP AU BF CLH. Contributed reagents/materials/analysis tools: JAP AU CH JTK BF BL. Wrote the paper: JAP AU JRH.

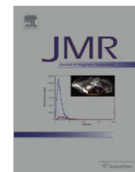
Appendix E

A Selective ^{15}N -to- ^1H Polarization Transfer Sequence for More Sensitive
Detection of ^{15}N -Choline



Contents lists available at ScienceDirect

Journal of Magnetic Resonance

journal homepage: www.elsevier.com/locate/jmr

A selective ^{15}N -to- ^1H polarization transfer sequence for more sensitive detection of ^{15}N -choline

Jessica A. Pfeilsticker, Jason E. Ollerenshaw, Valerie A. Norton, Daniel P. Weitekamp *

A.A. Noyes Laboratory of Chemical Physics, California Institute of Technology, Pasadena, CA 91125, USA

ARTICLE INFO

Article history:

Received 28 July 2009

Revised 17 March 2010

Available online 27 April 2010

Keywords:

INEPT

PASADENA

^{15}N -choline

Hyperpolarization

Selective coherence transfer

REBURP

ABSTRACT

The sensitivity and information content of heteronuclear nuclear magnetic resonance is frequently optimized by transferring spin order of spectroscopic interest to the isotope of highest detection sensitivity prior to observation. This strategy is extended to ^{15}N -choline using the scalar couplings to transfer polarization from ^{15}N to choline's nine methyl ^1H spins in high field. A theoretical analysis of a sequence using nonselective pulses shows that the optimal efficiency of this transfer is decreased by 62% as the result of competing ^{15}N - ^1H couplings involving choline's four methylene protons. We have therefore incorporated a frequency-selective pulse to support evolution of only the ^{15}N -methyl ^1H coupling during the transfer period. This sequence provides a 52% sensitivity enhancement over the nonselective version in *in vitro* experiments on a sample of thermally polarized ^{15}N -choline in D_2O . Further, the ^{15}N T_1 of choline in D_2O was measured to be 217 ± 38 s, the ^{15}N -methyl ^1H coupling constant was found to be 0.817 ± 0.001 Hz, and the larger of choline's two ^{15}N -methylene ^1H coupling constants was found to be 3.64 ± 0.01 Hz. Possible improvements and applications to *in vivo* experiments using long-lived hyperpolarized heteronuclear spin order are discussed.

© 2010 Elsevier Inc. All rights reserved.

1. Introduction

It is now possible to routinely generate samples of certain small biomolecules with nuclear polarizations on the order of 10% using parahydrogen and synthesis allow dramatically enhanced nuclear alignment (PASADENA) [1] or dynamic nuclear polarization (DNP) [2,3]. These technologies show promise for clinical applications based on the *in vivo* characterization of metabolic processes on the seconds timescale. Experiments of this nature rely on storage of the polarization on heteronuclei with long population relaxation times, such as carbonyl ^{13}C or quaternary ^{15}N nuclei, in order to minimize relaxation losses during sample delivery and to provide time for transport, binding, and metabolism. However, the sensitivity enhancement afforded by this strategy is partly lost if the final signal is also detected on a low- γ heteronucleus. Chekmenev et al. [4] have proposed that optimal sensitivity can be obtained by storing polarization on a slowly-relaxing heteronuclear spin and then using an INEPT [5] sequence to coherently transfer magnetization to nearby ^1H nuclei for detection, and have demonstrated the method with two hyperpolarized reagents, $1\text{-}^{13}\text{C}$ -succinate- d_2 and $2,2,3,3\text{-tetrafluoropropyl } 1\text{-}^{13}\text{C}$ -propionate- d_3 (TFPP). Those experiments were designed numerically assuming that the relevant ^1H and ^{13}C sites

were 3-spin ABX systems. A similar strategy has been applied to ^{15}N -choline, where the hyperpolarized ^{15}N polarization was transferred by nonselective INEPT resulting in detectable signal on some of the proton sites [6].

Here we demonstrate a selective version of this polarization transfer strategy with ^{15}N -choline, an $\text{A}_9\text{B}'\text{C}'\text{C}'\text{X}$ system of 14 spin $1/2$ nuclei [7]. Choline is a useful biomarker, showing significantly altered uptake and metabolism in diseased brain tissue [8] and in malignant tumor cells in the breast and prostate [9,10], though toxicity may limit the dose in some applications. Hyperpolarization of ^{15}N -choline to $(4.6 \pm 1)\%$ has been reported after 2 h of DNP at 1.4 K [3,6]. The ^{15}N longitudinal relaxation time of $T_1 = 120$ s in blood [3] is promising for metabolic studies.

We have investigated two INEPT-based pulse sequences for ^{15}N -to- ^1H polarization transfer in ^{15}N -choline. The first is a nonselective refocused INEPT sequence similar to that used in recent hyperpolarized experiments [4,6]. While this sequence is effective, a product operator analysis shows that significantly greater sensitivity can be obtained by using a selective sequence, as demonstrated by targeting choline's nine degenerate methyl ^1H spins. We therefore also present a selective refocused INEPT transfer that uses a REBURP pulse to support coherence transfer from ^{15}N to choline's methyl ^1H spins while suppressing competing transfer pathways to methylene ^1H nuclei. These pulse sequences are experimentally demonstrated *in vitro* using a thermally polarized sample of ^{15}N -choline in aqueous solution.

* Corresponding author. Fax: +1 626 395 6948.

E-mail address: weitekamp@caltech.edu (D.P. Weitekamp).

glycoprotein gp41. The performance of that assay is compared against the gold standard chimeric protein antigen using sera collected from a cohort of HIV-1-positive human subjects, plus controls. We also report on the thermal stability of the capture agent cocktail, with an eye towards point-of-care HIV diagnostics assays that are needed in environments where refrigeration chains may not exist.

Materials and Methods

For detailed protocols see **Materials and Methods S1**.

Ethics Statement

All study documents and procedures regarding the patient serum assays were approved by the UCLA and Caltech Institutional Review Boards. All subjects provided written informed consent prior to initiation of study procedures.

Results and Discussion

The development of a PCC Agent against a protein target utilizes the target itself to promote the 1,3-dipolar cycloaddition between an acetylene and an azide group to form a triazole linkage (the *in situ* ‘click’ reaction) [12]. The protein effectively plays the role of an extremely selective, but much less efficient, variant of the Cu(I) catalyst that is commonly used for such couplings [13,14]. For the present work, the two reacting species are peptides – one peptide (the anchor) is a chemically modified variant of a conserved, immunogenic epitope on the HIV-1 gp41 protein, and the second peptide is selected via an *in situ* click screen from a large (10^6 element) one-bead-one-compound (OBOC) [15] peptide library. The protein targets are human monoclonal antibodies raised against variants of the gp41 epitope represented by the anchor peptide.

The PCC Agents developed here were designed to capture antibodies that are selective for residues 600–612 (IWCGSGK-LICTTA) of gp41. Previous studies have shown that a large fraction of HIV-1-positive patients develop antibodies against this epitope [16,17]. Our strategy for sampling the polyclonal diversity of such antibodies was to develop PCC Agents that exhibited both differential, as well as similar avidities for human monoclonal antibodies (mAbs) raised against different parts of this epitope. A key decision in this regard involves the selection of the anchor peptides from which the PCC Agents are developed. For this task, we modified the polypeptide fragment corresponding to residues 600–612 of gp41 with artificial amino acids at multiple locations, and tested the ability of these modified peptides to detect two different monoclonal anti-gp41 antibodies 3D6 and 4B3 (Polymun, Klosterneuburg, Austria). The 3D6 mAb was raised against the epitope SGKLIIC, whereas the 4B3 mAb was raised against SGKLICTTA. One anchor peptide, A21, was synthesized by adding a propargyl glycine (Pra) residue at the C-terminus of the residues 600–612 of gp41. This anchor peptide was also N-terminally tagged with a polyethylene glycol (PEG) oligomer bridge and a biotin label. For a second anchor peptide (A22), Leu-607 was substituted with Pra. A22 also included an N-terminal PEG-biotin label. A21 equally detected 3D6 and 4B3 with an estimated dissociation constant (K_d) of 1–50 nM, while A22 differentially detected 3D6 ($K_d > 10 \mu\text{M}$) and 4B3 ($K_d = 1–50 \text{ nM}$) (**Figure S1** in Supporting Information). A21 and A22 were then separately developed into PCC agents against 3D6 and 4B3, respectively.

The *in situ* click screens are illustrated in **Figure 1**. The target IgG is incubated with an excess of the selected anchor peptide and

a large OBOC library at 4°C overnight (see **Materials and Methods S1**). The OBOC library is synthesized on TentaGel resin (Rapp Polymere, Tuebingen, Germany), and is a comprehensive library of 5-mers with a 6th amino acid at the N-terminus presenting an azide functionality. To help ensure chemical and biochemical stability, the OBOC library is comprised of non-natural (D) stereoisomers of the 20 natural amino acids, excluding cysteine and methionine. The *in situ* screen is designed to identify a secondary (2°) peptide that, when coupled to the anchor, forms a biligand with increased selectivity and/or affinity for the target IgG. The screen proceeds stepwise. In the first step (not shown in **Figure 1**) the OBOC library is cleared of beads that exhibit non-specific binding to alkaline phosphatase-conjugated streptavidin (SA-AP), which is used as a detection reagent in a later step. Step 2 is a target screen, and so is designed to detect the presence of the bound IgG target to specific beads, and defines possible hits. The step 3 screen is designed to remove those beads from the pool of potential hits that also exhibit binding to off-target serum proteins. Step 4 is called a product screen, and is unique to sequential *in situ* click screens [11]. This screen is designed to detect for the presence of *in situ* clicked reaction products, which are those hit beads containing the triazole-linked anchor peptide. Typically, Step 2 yields a few hundred hits (~0.05% of the OBOC library). Step 3 reduces that pool by a factor of 2 or 3 to about 100 hits, and Step 4 further reduces the number of hits to around 10. This is a manageable number, meaning that each hit can be separately synthesized as a biligand using Cu(I) catalyzed click chemistry to couple the anchor and 2° peptides. The performance of these biligands is then characterized using immunoprecipitation (pull-down) assays detected by Western blotting from spiked serum samples for specificity (data not shown), and sandwich ELISAs and surface plasmon resonance (SPR) assays for affinity estimations (**Figure S2**, **Figure S3**). A complete list of the hits for the A21/3D6 and A22/4B3 screens is given in **Table S1**. This approach yielded two equivalently performing biligands against 3D6, and one biligand against 4B3 (**Figures S2**, **Figure S3**). These three PCC agents (**Figure 2**) were combined, in equal parts, to form a capture agent cocktail. The cocktail slightly outperformed both the standard commercial chimeric antigen and A21, when tested against healthy human serum spiked with both 3D6 and 4B3 (**Figure S4**). A21 is the equivalent of the original antigenic epitope of gp41.

The PCC Agent cocktail and the standard antigen were co-evaluated against a panel of clinical samples using sandwich ELISAs. Serum samples were collected from nine HIV-1-positive patients in Southern California. The standard antigen is a recombinant chimeric protein containing a fragment of HIV-1 gp41 (residues 546–692), the ‘O’ group HIV-1 gp41 immunodominant region (residues 580–623), and a fragment of HIV-2 gp36 (residues 591–617). A good performance of this chimeric antigen has been reported elsewhere [18]. For the comparison assays, streptavidin-coated 96-well plates were saturated with the PCC Agent cocktail or chemically biotinylated chimera in triplicates. Serum samples were diluted to 1% v/v in Tris-buffered saline (TBS) supplemented with 0.1% w/v bovine serum albumin (BSA), and incubated in the wells for 1 hr at room temperature. Unbound proteins were washed off and captured IgG was detected with a peroxidase-conjugated mouse monoclonal anti-human IgG-Fc antibody. The comparison assay results for the patient serum samples along with a healthy control are shown in **Figure 3A**. The signal-to-noise (S/N) ratio in these assays is defined as the measured ELISA signal for a given patient sample, divided by that for the healthy control. The PCC Agent cocktail performed at least as well, and typically much better, than the standard chimeric

A proportionality constant A_{non} and a DC offset constant C have again been included. Maximizing this function numerically for the best known values of the three coupling constants for choline, $J_m = 0.82$ Hz, $J_a = -0.57$ Hz, $J_b = 3.64$ Hz, gives an optimal transfer delay $\tau_1 = 0.233$ s, which yields a signal of $S_{non} = 0.721A_{non} + C$.

Comparing the maximum values of S_{sel} and S_{non} , it is apparent that the ^{15}N -methylene ^1H couplings have the effect of reducing the observable ^1H signal by 62% in the idealized case of an experiment for which $A_{sel} = A_{non}$ and $C = 0$. It would clearly be advantageous to suppress these couplings. This can be achieved by replacing the ^1H π pulse in the middle of τ_1 with a selective pulse tailored to invert the methyl ^1H spins without affecting the methylene ^1H spins.

3. Experimental

Data were collected on a Varian UNITY/INOVA spectrometer operating at a ^1H resonance frequency of 500 MHz. The sample was prepared by dissolving 20 mg ^{15}N -choline chloride (ISOTEC, Miamisburg, Ohio) in 700 μl D_2O . Refocused INEPT experiments were performed using the pulse sequence shown in Fig. 3, which implements the selective ^{15}N -methyl ^1H transfer described in the theory section using a 6.695 ms ^1H REBURP pulse [12] centered at the methyl ^1H frequency. A time $\tau_{reb} = 6.4$ ms, equal to the effective evolution time of the ^{15}N -methyl ^1H coupling during the REBURP pulse, was subtracted from the transfer delay as indicated in Fig. 3. For nonselective INEPT experiments, the REBURP was replaced with a nonselective π pulse and τ_{reb} was set to zero.

To allow efficient testing in the absence of hyperpolarization, the sequence includes a ^{15}N purge element before the recycle delay d_1 to ensure that the system reaches a consistent state at the start of each transient. This measure is necessary because it is impractical to allow full relaxation of the choline ^{15}N spin after each transient owing to its very long T_1 . The sequence includes a ^{15}N $\pi/2$ pulse immediately prior to acquisition in order to purge any ^1H coherence that remains antiphase with respect to ^{15}N after the refocusing period. In the absence of this pulse, intermittent phase aberrations were observed in the methyl ^1H resonance.

For ^{15}N T_1 measurements by inversion-recovery, the pulse sequence of Fig. 3 was modified by adding a ^{15}N π pulse and a variable recovery delay immediately before the ^1H purge pulse. For these experiments, the ^{15}N purge element before d_1 was removed and d_1 was increased to 600 s.

Data analysis was performed in MATLAB (The MathWorks, Natick, MA) using scripts developed in house. Spectral data were quantified by fitting to a complex Lorentzian lineshape function, except for inversion-recovery data, which was quantified by integration. A downhill simplex algorithm was used for least-squares data fitting, and uncertainties in the extracted parameters were estimated using a bootstrap Monte Carlo method [13].

The value of τ_{reb} , which is subtracted from the INEPT transfer delay in order to account for evolution of the ^{15}N -methyl ^1H scalar coupling during the long REBURP pulse, was determined using a numerical simulation of the pulse sequence. Calculations were performed in GAMMA v4.1.2 [14] in Hilbert space using a spin system of practical size, consisting of one ^{15}N and six methyl ^1H spins, with $J_m = 0.82$ Hz. The ^1H resonance frequency was set to 500 MHz and the carrier frequencies were set on resonance with the ^{15}N and methyl ^1H spins. The REBURP and the nonselective pulses were simulated with finite widths corresponding to the experimental

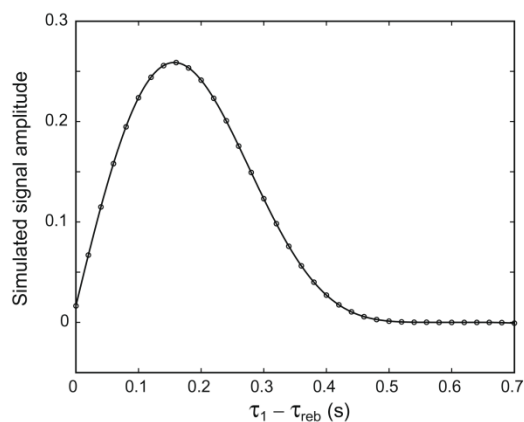


Fig. 4. Numerical simulation of the selective ^{15}N -to- ^1H INEPT pulse sequence acting on a simplified spin system. Circles are simulated methyl ^1H signal amplitudes for different values of the INEPT transfer delay ($\tau_1 - \tau_{reb}$). The line was calculated using a modified form of Eq. (1) with parameter values from a least-squares fit to the data. This fit was used to determine τ_{reb} , the effective evolution time of the ^{15}N -methyl ^1H coupling during the sequence's REBURP pulse.

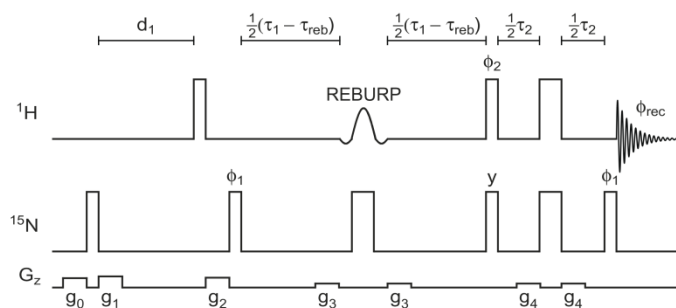


Fig. 3. Selective refocused INEPT pulse sequence for coherent polarization transfer from ^{15}N to methyl ^1H in ^{15}N -choline. Narrow (wide) rectangles denote radiofrequency pulses with a tip angle of $\pi/2$ (π), applied with B_1 field strengths of 23.9 kHz for ^1H and 15.6 kHz for ^{15}N . The shaped ^1H pulse is a 6.695 ms REBURP [12] centered on the methyl ^1H frequency. A four step phase cycle ($\phi_1 = x, x, x, x$; $\phi_2 = x, y, x, y$; $\phi_{rec} = x, y, x, y$) was used to suppress signals originating from ^1H magnetization and to prevent carry over of signal from one transient to the next. A recycle delay d_1 of 60 s ($\sim 0.25 T_1$) was used. Since it is impractical to make this delay long enough to allow full relaxation of the choline ^{15}N spin, a purge element consisting of a ^{15}N $\pi/2$ pulse sandwiched by gradients g_0 and g_1 is used to eliminate ^{15}N magnetization at the start of d_1 , ensuring a consistent starting magnetization for all experiments. A ^1H purge element comprising a ^1H $\pi/2$ pulse and gradient g_2 is used at the start of each transient. Gradients g_3 and g_4 are used to suppress coherence transfer pathways created by imperfect π pulses.

values. Relaxation and phase cycling were neglected. The pulse sequence shown in Fig. 3 was simulated, and the methyl ^1H signal amplitude was calculated, for each of a series of values of the INEPT transfer delay ($\tau_1 - \tau_{\text{reb}}$). The signal data, shown in Fig. 4, was then subjected to least-squares fit to a version of Eq. (1) appropriate for a system containing six methyl ^1H spins and including τ_{reb} as an adjustable parameter, resulting in the value of $\tau_{\text{reb}} = 6.4$ ms used experimentally.

4. Results and discussion

Fig. 5 shows a spectrum of ^{15}N -choline recorded using the selective ^{15}N -to- ^1H INEPT sequence of Fig. 3, alongside a ^{15}N -detected spectrum of the same sample recorded in a similar measurement time. It is not meaningful to compare these spectra quantitatively because they were both recorded using a probe that is optimized for direct heteronuclear observation, a factor which diminishes the sensitivity advantage of ^1H detection. However, even under these unfavorable circumstances the sensitivity to ^{15}N magnetization is more than an order of magnitude better in the selective INEPT spectrum (Fig. 5a) than in the ^{15}N -detected spectrum (Fig. 5b).

A modified version of the selective ^{15}N -to- ^1H INEPT experiment was used to measure the ^{15}N longitudinal relaxation time of ^{15}N -

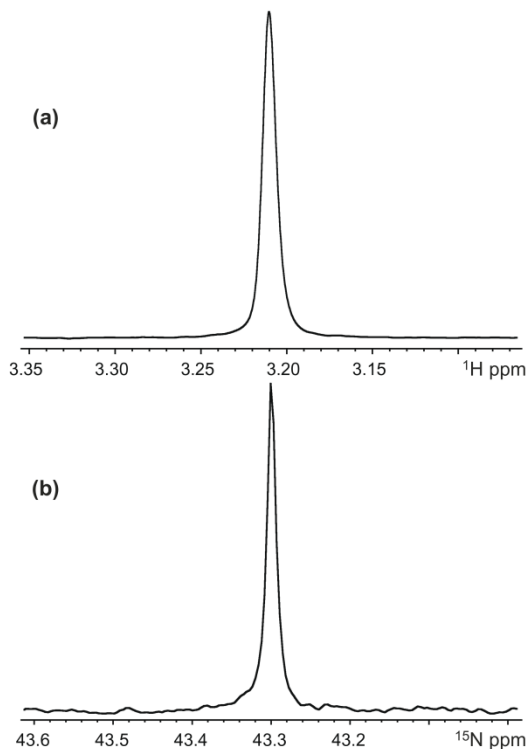


Fig. 5. (a) ^1H spectrum of ^{15}N -choline recorded using the selective ^{15}N -to- ^1H INEPT sequence of Fig. 3. Only the methyl resonance is shown. (b) Single-pulse ^{15}N spectrum of ^{15}N -choline, recorded with tip angle $\pi/2$. Spectra (a) and (b) were each collected on the same Varian AutoX Dual Broadband probe, taking the sum of four transients with a recycle delay of 60 s. Monte Carlo fits of (a) and (b) to Lorentzian lineshapes show that, relative to direct ^{15}N detection, the fractional uncertainty in the initial ^{15}N magnetization is reduced by a factor of 11.0 when using the selective ^{15}N -to- ^1H INEPT sequence, even though the probe design is optimized for the ^{15}N channel.

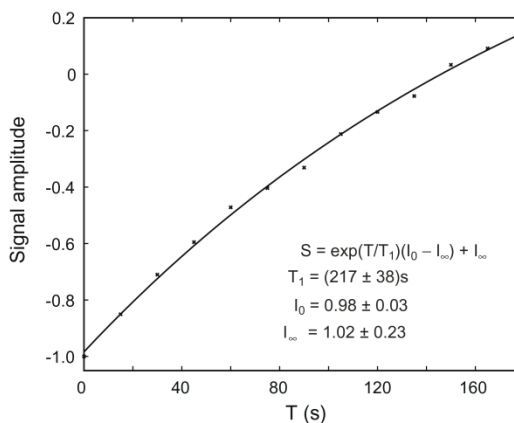


Fig. 6. Measurement of the ^{15}N longitudinal relaxation time of ^{15}N -choline in D_2O solution using a modified version of the pulse sequence shown in Fig. 3. The experiment was repeated for 13 values of the inversion-recovery delay $T = 0.001, 15, 30, 45, \dots, 180$ s. Crosses are experimental methyl ^1H signal amplitudes obtained by integrating the spectral data. The line was calculated using the indicated equation and parameter values from a least-squares fit to the data.

choline in D_2O solution, yielding a value of $T_1 = (217 \pm 38)$ s (Fig. 6). This is comparable to the value $T_1 = (285 \pm 12)$ s previously reported by Gabellieri et al. [3] for ^{15}N -choline in 90% $\text{H}_2\text{O}/10\%$ D_2O .

A series of ^{15}N -choline ^{15}N -to- ^1H INEPT spectra were recorded using both selective and nonselective versions of the pulse sequence of Fig. 3 with values of the transfer delay τ_1 ranging from 6.4 ms to 700 ms. The methyl ^1H signal amplitudes observed in these experiments are plotted in Fig. 7. The selective INEPT sequence allows ^{15}N -choline to be detected with 52% greater sensitivity than the nonselective sequence, comparing the maximum signal amplitude observed in each case. In the Theory section, the amplitude of the methyl ^1H signal was predicted as a function of the transfer delay for the selective (Eq. (1)) and nonselective (Eq. (2)) experiments using a product operator analysis. By fitting the

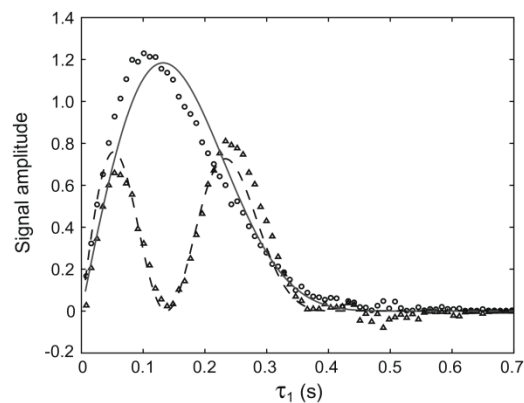


Fig. 7. Amplitude of the methyl ^1H signal observed in ^{15}N -to- ^1H INEPT spectra of ^{15}N -choline using selective (circles) and nonselective (triangles) versions of the pulse sequence shown in Fig. 3, as a function of the INEPT transfer period τ_1 . The lines were calculated using Eq. (1) (solid line) and Eq. (2) (dashed line) with parameter values from a least-squares fit to the data.

observed signal amplitudes to Eqs. (1) and (2), the optimal length of τ_1 for each experiment can be determined, as well as precise values of choline's ^{15}N – ^1H coupling constants.

A simultaneous least-squares fit to both datasets yields parameter values $A_{\text{sel}} = 0.632 \pm 0.001$, $A_{\text{non}} = 1.000 \pm 0.005$, $J_m = (0.817 \pm 0.001)$ Hz, $J_b = (3.64 \pm 0.01)$ Hz, and $C = 0.000 \pm 0.001$. These values for the coupling constants are similar to ones derived from previously published ^1H – ^{14}N values ($J_m = 0.80$ Hz and $J_b = 3.61$ Hz) [15] or observed recently [6] with ^{15}N -choline ($J_m = 0.8$ Hz and $J_b = 3.7$ Hz). The value of the smaller ^{15}N -methylene ^1H coupling constant was found to have a negligible effect on the fitting process, so this parameter was fixed at a reasonable value of $J_a = -0.57$ Hz.

Note that, for experiments using the selective and nonselective versions of the pulse sequence of Fig. 3 on the same spectrometer hardware and sample, the constants in Eqs. (1) and (2) should ideally be the same. The observation that A_{sel} is smaller than A_{non} may be due to signal losses during the selective sequence's REBURP pulse. Comparing the values of A_{sel} and A_{non} from the least-squares fit it appears that 36% of the signal is lost in this way. This can be attributed in part to miscalibration of the REBURP pulse. A three pulse sequence ($\pi/2$ – REBURP – $\pi/2$) was used to calibrate the REBURP pulse by seeking pulse width and power parameters that gave the best null signal. It would be more appropriate to choose a calibration sequence that uses the REBURP pulse for inversion, as it is used in the selective INEPT sequence, rather than for refocusing. Another possibility for the relative deviations of the selective and nonselective experiments from the theory is that ^1H – ^1H couplings are neglected in the analytical theory given for the dynamics. Including these numerically is beyond our present computer capabilities.

We have presented a pulse sequence that suppresses the effects of the four methylene protons on the INEPT transfer from ^{15}N to methyl ^1H in ^{15}N -choline. Note that the same result can be achieved by selective deuteration of ^{15}N -choline. This approach might provide the additional benefit of increasing the molecule's ^{15}N longitudinal relaxation time and would be an option for DNP experiments. However, the present selective recoupling strategy is clearly advantageous for ^{15}N -choline hyperpolarization using PASADENA. In these experiments, two of the methylene ^1H spins derive from a parahydrogen molecule which reacts with an unsaturated precursor to initiate the hyperpolarization process. Although deuteration of the alkene precursor can remove two of the methylene ^1H spins, those which supply the spin order cannot be eliminated.

The success of this selective coherence transfer strategy in ^{15}N -choline has clear implications for studies of other hyperpolarized small biomolecules. By directing the spin order to a subset of the possible detection spins, sensitivity is improved. The recoupling strategy demonstrated here accomplishes this by way of a frequency selective π pulse, which simplifies, and often shortens, the polarization transfer step. Similar selective INEPT sequences could be used to improve the sensitivity of the ^{13}C -to- ^1H polarization transfer experiments demonstrated by Chekmenev et al. in hyperpolarized TFPP [4] by directing the spin order to one of the resolved ^1H sites.

The selective ^{15}N -choline transfer presented here also has potentially useful applications to thermally polarized *in vivo* ^{15}N spectroscopy. Pulse sequences can be devised to transfer methyl ^1H polarization to ^{15}N for an encoding period and then back to methyl ^1H for detection. Such sequences would benefit from choline's long ^{15}N T_1 , while making use of the strong thermal polarization of the nine methyl ^1H spins. This strategy is equally applicable if the ^{15}N polarization is selectively recoupled to the methylene protons adjacent to the oxygen, which more readily resolve choline

from acetylcholine and phospholine [6]. To lengthen the time available for the metabolic interconversion of choline and related compounds, chemical exchange is best encoded in the difference between longitudinal ^{15}N magnetization of the various species, prior to selective polarization transfer.

5. Conclusion

As part of a strategy to improve the sensitivity of *in vivo* experiments on hyperpolarized small biomolecules, we have investigated INEPT pulse sequences for the transfer of magnetization from ^{15}N to the methyl ^1H spins in ^{15}N -choline. Product operator analysis of a simple refocused INEPT sequence shows that the optimized efficiency of this transfer is diminished by 62% by the action of competing couplings between ^{15}N and choline's methylene ^1H spins. A selective INEPT sequence, using a ^1H REBURP pulse to suppress undesired couplings during the transfer period, was devised and tested *in vitro* on a thermally polarized ^{15}N -choline sample. It was demonstrated that the selective INEPT sequence leads to a 52% stronger methyl ^1H signal than the nonselective version.

Acknowledgments

This work was supported by the Beckman Institute pilot program, "Spin-Polarized Molecules for Structural and Systems Biology". JEO was supported by a Postdoctoral Fellowship from the Natural Sciences and Engineering Research Council of Canada.

References

- [1] E.Y. Chekmenev, J. Hovener, V.A. Norton, K. Harris, L.S. Batchelder, P. Bhattacharya, B.D. Ross, D.P. Weitekamp, PASADENA hyperpolarization of succinic acid for MRI and NMR spectroscopy, *J. Am. Chem. Soc.* 130 (2008) 4212–4213.
- [2] K. Golman, R.I. Zandt, M. Lerche, R. Pehrson, J.H. Ardenkjaer-Larsen, Metabolic imaging by hyperpolarized ^{13}C magnetic resonance imaging for *in vivo* tumor diagnosis, *Cancer Res.* 66 (2006) 10855–10860.
- [3] C. Gabellieri, S. Reynolds, A. Lavie, G.S. Payne, M.O. Leach, T.R. Eykyn, Therapeutic target metabolism observed using hyperpolarized ^{15}N choline, *J. Am. Chem. Soc.* 130 (2008) 4598–4599.
- [4] E.Y. Chekmenev, V.A. Norton, D.P. Weitekamp, P. Bhattacharya, Hyperpolarized ^1H NMR employing low γ nucleus for spin polarization storage, *J. Am. Chem. Soc.* 131 (2009) 3164–3165.
- [5] G.A. Morris, R. Freeman, Enhancement of nuclear magnetic resonance signals by polarization transfer, *J. Am. Chem. Soc.* 101 (1979) 760–762.
- [6] R. Sarkar, A. Comment, P.R. Vasos, S. Jannin, R. Gruetter, G. Bodenhausen, H. Hall, D. Kirik, V.P. Denisov, Proton NMR of ^{15}N -choline metabolites enhanced by dynamic nuclear polarization, *J. Am. Chem. Soc.* 131 (2009) 16014–16015.
- [7] J.A. Pfeilsticker, J.E. Ollershaw, V.A. Norton, D.P. Weitekamp, Reverse ^{15}N rINEPT with selective recoupling in choline, in: 50th Experimental NMR Conference, Asilomar, 2009.
- [8] Y. Boulanger, M. Labelle, A. Khait, Role of phospholipase A_2 on the variations of the choline signal intensity observed by ^1H magnetic resonance spectroscopy in brain diseases, *Brain Res. Rev.* 33 (2000) 380–389.
- [9] R. Katz-Brull, D. Seger, D. Rivenson-Segal, E. Rushkin, H. Degani, Metabolic markers of breast cancer: enhanced choline metabolism and reduced choline-ether-phospholipid synthesis, *Cancer Res.* 62 (2002) 1966–1970.
- [10] E. Sutinen, M. Nurmi, A. Roivainen, M. Varpula, T. Tolvanen, P. Lehtikoinen, H. Minn, Kinetics of [^{11}C]choline uptake in prostate cancer: a PET study, *Eur. J. Nucl. Med. Mol. Imaging* 31 (2004) 317–324.
- [11] D.M. Doddrell, D.T. Pegg, W. Brooks, M.R. Bendall, Enhancement of ^{29}Si or ^{119}Sn NMR signals in the compounds $\text{M}(\text{CH}_3)_n\text{Cl}_{4-n}$ ($\text{M} = \text{Si}$ or Sn , $n = 4, 3, 2$) using proton polarization transfer. Dependence of the enhancement on the number of scalar coupled protons, *J. Am. Chem. Soc.* 103 (1981) 727–728.
- [12] H. Geen, R. Freeman, Band-selective radiofrequency pulses, *J. Magn. Reson.* 93 (1991) 93–141.
- [13] W.H. Press, S.A. Teukolsky, W.T. Vetterling, B.P. Flannery, Numerical Recipes in C: The Art of Scientific Computing, second ed., Cambridge University Press, Cambridge, UK, 1992.
- [14] S.A. Smith, T.O. Levante, B.H. Meier, R.R. Ernst, Computer simulations in magnetic resonance. An object-oriented programming approach., *J. Magn. Reson.* A106 (1994) 75–105.
- [15] V. Govindaraju, K. Young, A.A. Maudsley, Proton NMR chemical shifts and coupling constants for brain metabolites, *NMR in Biomedicine* 13 (2000).